MULTICOLOUR PHOTOMETRY OF MIRA VARIABLES

B. D. Kelly

A Thesis Submitted for the Degree of PhD
at the
University of St Andrews

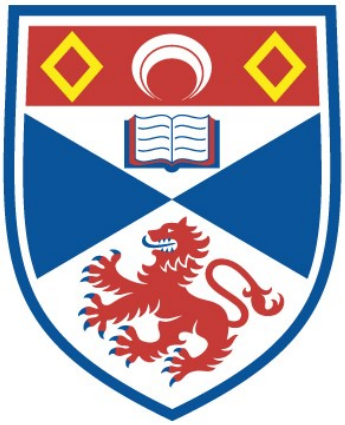

1977

MULTICOLOUR PHOTOMETRY

OF

MIRA VARIABLES

BY

B. D. KELLY

PhD. THESIS 1977

ProQuest LLC.
789 East Eisenhower Parkway
P.O. Box 1346
Ann Arbor, MI 48106 – 1346

Thesis Summary B. D. Kelly.

Multicolour Photometry of Mira Variables.

In Part 1, a background to the project is provided by summarizing the general properties of Miras. A section is devoted to describing pulsating variables from a theoretical viewpoint, and this is followed by a discussion of past photometric work. Finally, a comparison is made between the theory and observations of Miras, which points out the well-known incompatibilities between the two approaches.

Part 2 begins by underlining the desirability of observing Miras in UBVRI, and then goes on to describe the mechanical design of the St. Andrews ten colour, two photo-multiplier, automated photometer. This photometer was designed as a general user instrument for the South African Astronomical Observatory, where the observing programme was carried out between May 1973 and October 1974.

The photometric characteristics of Miras are then re-considered, and the adopted ten colour photometric system, which adds five 200 Å wide filters to UBVRI, is described. The procedures used for obtaining the observations, and the reduction methods are summarized, along with the likely sources of error. This is followed by the analysis of the results, which consists mainly of a description of the properties of the various two-colour diagrams, particular emphasis being placed on those such as (V-R,R-I) and (V,R-I)

which show unexpectedly narrow sequences. In addition, considerable attention is directed at the scatter in the (U-B,R-I) diagram, and also at the interesting R Aqr system.

The data are then considered from the period-luminosity-colour viewpoint, enabling a discussion of absolute magnitudes and the value of the pulsation constant, as well as an investigation of the possible harmonic relationships between Miras of differing periods. Finally, an attempt is made to place the Me Miras in the (M_{bol} , log Te) diagram, and the conclusion is drawn that the discrepancies between theory and observation can probably be mostly attributed to the methods of interpretation of the latter.

Declaration

Except where reference is made to the work of others, the research described in this thesis and the composition of the thesis are my own work. No part of this work has been submitted for a higher degree at this or any other University. Under Ordinance General No. 12, I was admitted to the Faculty of Science of the University of St. Andrews on the 1st October 1968, to carry out design work in connection with an automated photoelectric photometer and subsequently to use the photometer in a programme of multicolour photometry of Mira Variables. I was accepted as a candidate for the degree of Ph.D. on the 1st October 1969, under Resolution of the University Court, 1967, No. 1.

Certificate

I certify that Bruce Dennis Kelly has spent nine terms in research work at the University Observatory, St. Andrews, that he has fulfilled the conditions of Ordinance General No. 12 and Senate Regulations under Resolution of the University Court, 1967, No. 1, and that he is qualified to submit the accompanying dissertation in application for the degree of Ph.D.

ACKNOWLEDGEMENTS

Many people have been very helpful during the long period I have been working on this project, and so it is convenient to group them geographically.

Scotland

All the staff of the University Observatory have been of assistance at some stage of the work. I should especially like to thank Dr. I. G. van Breda for his patience whilst supervising a very protracted investigation, and for his help, particularly during the photometer design period. I am grateful to Professor D. W. N. Stibbs for the use of facilities at St. Andrews, and for the allocation of time on the James Gregory telescope. Drs. P. W. Hill, D. Kilkenny and D. C. B. Whittet all contributed to the long discussions associated with the mechanical design work, and in this connection I should also like to thank Mr. R. Beetles of R.O.E. Messrs. Crabe, Bird and Erskine of the University Observatory were responsible for most of the mechanical and electrical construction work, and incorporated many of their own refinements in the final structure. Mr. D. M. Carr, as well as his design work, also helped me greatly in my attempts to understand the relevant electronics.

South Africa

I wish to thank all the staff at S.A.A.O. for their help and hospitality during my stay there. In particular, I am grateful to Sir Richard Woolley for the use of office and computing facilities, and for the allocation of telescope time. Drs. A. W. J. Cousins and P. R. Warren gave unstintingly of their time during many long

discussions of photometric techniques and the interpretation of results, and Drs. T. G. Hawarden and L. A. Balona gave help concerning the distances of globular clusters and the importance of the pulsation constant respectively. Visitors to S.A.A.O. were also generally helpful, and Dr. E. Mallia obtained a small number of nonetheless important photoelectric measurements for me.

England

I wish to thank J. Ravest and M. Barker for their help, and for the use of calculators. I also wish to thank Miss E. Nicholson who typed the manuscript, and, of course, my wife for her continuing encouragement.

I wish to acknowledge S.R.C. support during most of the period covered by this work, and also the telescope time allocated by the L.T.U.P.

CONTENTS

INTRODUCTION

This investigation began in 1968 under the supervision of Dr. I. G. van Breda, and involved the production of an automated ten filter photometer, followed by its use in observing a selection of Mira variables. The photometer was completed in January 1973 and subsequently installed at the South African Astronomical Observatory, where the observational programme was carried out terminating in September 1974.

The photometer is now a general user instrument associated with the S. A. A. O. 100 cm telescope.

Fig.1. The Relative Intensities of Bright Lines in the Spectrum of Mira at Different Magnitudes.(Joy,1926)

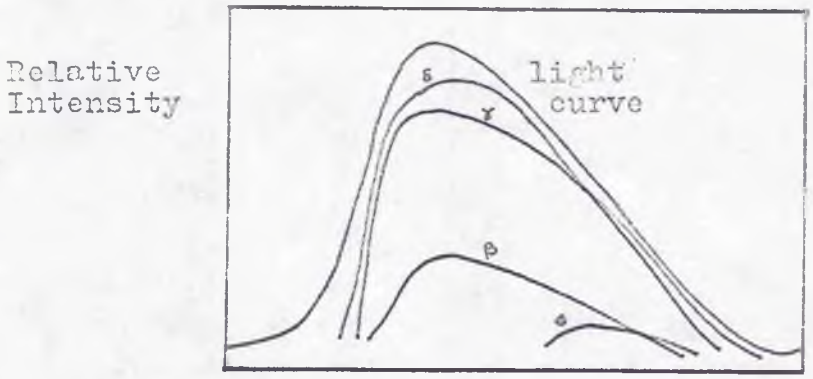

a) Hydrogen lines with visual light curve for comparison.

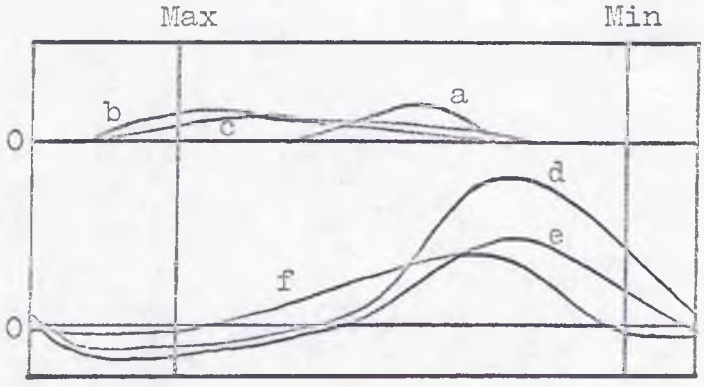

a 4511 In I
b 4179 Fe II
c 4233 Fe II
d 4571 Mg I
e 4308 Fe I
f 4202 Fe I

b) Metallic lines, showing the general division into high and low excitation groups. The curves below the zero line represent the intensities of absorption lines on an independent scale.

PART 1

A BACKGROUND TO THE STUDY OF MIRA VARIABLES

General

(I) Definitions

The Mira variables are cool variable stars with definable periods in the 100 day to 1000 day range. They also have large amplitudes in yellow light, in general greater than about two magnitudes. All Miras show strong emission lines (e.g. of H, Fe, Mg) at certain phases of their light curves, but in addition they show a diversity of elemental abundances in their atmospheres. Hence they can be divided by spectral type into Me, Se and Ce stars, and in this study the use of these terms will imply a variable of that type. For example, "Me star" means "Mira variable of type M".

(II) Me Stars

The Me Miras are by far the most numerous type and have approximately the solar composition. Their spectral types change with the phase of the visual light curve, earliest type occurring at maximum, and latest type near minimum. The emission lines are also phase dependent, appearing first on the rising branch of the light curve and changing in nature until they disappear after minimum. The emission lines for different elements appear and disappear at different phases (fig. 1).

PERIOD	GROUP I	II	III	IV	V
4	POTASSIUM	CALCIUM	SCANDIUM	TITANIUM	VANADIUM
	COPPER	ZINC	GALLIUM	GERMANIUM	ARSENIC
5	RUBIDIUM	STRONTIUM	YTTRIUM	ZIRCONIUM	NIOBIUM
	SILVER	CADMIUM	INDIUM	TIN	ANTIMONY
6	CAESIUM	BARIUM	LANTHANUM	HAFNIUM	TANTALUM
	GOLD	MERCURY	THALLIUM	LEAD	BISMUTH

FIG. 2

____ METALS ABUNDANT IN M STARS

_ _ METALS ABUNDANT IN S STARS

YTTRIUM APPEARS IN BOTH TYPES.

(III) Se and Ce stars

The Se variables differ from the Me type in that many of the metals have been replaced by their equivalents of higher atomic mass (fig. 2). For example Titanium and Scandium are replaced by Zirconium and Yttrium. In the visible part of the spectrum the most obvious result of this is the replacement of the strong TiO bands of the Me stars by the ZrO bands found in Se stars.

In Ce stars the atmospheric abundance of Carbon is higher than that of Oxygen, rather than the reverse which is the case for the M and S stars. The strong tendency for Carbon and Oxygen to combine in molecules results in the less abundant of the pair being "locked-up" in CO and CO_2. As these molecules do not produce bands in the visible spectral region, the apparent result is the disappearance of the less abundant element. Thus the "oxygen" stars are characterised by TiO and VO or ZrO and LaO respectively, while the "carbon" stars show C_2, CN, C_3 and SiC_2.

It has, of course, to be emphasised that these observed abundances apply only to the stellar atmospheres. It is quite feasible that all three types of star could have identical overall abundances. In general attempts to explain the differences between them fall back on appeals to some mechanism which mixes the contents of an evolved stellar core with a "normal" atmosphere, and whose effectiveness differs for different stars.

In general, the phase dependent behaviour of the Se and Ce stars is similar to that of the Me stars.

Most of the following discussion will be directed specifically at the Me stars since, being the most numerous group, more can be stated about them with confidence.

Fig.3. Luminosity-T_{eff} Diagram Showing Post-Main Sequence Evolutionary Tracks for $1M_o$, $3M_o$ and $5M_o$.(Barbaro et al.1966)

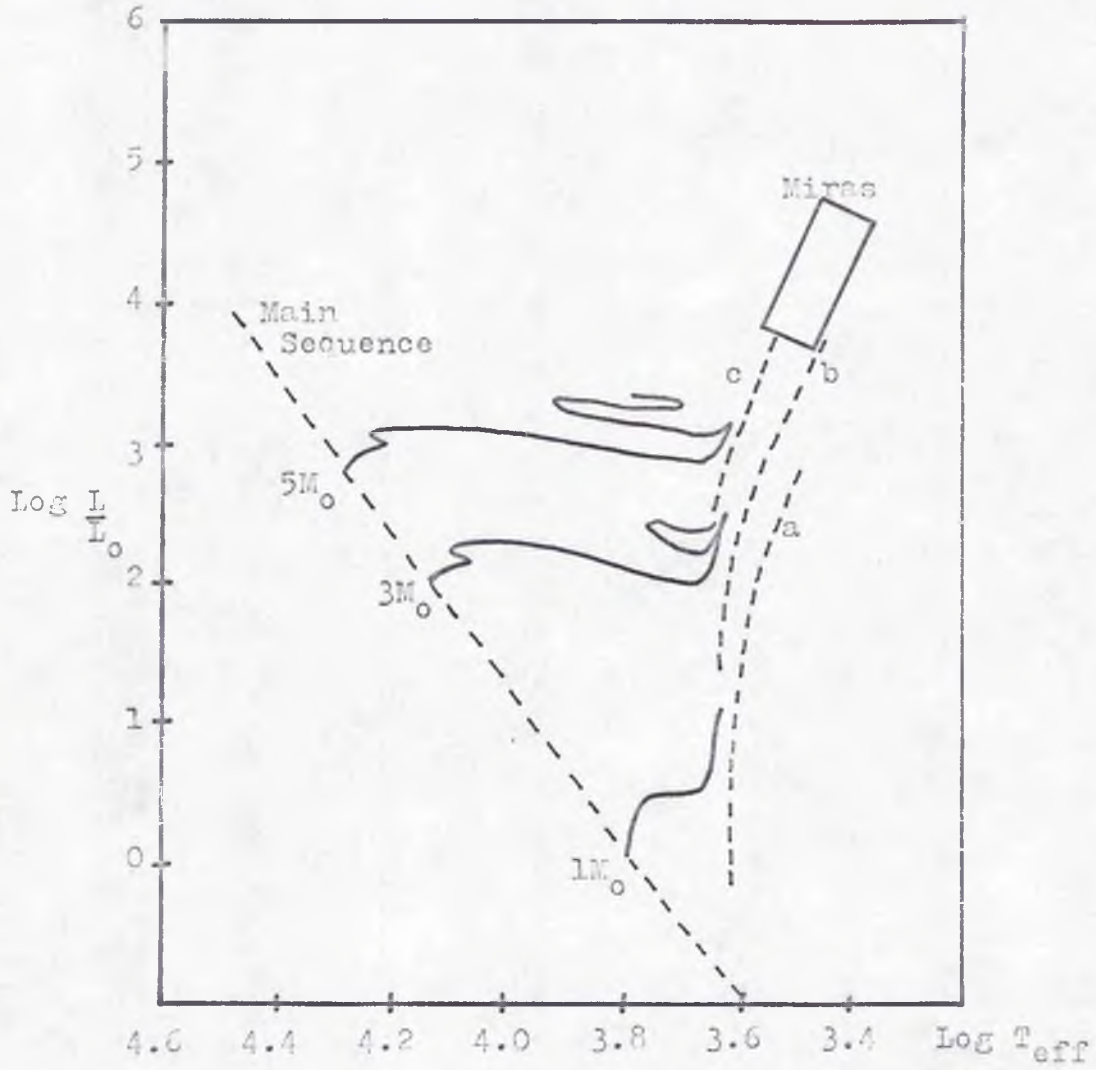

The dotted lines a, b, c are hypothetical Hayashi Lines for $1M_o$, $3M_o$ and $5M_o$ respectively. The position of the Mira variables is indicated.

Fig.4. Cores of Red Giants.

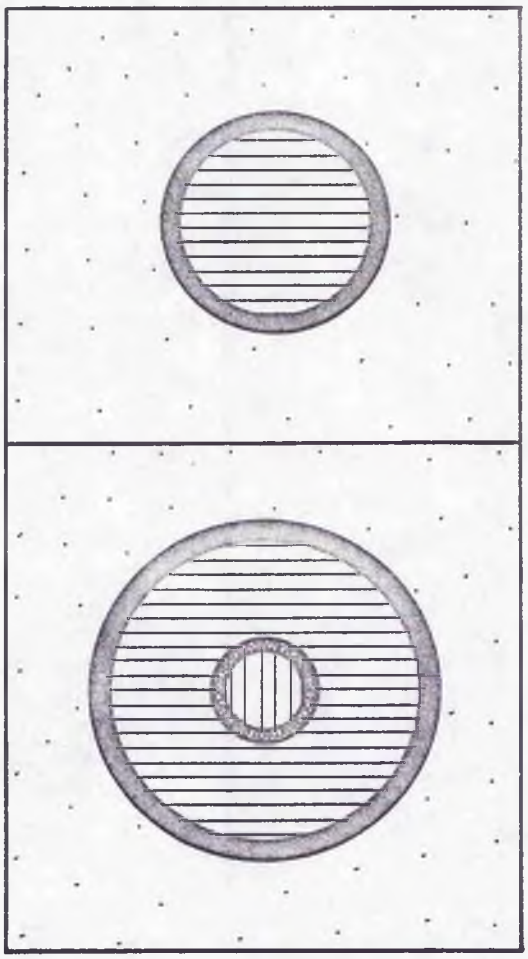

Shell H-burning
Shell He-burning
Helium
Carbon

(IV) Physical Conditions

(i) Kinematics

Studies of the kinematics of Miras (Wilson and Merrill, 1942; Osvalds and Risley, 1961; Clayton and Feast, 1969) show that the Me stars have mean M_v at maximum of about 0^m, and in addition that they share the motions of stars of intermediate age. Photometry (Pettit and Nicholson, 1933; Mendoza V, 1967) reveals them to have surface temperatures around $3000^\circ K$, which combined with their absolute magnitudes implies that they are red giants. Since one can take red giants to have masses equal to the main sequence turn-off mass of stars of similar age, and therefore similar kinematic characteristics, the Me stars are deduced to be about 1 - 2 solar masses (Feast, 1963).

(ii) Spatial Distribution

Consistent with their kinematics, the Me stars show only a moderate degree of concentration towards the plane of the Galaxy. In addition a few are found in metal-rich globular clusters, but none are found in open clusters.

(iii) Evolutionary State

The Me stars are found at the extreme red end of the giant region in the H-R diagram, and therefore are presumably in a post main sequence stage of evolution (fig. 3). Their position is consistent with that of a star having no thermonuclear energy sources in its core, relying instead on core gravitational contraction and nuclear reactions in a shell or shells at the base of the atmosphere. More specifically, one is considering stars which have either exhausted the hydrogen in their cores and have not yet begun helium burning, or have exhausted the core helium and are not burning carbon (fig. 4).

Pulsation theory of Variable Stars

This section has been taken principally from Cox and Giuli (1968).

(I) Simple Approach

Define Π = pulsation period

v_s = velocity of sound

R = stellar radius

$\Gamma_1 = \left(\frac{d \ln P}{d \ln \rho}\right)_{ad}$

= the adiabatic logarithmic gradient of pressure with respect to density

Ω = gravitational potential energy of system.

The fundamental period of a star should be approximately the time required for a sound wave to propagate through it.

$$\Pi \approx \frac{2R}{v_s}$$

Now $$v_s = \sqrt{\frac{\Gamma_1 P}{\rho}}$$

which combined with the virial theorem

$$-\Omega = 3 \int_V P dV$$

gives $$-\Omega = 3 \left\langle \frac{v_s^2}{\Gamma_1} \right\rangle M$$

$$\approx 3 \frac{\overline{v_s^2}}{\overline{\Gamma_1}} M$$

In addition, for a spherically symmetric star,

$$-\Omega = q \frac{GM^2}{R}$$

where q is a constant depending upon the degree of central concentration.

q = 0.6 for a homogeneous star

= 1.5 for a main sequence star

= 3/(5-n) for a polytrope of order n.

Combining these results gives

$$\Pi \approx 2 \left(\frac{3}{\overline{\Gamma_1}}\right)^{\frac{1}{2}} \left(\frac{R^3}{qGM}\right)^{\frac{1}{2}}$$

Defining $Q = \Pi \sqrt{\frac{\overline{\rho}}{\overline{\rho_0}}}$

We have $\Pi\sqrt{\overline{\rho}} = 2 \left(\frac{3}{\overline{\Gamma_1} q}\right)^{\frac{1}{2}} \left(\frac{3}{4\pi G}\right)^{\frac{1}{2}} = Q\sqrt{\overline{\rho_0}}$

Hence Q is a constant if $\overline{\Gamma_1}\, q$ = const., which one expects for a group of stars of similar internal structure. Because of this property, Q is called the PULSATION CONSTANT and its importance lies in the fact that its value depends on the internal structure of the star but it is also an observable quantity.

(II) The Wave Equation

For a spherical shell of radius r concentric with a star, which encloses a total mass of stellar material m, one can use the time derivative of the momentum equation combined with the equations for conservation of energy and mass to derive the equation of motion of the shell. This equation is made more manageable by assuming that the relative variations of the various parameters, for example $\delta P/P$, $\delta\rho/\rho$ etc., are all infinitesimal. This leads to the linearized equation of motion which is:-

$$\ddot{\xi} - \frac{\dot{\xi}}{r\rho} \frac{d}{dr} \left[(3\Gamma_1 - 4)\, P\right] - \frac{1}{\rho r^4} \frac{\partial}{\partial r} \left(\Gamma_1 P r^4 \frac{\partial \xi}{\partial r}\right)$$

$$= -\frac{1}{r\rho}\frac{\partial}{\partial r}\left[\rho(\Gamma_3 - 1)\delta\left(\varepsilon - \frac{\partial H}{\partial m}\right)\right]$$

Where r = radius of the mass shell

$$\xi = \frac{\delta r}{r}$$

$$\Gamma_3 - 1 = \left(\frac{d \ln T}{d \ln \rho}\right)_{ad}$$

= adiabatic logarithmic gradient of temperature with respect to density

ε = energy produced per unit mass in shell element by nuclear reactions

H = total energy flux (convection and radiation)

$\left(\varepsilon - \frac{\partial H}{\partial m}\right)$ = net rate of gain of energy per unit mass.

The linear theory of pulsation should give reasonable accuracy when used to determine stellar stability and periods, but of course it is unable to predict the amplitude of the pulsations.

a) <u>Adiabatic Treatment</u>

If all the stellar material is assumed to be undergoing only adiabatic changes, then the material can have no net gain or loss of heat and so $(\varepsilon - \partial H/\partial m)$ will be constant and zero. Hence the right-hand side of the wave equation is zero, and solutions can be obtained for the "adiabatic wave equation". These solutions are, of course, inherently non-realistic in as much as we have restricted the model to a series of equilibrium configurations which will therefore not be liable to periodic pulsations. Nonetheless, one can determine the fundamental

period of the model and also investigate how the behaviour of Q is modified. The adiabatic solutions to the problem can thus be used as a half-way house between the oversimplified and the realistic solutions, and so help in the physical interpretation of the latter.

An analytical solution of the wave equation is possible if one considers extremely simple cases, for example, assuming:-

$$\Gamma_1 = \text{constant} \ (\neq 4/3)$$
$$\delta r \propto r \quad (\text{i.e. } \xi \text{ is independent of } r),$$

then one can show that the equilibrium density ρ_o is independent of r, that is the model is a homogeneous star. Furthermore for $\Gamma_1 > 4/3$, there exists a periodic solution with

$$Q = \pi\sqrt{\rho_o} = \frac{2\pi}{\sqrt{(3\Gamma_1 - 4)(4/3)\pi G}} = \text{const.}$$

where ρ_o is now measured in solar units.

Less restrictive models lead to results such as

$$\pi\sqrt{\rho_o} = 2\pi\left[\overline{(3\Gamma_1 - 4)}(-\Omega/I)\right]^{\frac{1}{2}}$$

Where Ω = gravitational potential

I = moment of inertia about star's centre

$$\overline{3\Gamma_1 - 4} = \frac{\int (3\Gamma_1 - 4)\, P\,dV}{\int P\,dV}$$

= the pressure average.

The star will be dynamically unstable if $\overline{\Gamma_1} < 4/3$.

If simplifying assumptions are not made, then the linearised adiabatic wave equation has to be solved numerically. Under these circumstances it is found that the period of the star is determined principally by a function which has a strong maximum

Fig.5. Typical Dependence of Γ_1 upon Depth in a Real Stellar Atmosphere.

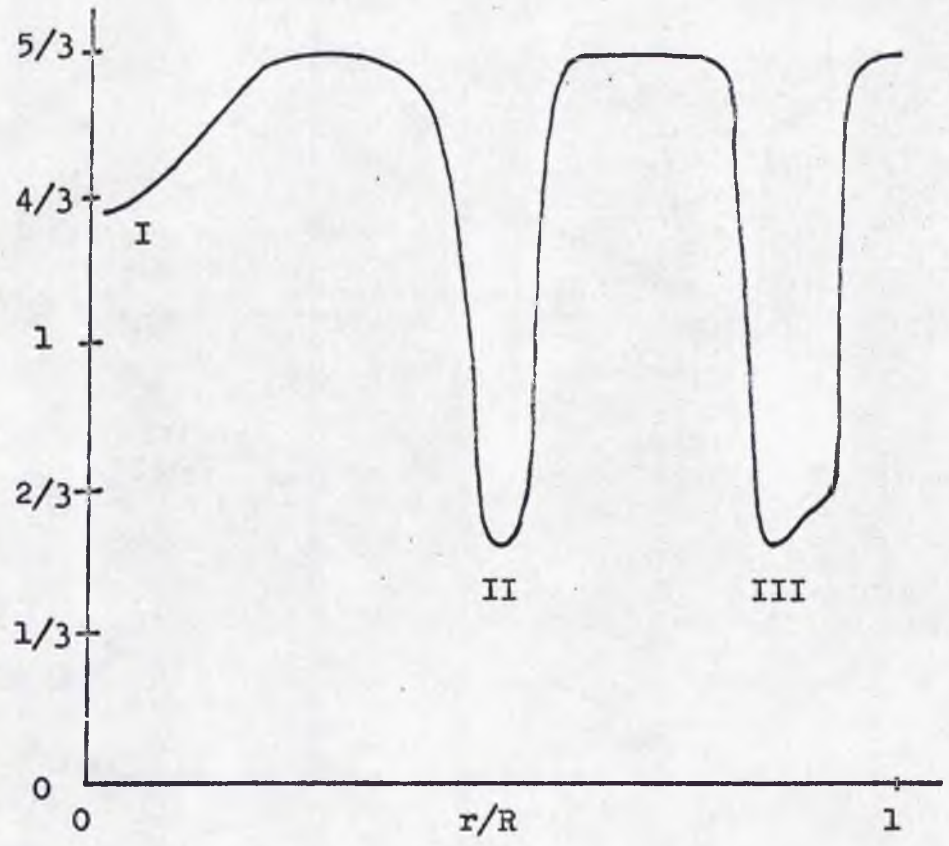

$\Gamma_1 = (d\ln P/d\ln)_{ad}$ is a function of depth in real stars, and three sizeable minima are shown here, corresponding to regions where

(I) radiation pressure makes an important contribution to P,

(II) He II is partly ionized to He III,

(III) He I and H I are partly ionized to He II and H II.

A depression would also occur, for example, where the molecule H_2 was partly dissociated.

Γ_3 behaves similarly, although the actual values of Γ_1 and Γ_3 are in general different.

in the atmosphere of the star ($r/R \approx 0.75$) and is very small in the central regions. By analogy with the above, one can write

$$Q = \Pi \sqrt{\bar{\varrho}_o} = 2\pi \left[\langle 3\Gamma_1 - 4 \rangle (-\Omega/I) \right]^{-\frac{1}{2}}$$

where $\langle 3\Gamma_1 - 4 \rangle$ is mainly determined around the region $r/R \approx 0.75$.

The temperature of this CRITICAL ZONE is given by

$$T_{crit} \approx (1.1 \text{ to } 1.8) \times 10^6 \frac{M}{R} \quad {}^{o}K$$

where M and R are in solar units.

In realistic models of stellar atmospheres, Γ_1 is not a constant with depth (fig. 5). The most obvious variation in the value of Γ_1 occurs in regions where a very abundant element (H or He) is partly ionised. In such a region the material has an extra degree of freedom in that an input of energy can result in an increase in ionisation rather than an increase in the kinetic motions of the atoms. Hence the material is more compressible and Γ_1 and Γ_3 both show marked minima.

For Cepheid variables, longer periods are associated with higher luminosity, lower surface temperature and larger radii. As a result, as one moves along the Cepheid sequence T_{crit} decreases with increasing period, and the position of the critical zone shifts with respect to the neighbouring He II → HeIII ionisation zone. Hence $\langle \Gamma_1 \rangle$, and therefore Q, varies with period for Cepheids.

The results of studies of the linear adiabatic wave equation can be summarized as follows.

1) For giant stars the amplitude of the pulsation becomes very small in the central regions, meaning that nuclear reactions do

not dominate the star's stability and the sources of pulsational instability must be sought in the envelope.

2) The pulsation period is primarily determined in a critical zone in the stellar envelope where $r/R \approx 0.75$.

3) Q varies in a systematic fashion even for a group of variables of similar internal structure.

b) Non-adiabatic Treatment

The non-adiabatic term in the wave equation has only a small direct effect on the solutions throughout most of the stellar mass, and so the adiabatic theory is capable of predicting the pulsation period satisfactorily.

It is instructive to inspect the linearized form of the Energy equation.

$$\frac{\partial}{\partial t}\left(\frac{\delta P}{P}\right) = \Gamma_1 \frac{\partial}{\partial t}\left(\frac{\delta \rho}{\rho}\right) + \frac{(\Gamma_3 - 1)\rho}{P}\,\delta\left(\varepsilon - \frac{\partial H}{\partial m}\right)$$

This equation reveals two important phenomena associated with the non-adiabatic effects introduced by the second term on the right hand side.

Firstly, one expects $\partial(\delta\rho/\rho)/\partial t$ to be approximately 90° out of phase with respect to $\delta\rho/\rho$. Assume that $\delta(\varepsilon - \partial H/\partial m)$ is approximately in phase with $\delta\rho/\rho$. Then, clearly, the result is a phase shift between $\partial(\delta P/P)/\partial t$ and $\partial(\delta\rho/\rho)/\partial t$. The non-adiabatic term will thus, in general, result in a phaseshift between the pressure and density variations which gives the solution of the wave equation the characteristics of a running wave. In addition the phase shift means that work is being done

either on or by any given mass shell during the pulsation. If the "restoring force" P lags behind the "displacement" ϱ, then one has a condition of overstability and the pulsation tends to grow.

The second effect is peculiar to the outer layers of the star. Here P/ϱ becomes very small and this in turn demands that $\delta(\varepsilon - \partial H/\partial m)$ become very small. However, $\varepsilon = 0$ in such regions, hence $\partial(\delta H)/\partial m$ must become small. Therefore the displacement δH from the equilibrium flux must be almost constant in space in the outer atmosphere, and this is described by saying that the flux variations are "frozen in". One can interpret this as being due to the small heat capacity of the outer stellar layers.

The cause of stellar pulsations can be understood intuitively through two complementary approaches which converge to produce the same mathematical result.

(i) Work Done

We have seen that in real stellar material one can expect the pressure and density changes in any selected shell of radius r to be out of phase. This leads to the conclusion that net work, either positive or negative, is being done on the material of that shell by pressure and gravity forces. By summing the work done during a cycle on all the shells making up the star, one can determine the total work being done. If this is positive, the star is clearly pulsationally unstable.

Mathematically, one searches for solutions of the wave equation of the form

$$\dot{\xi}(r,t) = \xi(r)\, e^{\pm i\sigma t}\, e^{-\chi t}$$

where $\sigma = \frac{2\pi}{\Pi}$

and $\mathcal{K} \approx -\frac{Cr}{2J\sigma^2}$ = the stability coefficient

$J = \int_m |\xi|^2 \, r^2 \, dm$

= oscillatory moment of inertia

$Cr \propto \left\langle \frac{dW}{dt} \right\rangle$ = average rate at which pressure and gravity forces do work on the whole star during a cycle

clearly,

$Cr < 0 \quad \Rightarrow \mathcal{K} > 0 \quad \Rightarrow$ DAMPING

$Cr > 0 \quad \Rightarrow \mathcal{K} < 0 \quad \Rightarrow$ DRIVING

(ii) Energy Flow

If the total energy flux leaving the surface of a star varies, and yet the energy produced in the star by nuclear reactions is constant, then clearly the star must be capable of storing energy at one time and releasing it subsequently.

Consider the He II $\longrightarrow$ He III ionisation zone. We have already seen that inside such a zone $(\Gamma_3 - 1) = (d \ln T / d \ln \rho)_{ad}$ becomes small, and so a compression of such a region results in a relatively small increase in temperature. Outside the ionization zone the temperature increase will be larger. Hence the temperature gradient in the lower part of the zone will be increased, and that in the outer part reduced. If the state of the material is approximately adiabatic, then the energy flow will behave similarly, being increased in the lower part of the zone and reduced in the higher part. Clearly, relative

to the equilibrium state, energy is being stored in the inner part of the zone and liberated in the outer. If the compression of a region results in a reduction in the energy flux through it, then that region has a destabilising influence. Hence the lower and upper parts of an ionisation zone act as driving and damping regions respectively. If the stellar material is approximately adiabatic, the effects of these two regions cancel one another, and so the ionisation zone as a whole does not contribute to stellar instability.

(iii) Non-adiabatic Effects and Pulsational Stability

Mathematically, (i) and (ii) above produce the same result since

$$Cr \approx -L \int_m (\Gamma_3 - 1)\, e_1 \frac{dH_1}{dm}\, dm$$

where L = total luminosity of the star

e_1 = real part of the spatial variation in the density displacement

≡ amplitude of density variation

H_1 = real part of the spatial variation in the flow displacement

≡ amplitude of flux variation

≈ δ H at maximum density.

It is seen that regions where H_1 is decreasing outwards produce a positive contribution to Cr and are therefore driving regions.

We have seen that non-adiabatic effects dominate only in the outer stellar layers. Elsewhere the stellar material acts approximately adiabatically. We can express this by saying that a TRANSITION REGION exists, and that below this,

Fig.6. The Possible Interactions Between an Ionization Zone and the Transition Region.

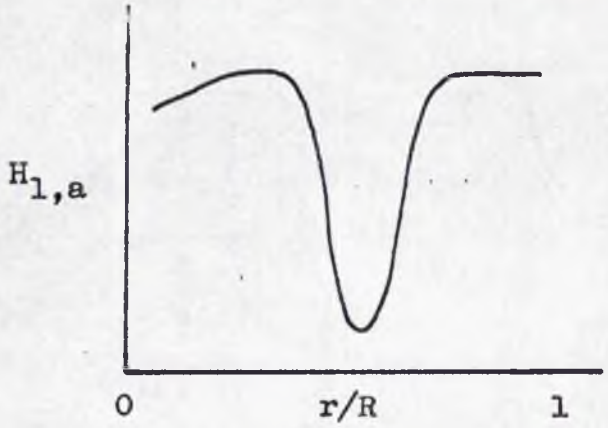

Computed adiabatically, the flux amplitude shows a sharp minimum in an ionization zone.

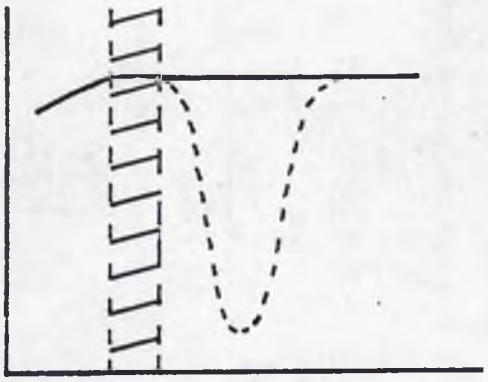

(a) Transition region annuls effect of ionization zone.

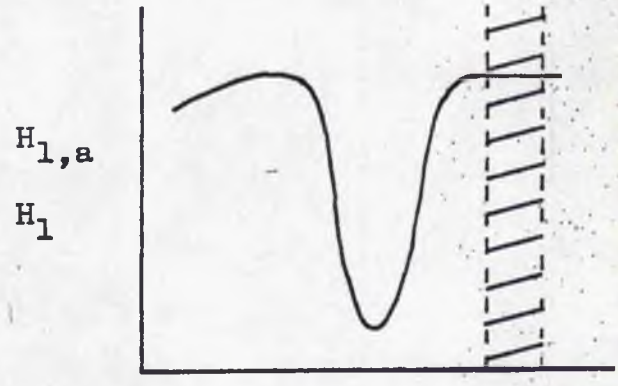

(b) Transition region has no effect on flux amplitude.

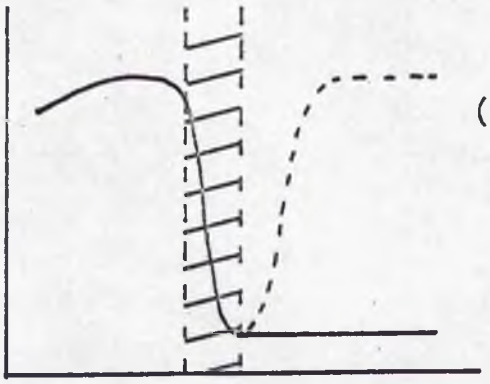

(c) Transition region "freezes" actual flux amplitude H_1 at a low level.

$H_1 \approx H_{1,a}$ = flux computed adiabatically. Outside the transition region $H_1 \approx$ constant.

Fig. 6 shows the result of the possible interactions between an ionisation zone and the transition region. The only important case occurs when the two coincide and the transition region "freezes" H_1 at a low level, thereby annulling the damping effect of the outer edge of the ionisation zone. In this case there is a net storage of energy occurring at maximum compression and the star as a whole will be pulsationally unstable.

It must be emphasised that H_1 is the real part of the complex amplitude of δH. The energy storage revealed in fig.6c will be compensated by an energy release occurring at some other phase of the pulsation.

(III) Summary: The Importance of Γ_1 and Γ_3

We have seen that from the point of view of pulsation theory the vital characteristic of a star lies in the interaction between the zone of ionisation of an abundant element and a "sensitive" region in the stellar atmosphere. Firstly the star will be pulsationally unstable if the transition region occurs in a zone where Γ_3 is strongly depressed. Secondly the value of the pulsation constant depends on the interaction between Γ_1 and a weighting function having a strong maximum in the region $r/R \approx 0.75$, which is called the critical zone. The test occurs for Cepheid variables, in which the critical zone, transition region and He II $\rightarrow$ He III ionisation zone all lie at comparable depths and produce the sort of effects one might

expect. Indeed, the position in the H - R diagram of the blue edge of the Cepheid instability strip, and the variation of Q with period are both explicable by pulsation theory. Problems, however, occur when the red edge of the instability strip is considered. One might expect that pulsations will stop for cooler stars, as the transition region moves outside the He II $\rightarrow$ He III ionisation zone. However, it is found that the interaction involving the (H I $\rightarrow$ H II) + (He I $\rightarrow$ He II) zone occurs almost immediately. The red edge of the instability strip seems to require explanation in terms of convection currents contributing a stabilising influence. One then finds, however, that it is difficult to explain pulsation occurring for much cooler stars, namely the Miras. We return to the theory of Miras in a later section.

PHOTOMETRIC OBSERVATIONS

The effective temperature of a star is the actual temperature of the black body which would produce the same total energy per unit surface area as the star. The observed energy received from a star is proportional to the square of its apparent angular diameter.

Hence $m_{bol} = f(Te, \alpha)$, and given any two of these variables one can compute the third.

(I) Pettit and Nicholson (1933)

Pettit and Nicholson made radiometer measurements of m_{bol} for a collection of Miras at various phases, and also used a water-cell acting as a filter, thereby producing an extremely broad band two colour system which they calibrated in terms of Te. They attempted an absolute calibration of both m_{bol} and Te which therefore enabled them to calculate the angular radii α of the stars they observed. Although modern work disagrees with the absolute calibrations, the system would appear to have been self-consistent in that the values of α produced agree extremely well with the values obtained from interferometry (Pease 1931), speckle interferometry (Bonneau and Labeyrie, 1973) and occultation studies (Nather and Wild, 1973).

For a variable star, it is useful to express the surface brightness and the angular radius in terms of magnitudes m_σ and m_α respectively, so that $m_\lambda = m_{\sigma,\lambda} + m_{\alpha,\lambda}$ at some wavelength λ. In general, m_α will be relatively weakly dependent on λ, and for a black body it will be independent of λ. Considering a black body whose temperature and

Fig.7. Average Radiation Curves of Miras.

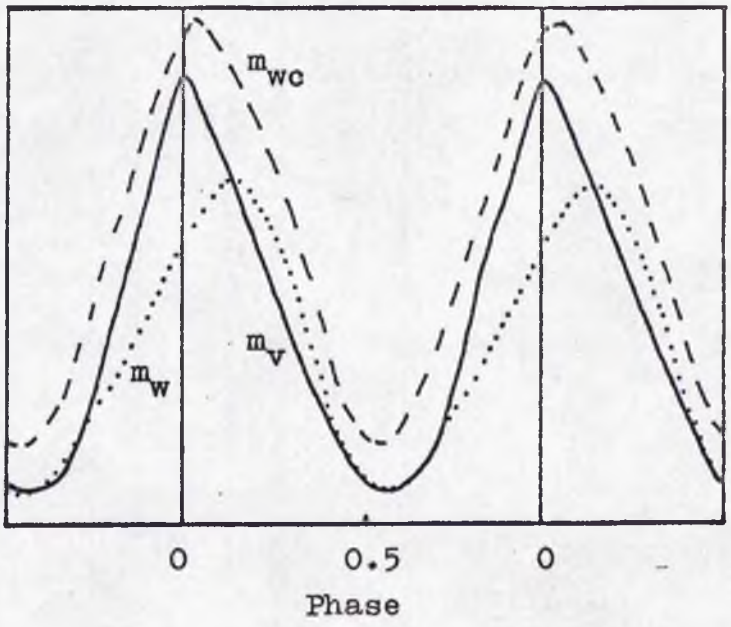

m_v - visible

m_{wc} - visible + near IR

m_w - radiation longward of 1.3 microns

radius are varying, and are not necessarily in phase with one another, we see that the variations in m_λ need not be in phase with either $m_{\sigma,\lambda}$ or m_α. More specifically, the relative phases of the maxima and minima of the three quantities will depend on the amplitudes of $m_{\sigma,\lambda}$ and m_α.

For Miras, Te $\approx$ 3000°K, so the maximum of the energy curve will lie in the near infrared (I). The photometric V band, therefore, lies on the short-wave tail of the intensity curve and so $m_{\sigma,V}$ varies more strongly with temperature than $m_{\sigma,I}$. For Miras this effect is exaggerated because of the strong TiO absorption bands, which are temperature sensitive, and occur in V. Fig. 7 summarizes the result of this as indicated by Pettit and Nicholson's measurements. It is seen that the observed light curve shows a maximum the timing of which depends on the wavelength of measurement, i.e. $t_{max}(\lambda) = f(\lambda)$.

It is important to emphasize two points.

(i) This effect would show for a true black body.

(ii) The wavelength dependence is in a sense spurious: $t_{max}(\lambda)$ <u>really</u> depends on the amplitude of $m_{\sigma,\lambda}$.

Pettit and Nicholson's measurements are consistent with the following properties for Miras.

(i) The amplitude of $m_{\sigma,V}$ is so large with respect to the amplitude of m_α that maximum $m_{\sigma,V}$ (and therefore maximum Te) occurs at the same time as maximum V.

(ii) Minimum m_α (minimum radius) occurs at maximum $m_{\sigma,V}$.

(iii) Maximum m_α (maximum radius) occurs at about phase 0.3.

Fig.8.

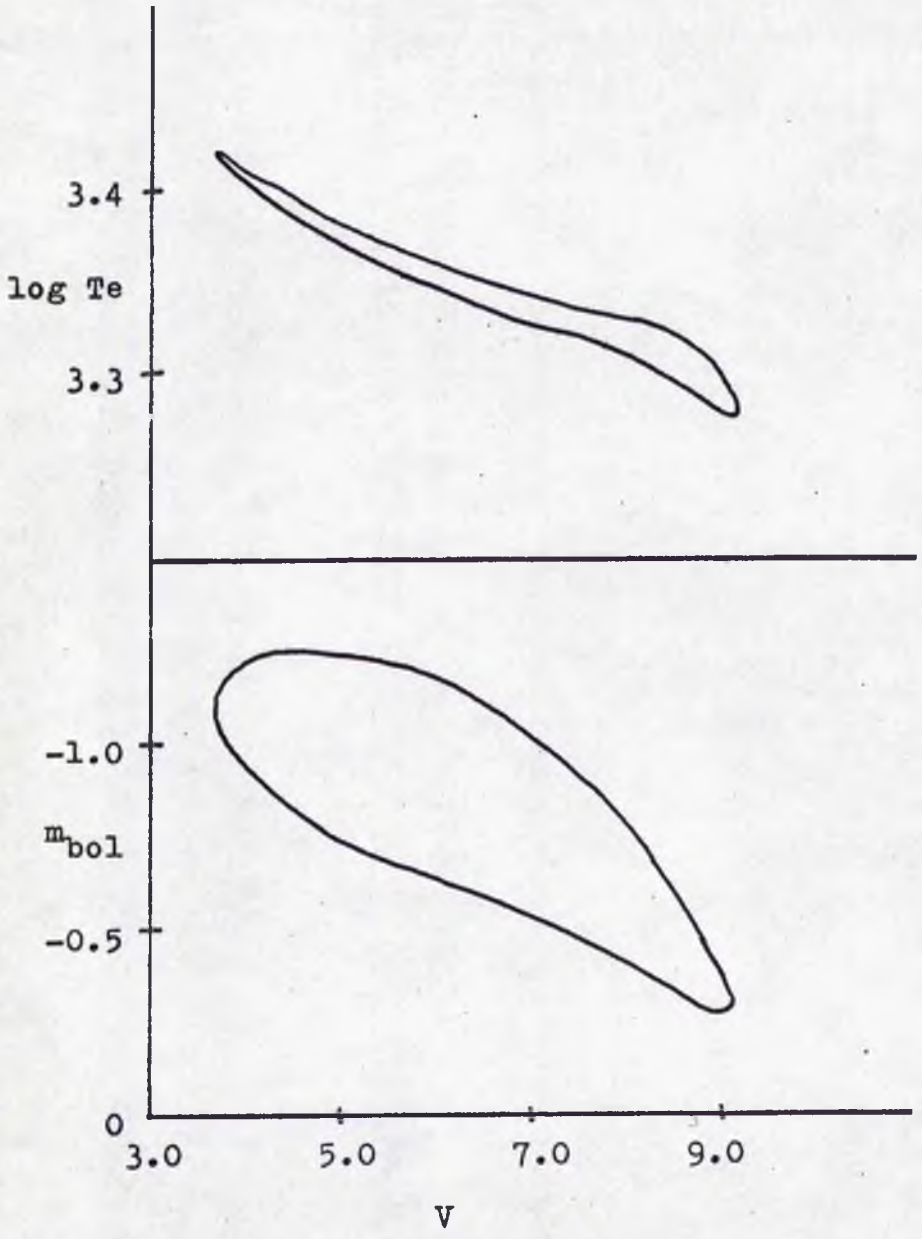

Fig.9.

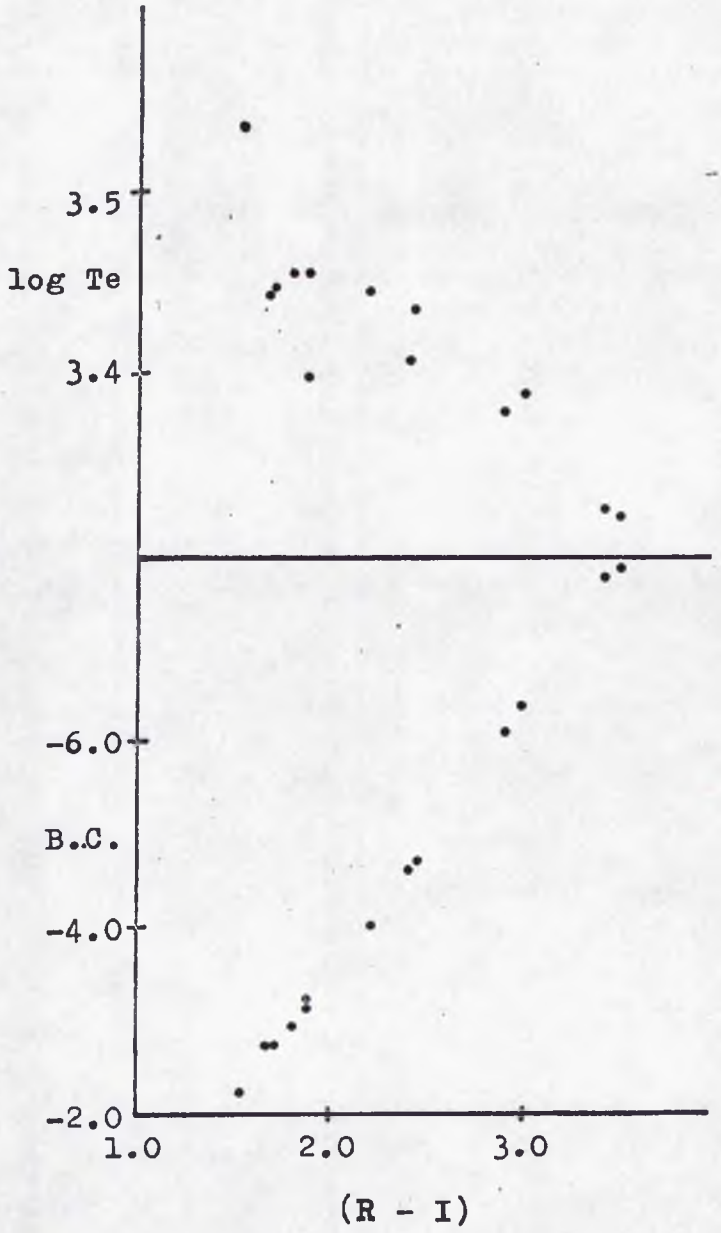

These properties are not, however, consistent with the radial velocity changes exhibited by the absorption lines. Scott (1942) has shown that they are consistent with the assumption that the photosphere's velocity changes are indicated by the emission line velocities. However the actual velocities given by the emission lines cannot be those of the photosphere since this leads to unacceptable results when the kinematics of the stars are investigated.

Pettit and Nicholson's measurements can be presented in a different form if we make use of their data relating m_{bol} and Te of Mira with phase, combined with the mean V curve taken from Campbell (1955). Fig. 8 shows the relationships (m_{bol}, V) and (Te, V), and reveals the loop produced by the radius variations which prevent these two relationships from being unique.

(II) Mendoza V (1967)

Mendoza V has observed Miras on the U B V R I J H K L M N system and has followed Johnson's (1966) method of calibrating m_{bol} and Te. This method measures m_{bol} "directly" by integrating the energy curve indicated by the photometry, after making allowances for known strong absorption, particularly by H_2O. The procedure is carried out for a number of stars for which α has been determined by some other method, enabling Te to be calculated. For these stars, Te is then plotted against I - L, allowing the construction of a calibration curve for stars of unknown α. The method leads to scales for Te and m_{bol} different from those produced by Pettit and Nicholson. In Fig. 9

Fig.10. Composite Light Curves of Me Variables (Smak,1966)

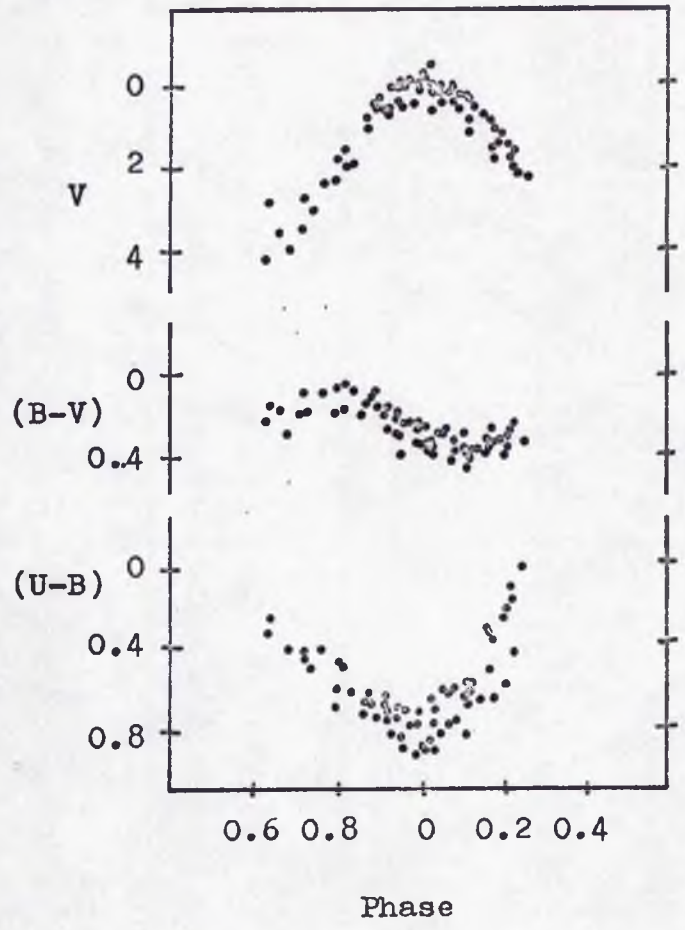

we have plotted Mendoza V's determined m_{bol}-V and Te against R - I for Me stars. These diagrams indicate the possibility of using R - I to determine effective temperatures and bolometric corrections provided one restricts consideration to Me stars only.

(III) Smak (1966)

Smak has summarised the properties of Me Miras as observed in U B V. Fig. 10 shows the variations in B - V and U - B as a function of phase, and it is noticeable that B - V has small variations out of phase with the light curve, its bluest value occurring at about phase 0.8. U - B has a sizeable amplitude approaching 1^m, but it is opposite in phase to what one might expect, reddest U - B occurring at phase 0, that is, when the stars are at their hottest.

The gross features of the U B V photometry, including the very large V amplitudes, are due to the effect of differential TiO blanketing. The TiO bands are strongest in V, but also have considerable strength in B. Hence B - V is almost independent of temperature since the changing blanketing in V cancels the change in colour which would be expected of a black body. U has no TiO bands, and so the growth of bands in B as the temperature falls results in the U - B colour becoming bluer.

The detailed properties are more confusing. Both the phase of the B - V variations and the large scatter found in the two colour diagram imply the presence of phase dependent effects which are not correlated with temperature. It must be assumed that these are caused by the emission lines.

Fig.11.

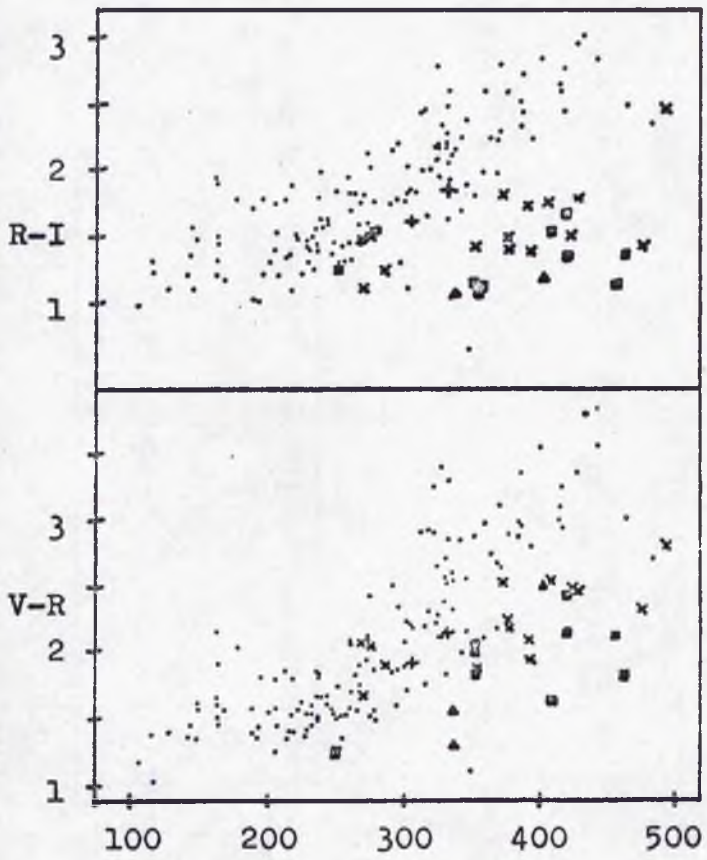

Colours at visual maximum (Barnes,1973).

- · Me
- \+ MSe
- × Se
- ▲ CSe
- ■ Ce

Fig.12.

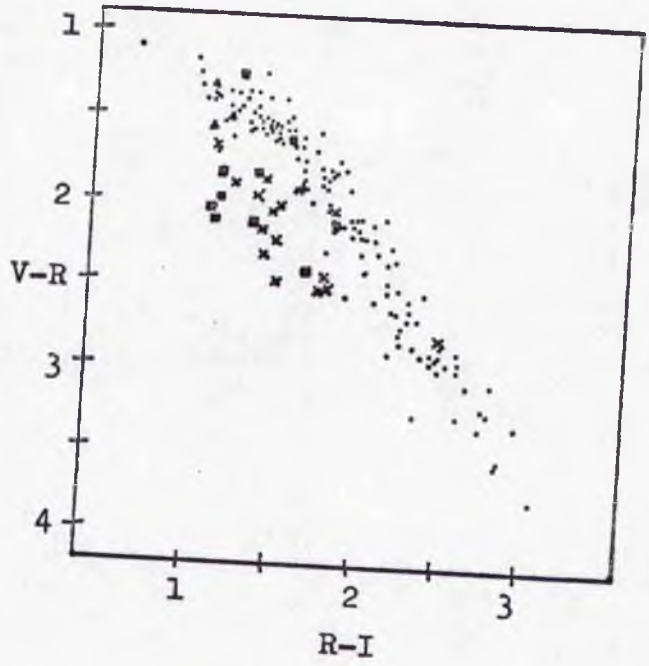

Colour - colour diagram for visual maxima (Barnes,1973).

(IV) Barnes (1973)

Barnes has published a collection of V R I photometry of Miras, mainly concentrated around phase 0.0. He has plotted the relationships between colour and period, and also the (V- R, R - I) diagram (Figs. 11 and 12). These diagrams show considerable scatter, although there is a clear separation between the typical characteristics of the Me, Se and Ce stars. Comparisons will be made between Barnes' photometry and the present results in a subsequent section.

Fig.13. Model of a Red Giant Envelope (Keeley,1970a)

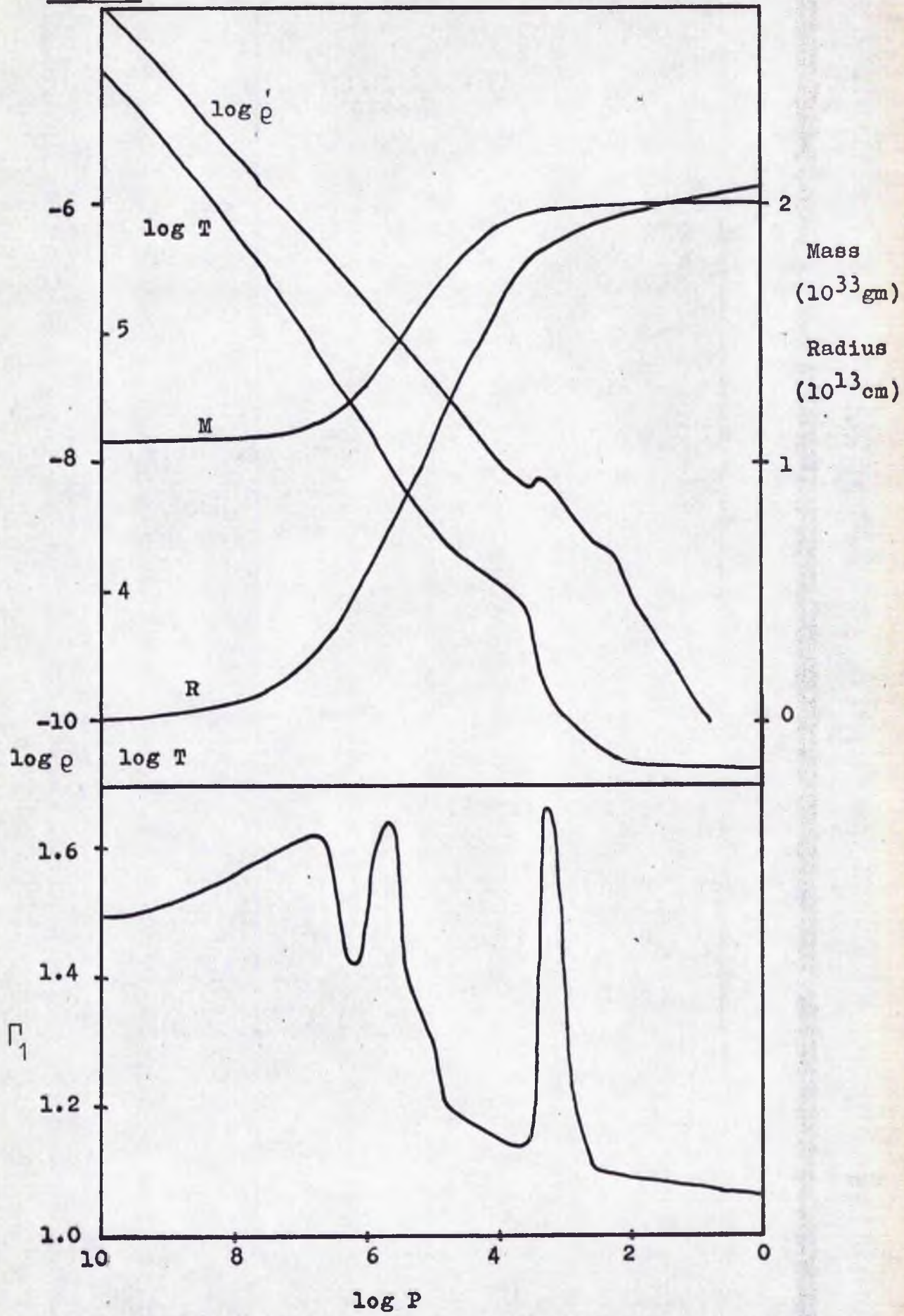

COMPARISON OF PULSATION THEORY WITH OBSERVATIONS

Theoretical models of Miras have been described in two papers by Keeley (1970a,b). The first paper concerns the construction of static models of extreme red giants in the mass range 1.0 to 1.3 Mo, and compares their positions in the H - R diagram with the observations of Pettit and Nicholson and also with data obtained by combining mean absolute magnitudes of the variables grouped by period and obtained from kinematic studies by Osvalds and Risley (1961) with bolometric corrections computed by Smak (1966). The second paper describes the results of perturbing the models and following the pulsations by using non-linear pulsation theory, incorporating a modified theory of convective transport. The latter is a "non-local" treatment which allows for the possible overshoot of convective cells beyond the equilibrium condition.

Fig. 13 is adapted from Keeley's first paper, and shows the behaviour of the physical parameters as a function of pressure, which Keeley uses as a convenient depth measurement. The behaviour of Γ_1 is very instructive and indicates the properties discussed earlier, showing a depression due to radiation pressure near the centre of the star, and also two sizeable minima due to the (He II $\longrightarrow$ He III) and the (He I $\longrightarrow$ He II) + (H I $\longrightarrow$ H II) zones. In fact, the latter contains about ten per cent of the total mass. One interesting feature is the region of low Γ_1 reaching out to the surface. This is due to the dissociation of the H_2 molecule, which means that the atmosphere only consists of neutral H atoms in the small

Fig.14. Red Giant Models and the H-R Diagram

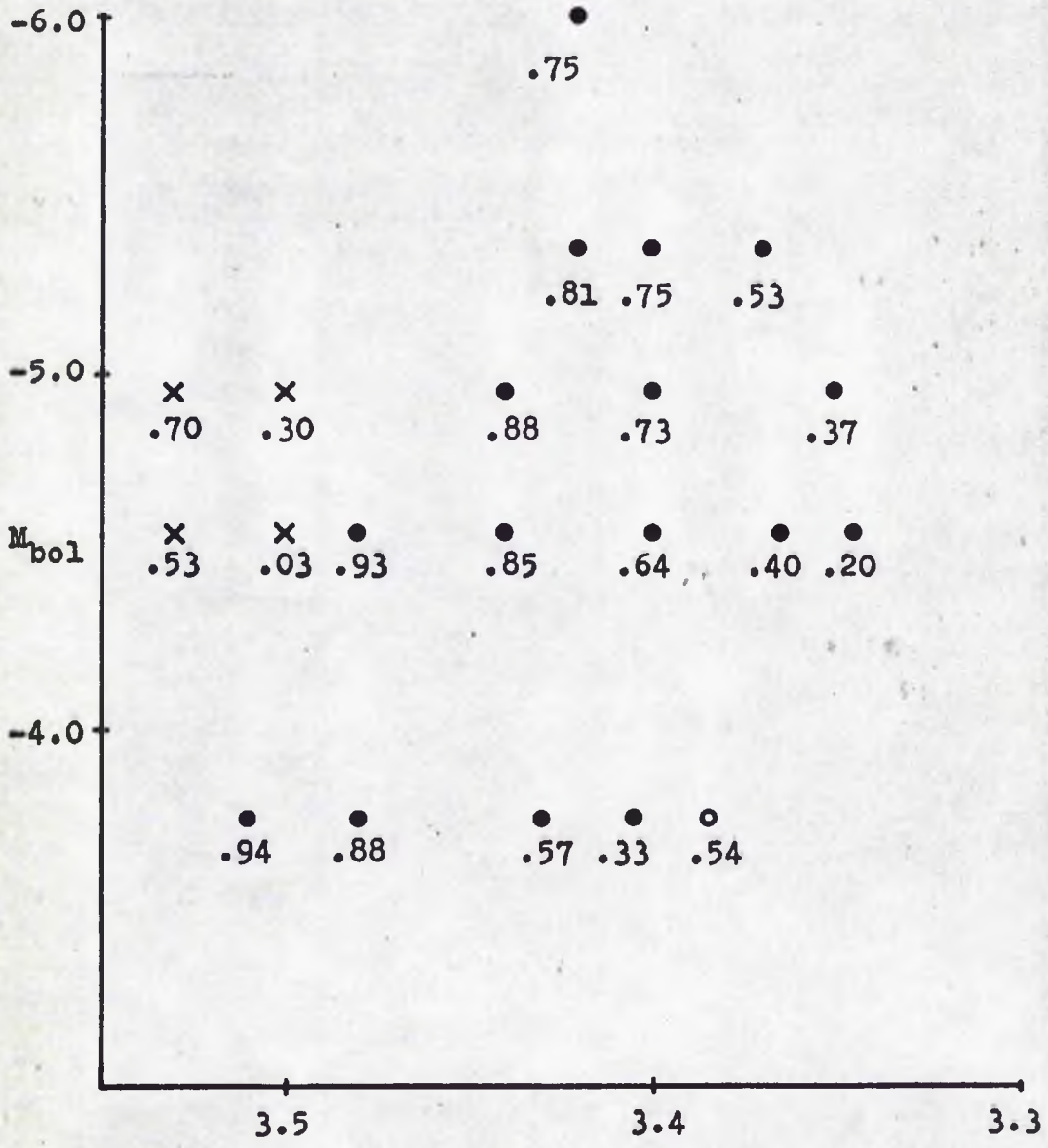

● $1.3M_0$

o $1M_0$

× $1.3M_0$ with low He and metal abundances

Numbers are the core mass fractions.

Fig.15. Comparison of Models with Observational Data

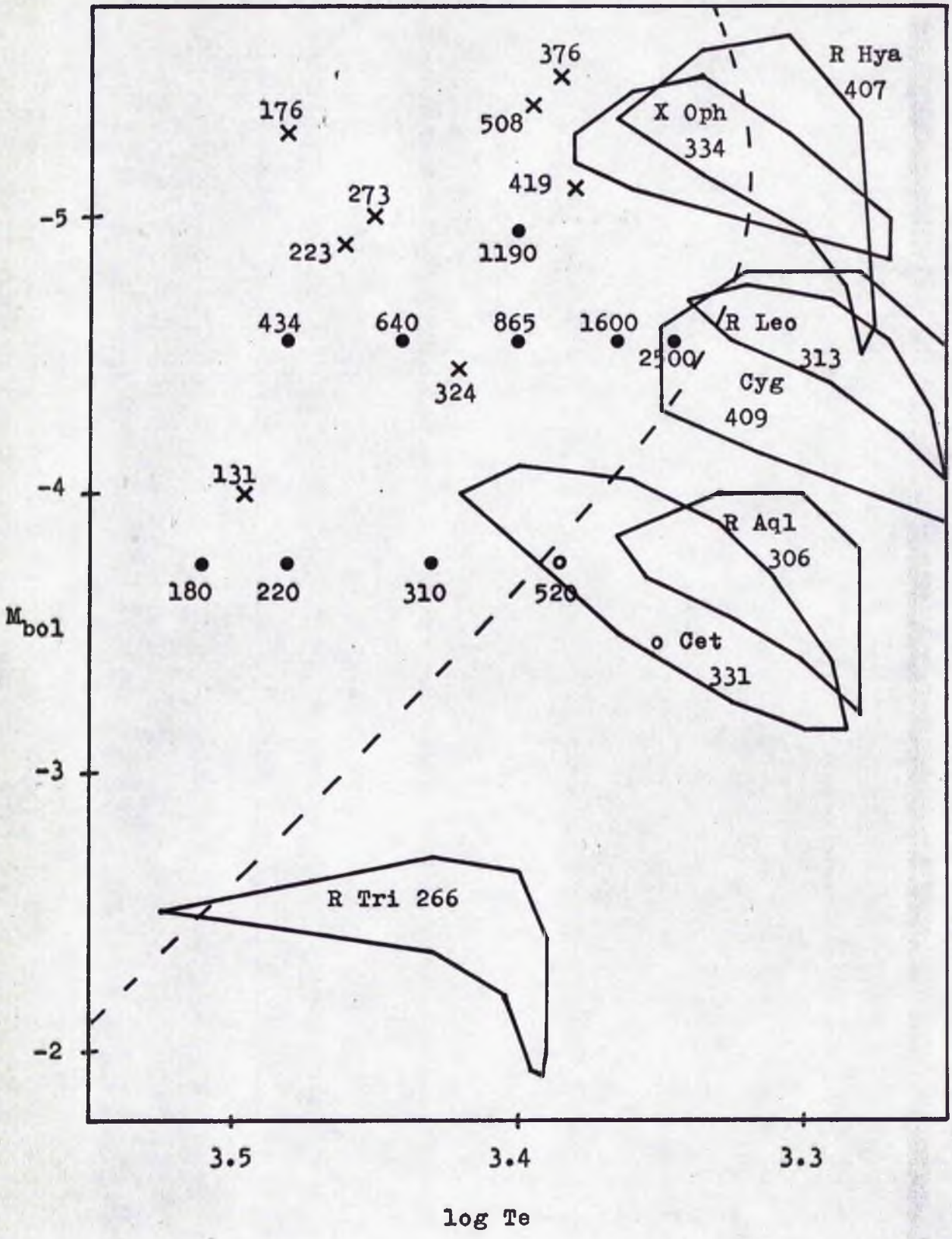

M_{bol}

— — Hayashi boundary for $1.3M_o$

× Statistical results of Osvalds and Risley

Loops are those observed by Pettit and Nicholson

region indicated by the sharp maximum in Γ_1. In addition it can be seen that Γ_1 does not reach very low values in the Helium ionisation zone, and assuming that Γ_3 behaves similarly, one can expect that, for Miras, this zone is not a vital contributor to the driving of the pulsations. This is a large but not unexpected difference from the case of the Cepheids. Finally, it must be noted that convection transports most of the energy through the envelope.

Keeley constructed the various stellar models by choosing likely combinations of mass, luminosity and effective temperature, and then carrying out the computations by working inward from the surface towards the region near log P = 10. The mass of the envelope having been determined, the mass of the core could be calculated although no attempt was made to continue the computations into the core. Fig. 14 is a copy of Keeley's diagram showing where his models sit in the H - R diagram. Recalling that the computed quantity is the core mass, the input parameters being luminosity, total mass and effective temperature, this figure should predict realistic values of core mass in the part of the diagram where stars are actually observed. The Hayashi boundary, which is the locus to the right of which stars of a given mass cannot exist, corresponds roughly to the locus of models with zero core mass. By taking Keeley's results one can add to his diagram a rough indication of the position of the Hayashi boundary, and this has been done in Fig. 15, which also shows the fundamental pulsation periods of the models. Keeley compares his results with the measurements made by Pettit and Nicholson, and also statistical values of luminosity and temperature obtained for various variables grouped

Fig.16. Kinetic Energy Production and Dissipation, and Radius Amplitude (Keeley,1970b).

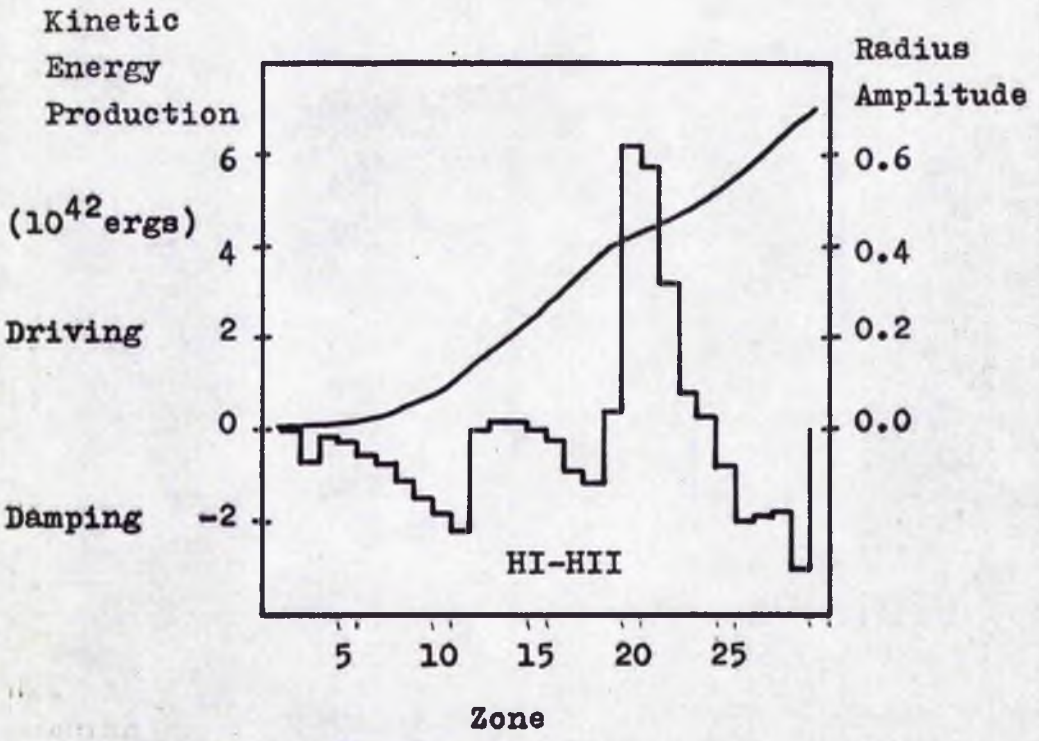

by period, deduced by combining work by Osvalds and Risley and by Smak. It is noticeable that, in particular, the results of Pettit and Nicholson lie to the right of the Hayashi boundary, which should be impossible. Keeley is inclined to attribute this to inaccuracies in his models, particularly the treatment of convection and the low-temperature opacities, but a considerable part of the discrepancy is due to the low temperatures given by Pettit and Nicholson's calibration. Mendoza's results imply values of log Te about .05 higher, which are also in better agreement with the Osvalds and Risley/Smak figures.

Fig. 16 summarizes the results obtained by Keeley's non-linear calculations, produced when a perturbation was applied to one of his static models. Strong driving occurs in the H I $\rightarrow$ H II ionisation zone, but not in the $H_2 \rightarrow 2H$ region which is very close to the surface and does not contain much mass. In fact, in this region there is strong damping due to the motion becoming a shock wave with consequent dissipation of energy.

Keeley also investigated the consequences of modifying the treatment of convection. Initially he used the normal mixing length theory, in which the motion of a convective cell depends only on the state of its immediate surroundings. He then repeated the calculations using a non-local treatment which spreads this dependence over a larger height in the atmosphere, and so can be seen as having a smoothing effect. A consequence of this is the introduction of the possibility of "overshoot" at the boundaries of the convective region. This provides an alternative means of energy transport in a nominally radiative zone, and this can reduce the driving by

this zone. Keeley suggests that this effect could explain why there is a red edge to the Cepheid instability strip. Perhaps it has become necessary to think of the region of the H - R diagram between the Cepheids and the red variables as being a "stability" strip, possibly caused by convective overshoot.

Keeley's models, particularly the hotter ones, have their strong driving region relatively near the surface, and this tends to favour overtone pulsation with the node lying near the middle of the H ionisation zone. The fundamental periods of the models are, in general, much longer than the observed periods, and this leads to the possibility that many Miras may be overtone pulsators.

An interesting effect found by Keeley concerned the comparison of the radii of the static models with the mean radii of the dynamic equivalents. He found that a pulsating model tended to have a mean radius about twelve per cent less than the static model. This emphasises a problem concerning observational determinations of Q, namely one does not know for certain the correct value of the mean density to be used in the calculation. Of course, the time average of the luminosity must be the same in the pulsating and the static models. This luminosity is that of the non-varying stellar core, and if the time average in the pulsating case did not have this value, it would imply that the envelope was secularly storing or losing energy.

PART 2

THE PRESENT WORK

General Introduction

U B V photometry produces rather ambiguous results when applied to Mira variables, in particular those of type Me. Strong TiO blanketing in B and V causes B - V to become independent of temperature, and the lack of such blanketing in U plus the presence of emission lines dominates U - B (Smak, 1966). For interpretable photometry of Miras, therefore, one must make use of the red and near infrared regions of the spectrum, where blanketing is weaker and emission lines are unimportant. Pursuing this line of reasoning, measurements have been made in Johnsons RI system (Mendosa UBVRI, 1967, Barnes VRI 1973) and also with narrow bands (Eggen, 1967, Lockwood and Wing, 1971).

It was decided to initiate a programme of photometry of Miras using UBVRI combined with five narrow bands selected to measure molecular features in the red and near infrared, and the first necessary step was the construction of a ten colour two photomultiplier photometer. Automatic filter and tube selection, signal digitization and teletype output were considered desirable for such a machine.

The project is discussed in three main sections, firstly the mechanical construction of the photometer, secondly the photometry of Mira variables, and finally the interpretation and discussion of the results.

Fig.17. Block Diagram of Photometer Measuring System

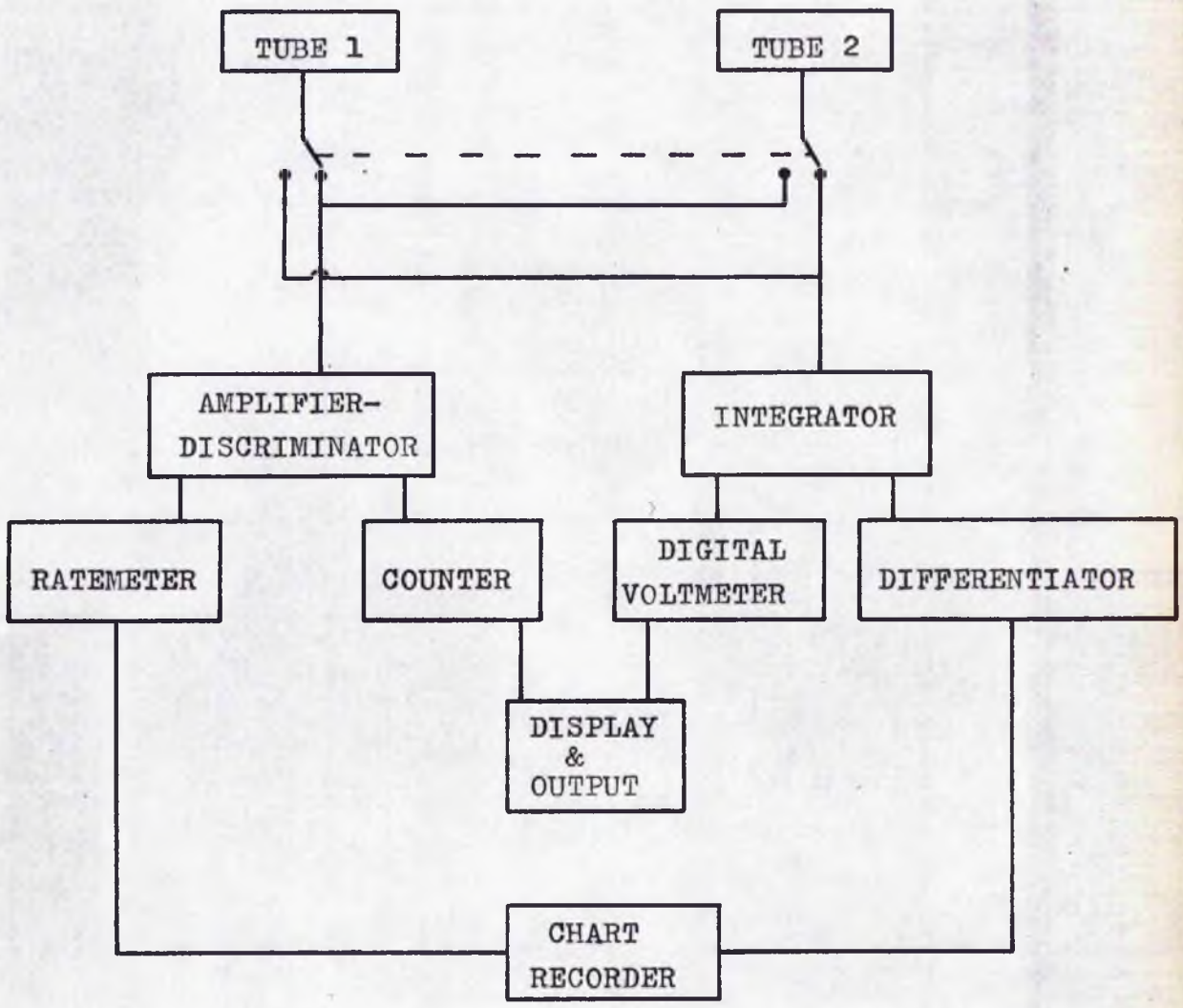

When Tube 1 is connected to the pulse counter, Tube 2 is feeding the integrator, and vice-versa. Only the signal from one of the tubes is processed at any instant. The control electronics ensures that the required tube is connected to the relevant measuring circuitry.

The Equipment

Three people were involved in the design of the photometer. Dr. I. G. van Breda, as well as having overall supervision of the project, was primarily concerned with the electronic system and provided the design for the logic units. Mr. D. M. Carr designed the analogue circuitry which comprised the integrator, digital voltmeter, differentiator and ratemeter, the latter being required to convert the signals generated by the system into a form suitable for chart recorder monitoring, (Fig. 17). The author was primarily involved with the mechanical design, which is therefore the only section considered here at length.

(I) Mechanical Design Requirements

1) The photometer was specifically intended for use on the 100 cm (40 inch) telescope of the Royal Observatory, Cape Town, operating at the f/20 cassegrain focus. During the progress of this project the South African Astronomical Observatory was formed, and the 100 cm telescope was removed to Sutherland and converted to f/16. It was decided to require the photometer to be operational at ratios as low as f/10, if necessary with the assistance of special fabry optics.

2) A separate acquisition box should be used for the location of objects, the actual photometer head having only a system for viewing the apertures.

3) The photometer should be compatible with the proposed standard interface plate (van Breda and Hill, 1972).

4) The two photomultipliers should be an EMI 6256 (S-13)

and an ITT FW-118 (S-1).

5) Filter selection for both phototubes should be achieved by a single stepping motor.

(II) Initial Problems

The use of filters operating in the one-micron region implied that a photomultiplier with an S-1 response was necessary. The high dark current associated with S-1 tubes has been a problem for a long time, especially when combined with the intrinsically low quantum efficiency of the S-1. ITT have managed to construct a usable S-1 tube (the FW-118) by eliminating all non-thermionic components of the dark current, combined with electrostatic focussing giving photocathodes of very small effective area. The dark current of such a tube can be reduced to arbitrarily low levels given a sufficiently low operating temperature.

Small photocathodes, however, produce their own problems. Firstly there is the difficulty of concentrating the light beam onto the sensitive area, and secondly, in Astronomy, one has magnified sensitivity to relative movement of the optical parts. It was therefore decided to use an FW -118 with the relatively large cathode diameter of 0.35 inch, and this implied the necessity of considerable cooling. It was decided that dry ice was the most suitable coolant available, and at that time the conventional approach was to use a slurry of dry ice and acetone or isopropyl alcohol, since dry ice does not make good thermal contact with solids. To minimise weight and surface area it was decided to construct a dry ice coldbox

Fig.18. First Photometer Design

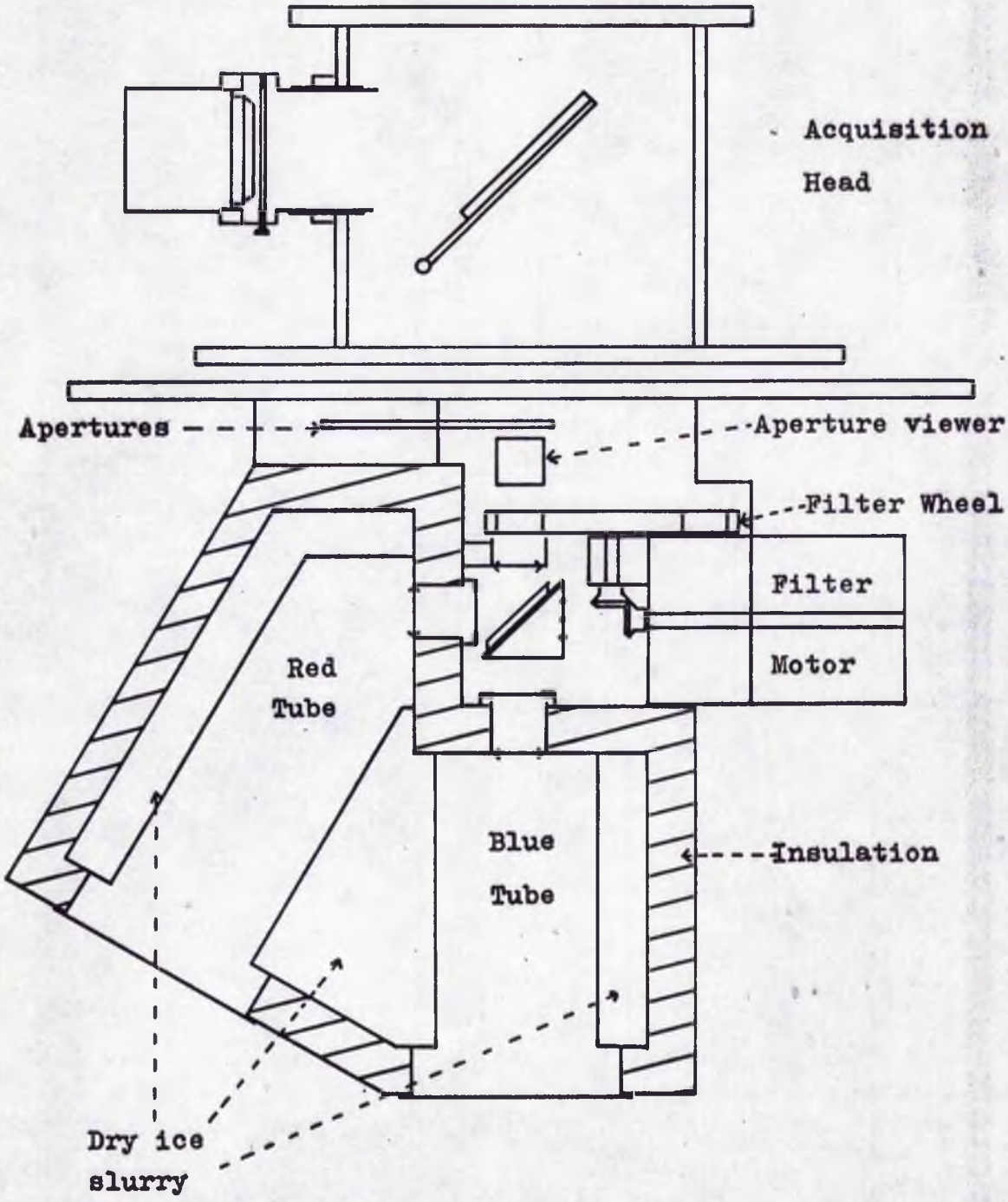

containing both photomultipliers. The blue tube would lie on the telescope axis, the red tube inclined at 30° to it. The red tube would be fitted with a reflecting hemisphere (Oke and Schild, 1968) to enhance quantum efficiency. The coldbox would be integral with the remainder of the photometer head (Fig. 18). Construction of this photometer was begun and continued for some time until it was decided to abandon the design. This decision was taken for a number of reasons.

(a) Internal Factors

1) The mechanical design was proving difficult to achieve accurately, it being based on the concept of relatively thin duralumin walls supported by a strong framework.

2) There had to be no risk of the liquid from the cooling slurry leaking into the photomultiplier chambers. Acetone and Isopropyl alcohol have a perishing effect on most likely gasketing substances, besides which, some parts of the structure were unsuitable for the gasket approach. An attempt was made to solve the problem by welding the aluminium, but the joints so formed would not remain water-tight after cooling with dry ice. This was the principal problem.

3) The configuration of the system required that the filter wheel be driven via a coupling mechanism. Bevel gears were chosen but it was found that this system generated more backlash than was desirable.

(b) External Factors

During the design period of the photometer, Products for Research Inc. began producing thermoelectrically cooled

Fig.19. Final Photometer Design

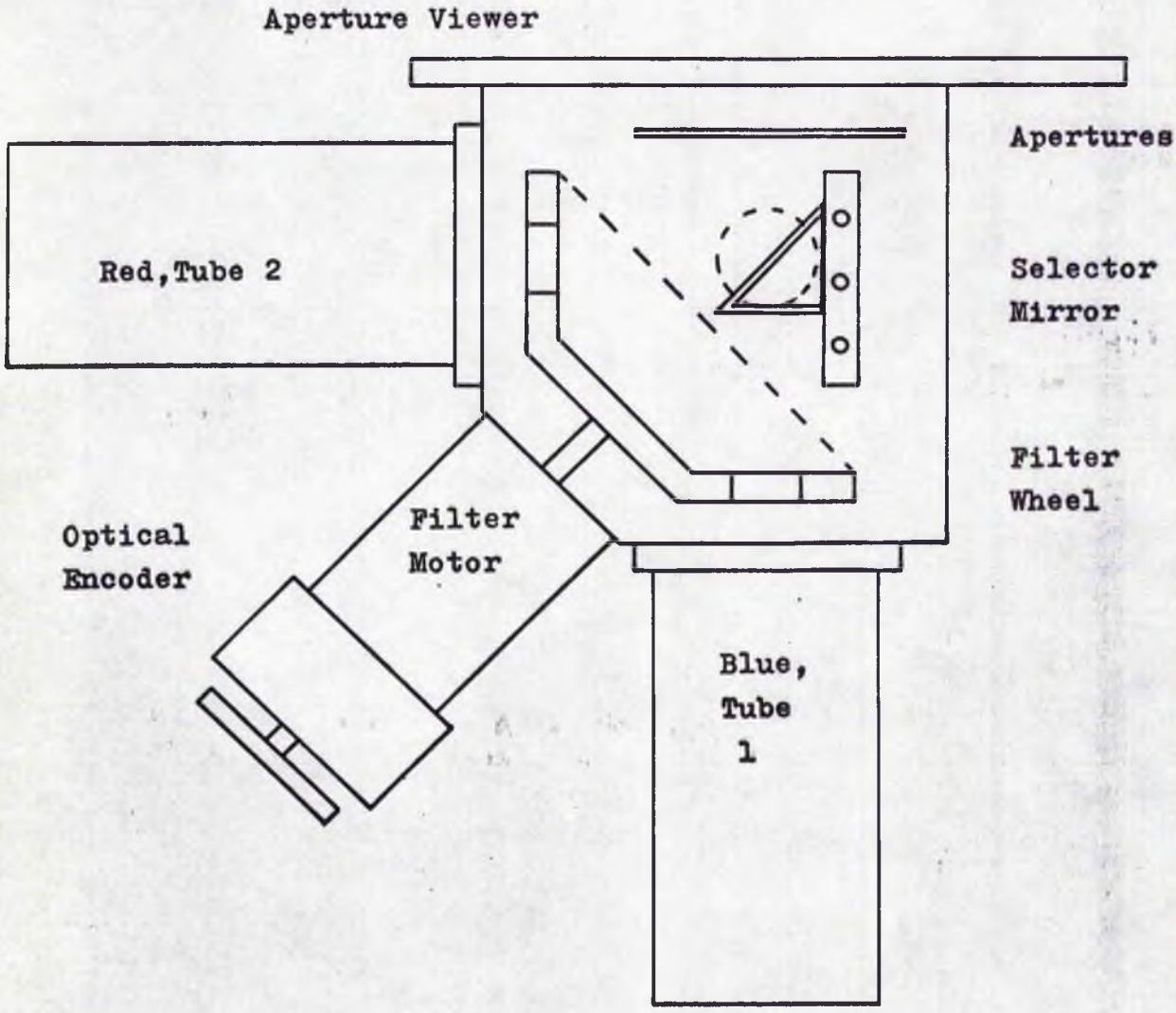

housings on a commercial basis. The Royal Greenwich Observatory produced the "Peoples" photometers which were designed to enable the attachment of coldboxes, and a "Peoples" photometer plus two Products for Research housings were acquired by the University Observatory, St. Andrews, on the recommendation of Dr P.W. Hill. These housings each had a fan drawing a constant stream of air through them, which acted as the receiving reservoir of the heat pump. The working temperature of the phototube was controlled by a sensor which switched the cooling current on and off as required. Temperatures down to $-20^{\circ}C$ could be selected.

These coolers were unsuitable for our purpose as the controlling mechanism proscribed pulse counting techniques and also the degree of cooling obtained was insufficient. Subsequently, Products for Research began producing housings suitable for pulse counting, and also developed housings which used piped water as a receiving reservoir. These housings were operational down to $-30^{\circ}C$, which is satisfactory provided one uses an ITT FW-118 with 0.1 inch diameter effective cathode.

(III) Final Photometer Design (Fig. 19)

A new photometer was designed to be used in conjunction with two water cooled housings, each fitted with a dark slide and cradles for increased rigidity. The use of cradles necessitated the construction of new window heaters. However, these are arranged to be identical to the originals with respect to physical contact and heat dissipation. The coldbox windows themselves are constructed of Perspex and have built-in

Fig.20. Fabry Windows

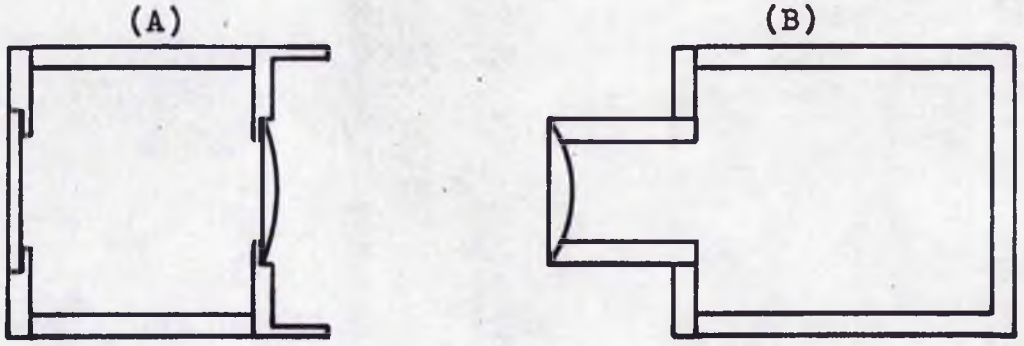

Window for tube 1. Perspex body with quartz lens and window.

Window for tube 2. Perspex body with glass lens.

Fig.21. Modified Fabry Window

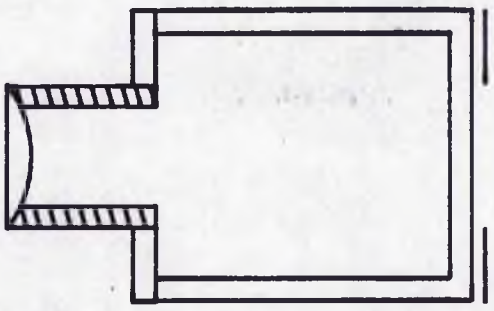

A perspex body, but with an aluminium lens support and a metal conducting annulus in contact with the front window.

fabry lenses (Fig. 20), the one for the blue tube having all-quartz optics. These were built at St. Andrews and flushed with Nitrogen to inhibit internal dewing. In design they follow essentially the style used by Products for Research themselves. The housings are positioned perpendicular to one another, one of them (tube 1) lying along the telescope axis. The light beam is deflected to tube 2 as required by a mirror riding on a threaded rod and driven by a D.C. motor along a path perpendicular to the axes of the two tubes. Hence the mirror travels parallel to its own surface, eliminating doubts about the reproducibility of the direction of the reflected beam. The mirror assembly is supported on the driving rod via a spring loaded captive nut which enables the assembly to be driven against a mechanical stop before the motor is switched off. This ensures that the same part of the mirror surface is always used. The mirror can be adjusted by means of three supporting screws enabling the light to be directed accurately at the cathode of the FW-118. The filter wheel is a right-angled truncated cone, rotation being about the axis of the cone. This system enables the filters for both photo-multipliers to be driven directly by the shaft of a single 200 steps per revolution stepping motor, and allows any number of filters up to the maximum of ten to be combined with either phototube.

Two filter wheels are provided, one accepting one inch diameter circular filters, the other, five one inch circular and five one inch square filters. The filters are held in place by springs and cover plates, and thicknesses up to approximately 8 mm are accepted readily. Thicker filters, up to approximately

3 cm, can be fitted if suitable cover plates are used.

The changing of filter wheels is not a simple operation as it involves removing coldbox 1 and unscrewing the side of the photometer body which supports coldbox 1. It is possible to perform this operation with the photometer on the telescope, but it is not classifiable as a night time procedure.

The opposite end of the motor shaft to the filter wheel operates an optical encoder, consisting of a slotted disc rotating between sets of light-emitting diodes and photo-transistors. This enables the current position of the filter wheel to be read out.

The aperture disc has eight holes corresponding to diameters of 200, 44, 31, 22, 15, 11, 8 and 4 arcsec. on the 100 cm telescope. The apertures are viewed for star centring purposes through a retractable prism assembly with a pair of back to back achromats followed by an eyepiece. This setup allows freedom of choice concerning the overall length of the viewing system and also gives good images over the field of view required. The prism assembly occupies the same space when in use as the phototube selector mirror. The position of the former is therefore sensed by a microswitch which causes the latter to move out of the way when necessary.

The photometer is constructed of 3/8 and $\frac{1}{4}$ inch duralumin plates held together by stainless steel screws, all joints being rebated for light-tightness. The design is such that the photomultiplier selector mirror can be replaced by a beam splitter, enabling simultaneous two filter photometry. Simultaneous star-sky measurements are not possible. Manual

standby knobs are provided for the filter wheel and selector mirror.

The photometer head also has mounted on it an electronics box incorporating the integrator, various power supplies and an SSR amplifier-discriminator. In addition there are displays showing the filter and photomultiplier in use, and start and clear switches. An acquisition head was constructed for use with the photometer. This is basically an eight inch diameter cylinder, fitted with a pivoted mirror, large eyepiece, and a graticule with X and Y motions for centring.

(IV) Later Modifications

Observers at the South African Astronomical Observatory have found that a small image intensifier is extremely useful for the finding and centring of faint stars (Hawarden, 1976). Therefore, subsequent to its arrival in South Africa, the photometer was fitted with an image intensifier viewing system. Filters were incorporated in this system to enable estimates of the colours of the stars being viewed to be made. The detailed design for this modification was by Mr. B. Hucklesby.

Laboratory experiments showed that the water-cooled housings would reach -30°C when provided with a stream of tap water. However, it was required that in use the water should be driven around a closed circuit system by a water pump. Under these circumstances the water temperature was higher and the minimum operating temperature of the housings was generally about -25°C. An attempt to improve the situation by using an immersion cooler failed. This meant that the dark current, zero point and possibly the colour equation associated with the FW-118 were functions of

ambient temperature. In addition, at the Sutherland out-station of S. A. A. O., this meant that satisfactory narrow band measurements could be made in winter when the tube temperature was -26°C, but not in summer when it rose to -20°C, increasing the dark current correspondingly. It clearly became necessary to revert to dry ice cooling.

Products for Research had been marketing a dry ice coldbox operating on the slurry principle for some time, but this could only be used in certain orientations without the liquid spilling out. Subsequently they developed a housing for astronomical purposes which used granulated dry ice pressed against the side of the photomultiplier chamber by a spring loaded plunger. One of these housings was obtained and found satisfactory. Its normal operating temperature is -65°C.

(V) Photometer Operating Problems

The first measurements made with the photometer produced satisfactory (U - B), (B - V) and (R - I) colours, but poor V and R magnitudes and poor (V - R) colours. At this time both water-cooled housings were in use, being operated at full cooling, and tube 2 was the FW-118 with the 0.1 inch cathode. Analysis of the results led to the conclusion that the R zero points were correlated with telescope position, but with a large additional scatter, whereas the poor V magnitudes were attributable to dewing of the window of the relevant coldbox. The latter effect was confirmed by increasing the operating temperature of the blue tube to -10°C, whereupon the effect disappeared. It was assumed that this problem arose because

the conduction path between the front lens surface and the window heater was rather indirect as compared with that normal for the windows produced by Products for Research themselves.

Strutting the coldboxes did not remove the apparent flexure, and also further tests revealed that the V zero points differed by $0^{m}.03$ when observations were made east and west of the meridian. The latter problem would seem to have been cured by packing the supports of the fabry window to ensure that it is held more securely, however the original discrepancy could possibly have been due to sky inhomogeneities.

The R zero points remained intractable, but it was thought that the problem was due to the use of small cathodes. The rigidity of the system was improved as for the blue tube, the rigidity of the selector mirror was checked and finally the coldbox was replaced by the dry ice housing containing the FW-118 with 0.35 inch diameter photocathode. Nevertheless the difficulties remained and it was finally decided that dewing of the window must again be the problem, despite this window being identical with Products for Research types. Laboratory experiments confirmed the existence of very heavy dewing on the window of the dry ice housing, and this was only eliminated by increasing the heater power dissipation by 50% and introducing a metal annulus to act as a conduction path between the heater and the central part of the front surface of the window. In addition it was observed that ice crystals

formed on the interior surface of the fabry lens. This was due to the residual moisture in the nitrogen condensing selectively on the glass lens rather than the perspex body because of the greater conductivity of the former. The ice would not introduce a variable R zero point, but would reduce sensitivity, and so it was largely eliminated by constructing the lens support from aluminium which then attracted the bulk of the interior condensation (Fig. 21).

(VI) Use of the Photomultipliers

The photometer electronics is designed to allow the operator the choice of using pulse counting or charge integration methods. These two techniques can be said to arise from two alternative pictures of the operation of a photomultiplier.

The output from a photomultiplier can be seen as a D.C. signal consisting of two currents, the first being constant and generally termed the dark current, the second being directly proportional to the amount of light falling on the photocathode. The measuring circuitry is then essentially a sensitive current meter capable of measuring values typically in the 10^{-10} to 10^{-6} amp range. The traditional means of achieving this is by using a high gain D.C. amplifier followed by a chart recorder; the latter being necessary since the signal is in general noisy, and by having a trace the observer can determine the average level of the signal by eye. In addition, this arrangement provides a monitoring system for the observer, since he can tell from the nature of the trace whether the observing conditions are satisfactory.

The approach has to be modified if the signal is to be output in a machine-readable form. In the St. Andrews Photometer this is achieved by using an integrator, which accumulates the photomultiplier current on a capacitor for an accurately specified period of time. At the end of the integration time, the voltage on the capacitor is determined by a digital voltmeter and the result printed out and punched on paper tape. There is a disadvantage in this system, namely the lack of the continual monitoring present in the traditional method. This was overcome in the present case by following the integrator by a differentiator so that during the integration time the chart recorder can display a trace of the signal.

The other approach to the use of a photomultiplier starts by considering the incoming light beam as a stream of photons. On striking the photocathode, a statistically constant fraction of the photons each give rise to the emission of a single electron. Each electron is then multiplied by the tube so that each gives rise to a burst of, typically, 10^8 electrons at the output. By amplifying the size of the electron bursts and then feeding them to a high speed counter, one can count the number of photons detected by the system. If the number counted in some time interval t is N, then random fluctuations in the original photon beam will mean that the signal has a noise $\sqrt{N}$ associated with it. The signal to noise ratio will then be $\sqrt{N}$. This limit to the accuracy of the measurement as imposed by the photon statistics is also valid when the D.C. techniques are being used, but unlike the photon

counting case, D.C. measurements do not give a direct measure of $\sqrt{N}$. This is the first advantage of the photon counting approach.

Suppose one is obtaining n_s counts per second due to the light from a star. In addition one will have n_b counts per second due to the sky brightness, and n_d counts per second generated inside the detection equipment. With "integration" time t, one has to make two measurements.

"Star count" = $(n_s + n_b + n_d)t$

Sky count = $(n_b + n_d)t$,

the value of $n_s t$ being deduced by subtraction. However, the signal to noise ratio has become:-

$$S/N = \frac{n_s t}{\sqrt{(n_s + 2n_b + 2n_d)t}}$$

This result, which is also true for the D.C. measurements, shows explicitly how the precision of the measurement improves with $\sqrt{t}$. It also demonstrates the requirement that n_b and n_d be kept as small as possible. Obviously, under given conditions, n_b can only be improved by using the smallest-sized diaphragm which allows all the starlight through. n_d, on the other hand, arises within the equipment and so requires closer scrutiny.

n_d consists of four main components.

(i) Thermionic emission by the photocathode.

This is the spontaneous emission of electrons by the photocathode in the absence of light. Signals from this source are indistinguishable from those caused by a light source. They are minimized by cooling, and also by usingaphotomultiplier with a small cathode (see e.g. Kelly and Kilkenny, 1973).

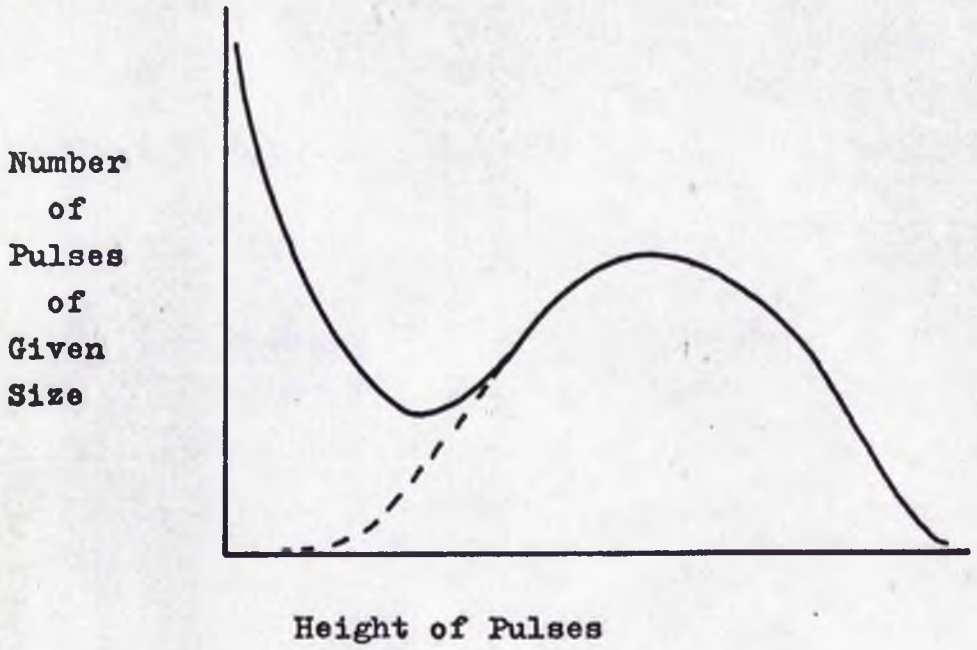

Fig.22. Typical Height Distribution of Pulses from a Photomultiplier.

The dotted line indicates the likely distribution of small pulses from the cathode alone.

(ii) Non-thermionic emission.

Cosmic rays can give rise to scintillation in the envelope of the photomultiplier, producing flashes of light which are seen by the photocathode. The same applies to flashes caused by the decay of radioactive elements present in the glass. These can be minimised to some extent by choice of the type of glass comprising the envelope.

(iii) Emission originating within the multiplier.

Typically, this may be thermionic emission occurring at the early stages of the multiplier. Such electrons are subject to less than the full multiplication experienced by electrons originating at the photocathode. As a result, at the output, these give rise to smaller electron bursts than those associated with the signal.

(iv) Electrical noise.

Leakage around the base of the photomultiplier, pickup in the signal leads, and noise in the associated circuitry give rise to spurious pulses not originating in the photomultiplier. With care these pulses can be kept very small, but not eliminated.

Fig. 22 is a diagram showing how the number of pulses of a given size varies with size in a typical situation. D.C. systems accept all these sources of noise uncritically, but photon counting systems are able to ignore the large number of small pulses, arising from cases (iii) and (iv) above, by using a discriminator. This ensures that only the pulses larger than a given size are counted, and so minimises n_d and improves the signal to noise ratio. This is the second

advantage of photon counting techniques.

As with the integration technique, chart recorder monitoring of measurements made using photon counting can only be done by the introduction of special circuitry, namely a ratemeter, which turns the rate at which counts are being detected into a D.C. signal.

The major disadvantage of the photon counting technique lies in the limited range of signal strengths it will accept. A photomultiplier has a linear response over a very wide range of signal strength. This useful range is limited at the lower end by photon statistics and at the upper end by internal heating as the stream of electrons in the multiplier becomes large. The D.C. methods can take full advantage of this range by simply altering the gain of the amplifier or by altering the size of the capacitor in an integrator. When photon counting there is no possibility of changing gain, and one soon finds that pulses of electrons are arriving too close together in time for the counting equipment to separate them.

The maximum rate at which the system will count is determined by the "dead time", τ. If two pulses arrive separated by a length of time less than τ, then only one pulse will be counted.

Suppose n pulses, randomly distributed in time, are arriving per second. Then the number of pulses lost per second will be

$$K = 2\tau \sum_{J=1}^{J=n} J$$

$$= \tau\, n(n-1)$$

Fig.23. Resistor Chain for EMI 6256.

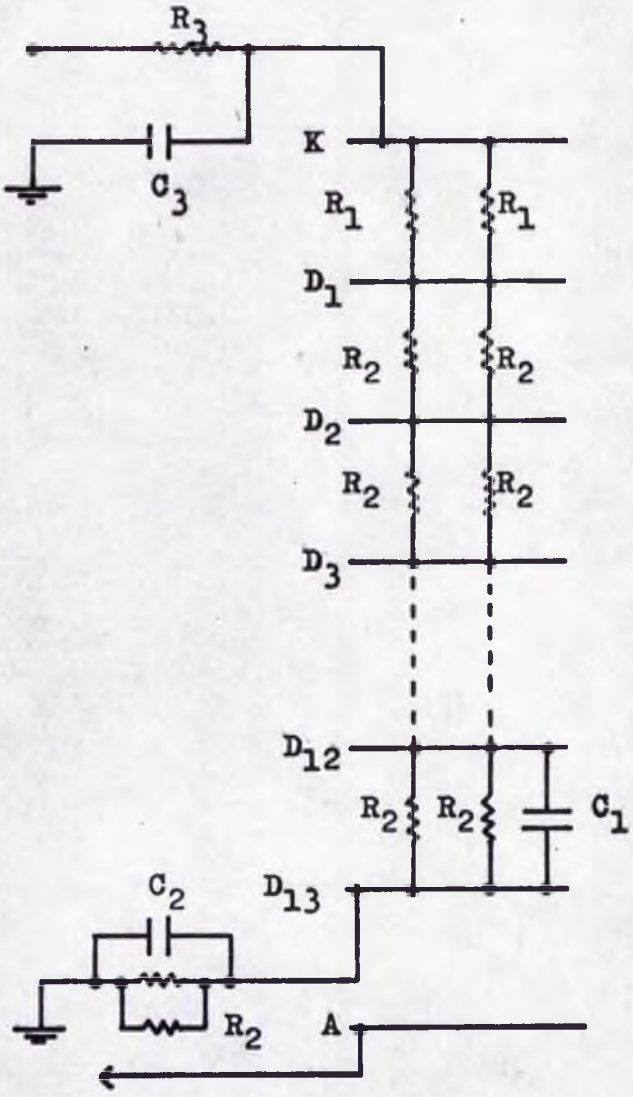

R_1 = 330 K

R_2 = 200 K

R_3 = 120 K

C_1 = 100 pF

C_2 = 1000 pF

C_3 = .001 F, 3 KV

Fig.24. Resistor Chain for FW 118.

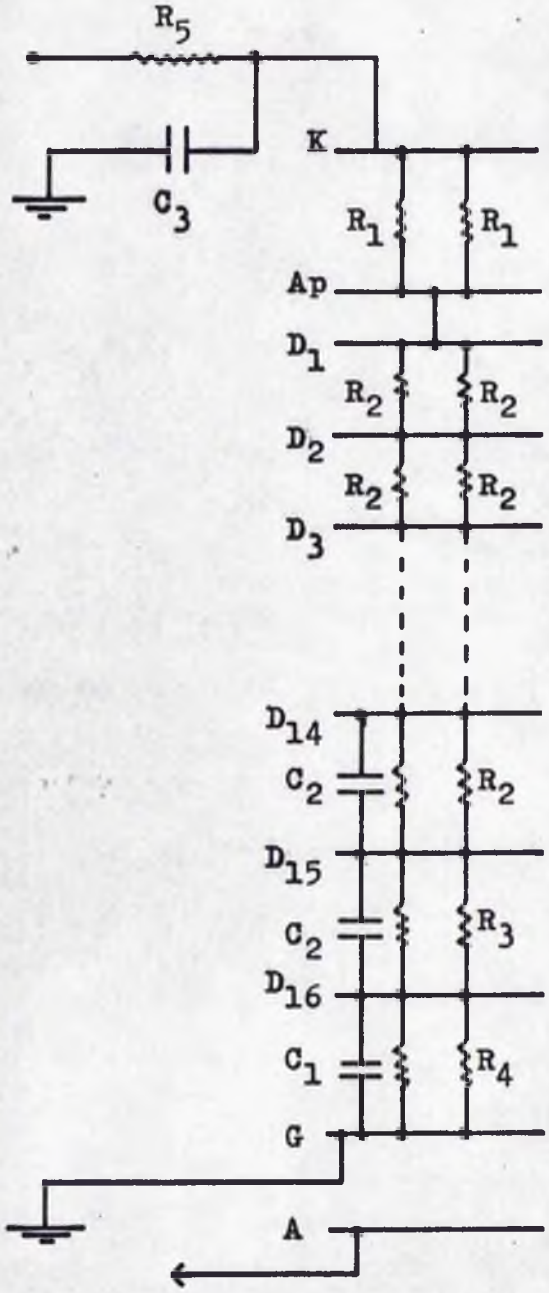

R_1 = 560 K
R_2 = 270 K
R_3 = 390 K
R_4 = 820 K
R_5 = 120 K
C_1 = 1000 pF
C_2 = 100 pF
C_3 = .001 F, 3 KV

Hence the percentage error introduced is $\tau(n-1).100$. This reveals that, due to the dead time effect, the photon counting method is inherently non-linear. In our case τ is about 7.5×10^{-8} sec., and so

$$\text{percentage loss} \approx 7.5 \times 10^{-6}\, n$$

One can, therefore, safely assume that the pulse counting results are linear for count rates less than 10^5 per second. Above that, a non-linear correction becomes necessary, and ultimately the system saturates.

The final disadvantages of photon counting methods are the sophisticated circuitry required and the extreme sensitivity of the system to pick-up. This has been mentioned in a previous section in connection with the unsuitability of coolers with their temperature controlled by an on-off switching system, and it reveals that in an instrument such as the St. Andrews Photometer, where both pulse counting and charge integration facilities are provided, it is the pulse counting requirement which is critical in determining the design.

Figs. 23 and 24 show the divider resistor chains used to distribute the applied E.H.T. voltage along the photomultipliers. These chains follow the design recommendations laid down by the manufacturers of the amplifier-discriminator used in the photon counting circuitry. The chains incorporate capacitors to prevent any voltage spikes in the E.H.T. generating spurious signals, and also have all the resistors in pairs as a precaution in case one of them should go open circuit.

Fig.25. Relationship between E.H.T. and Signal when Pulse Counting.

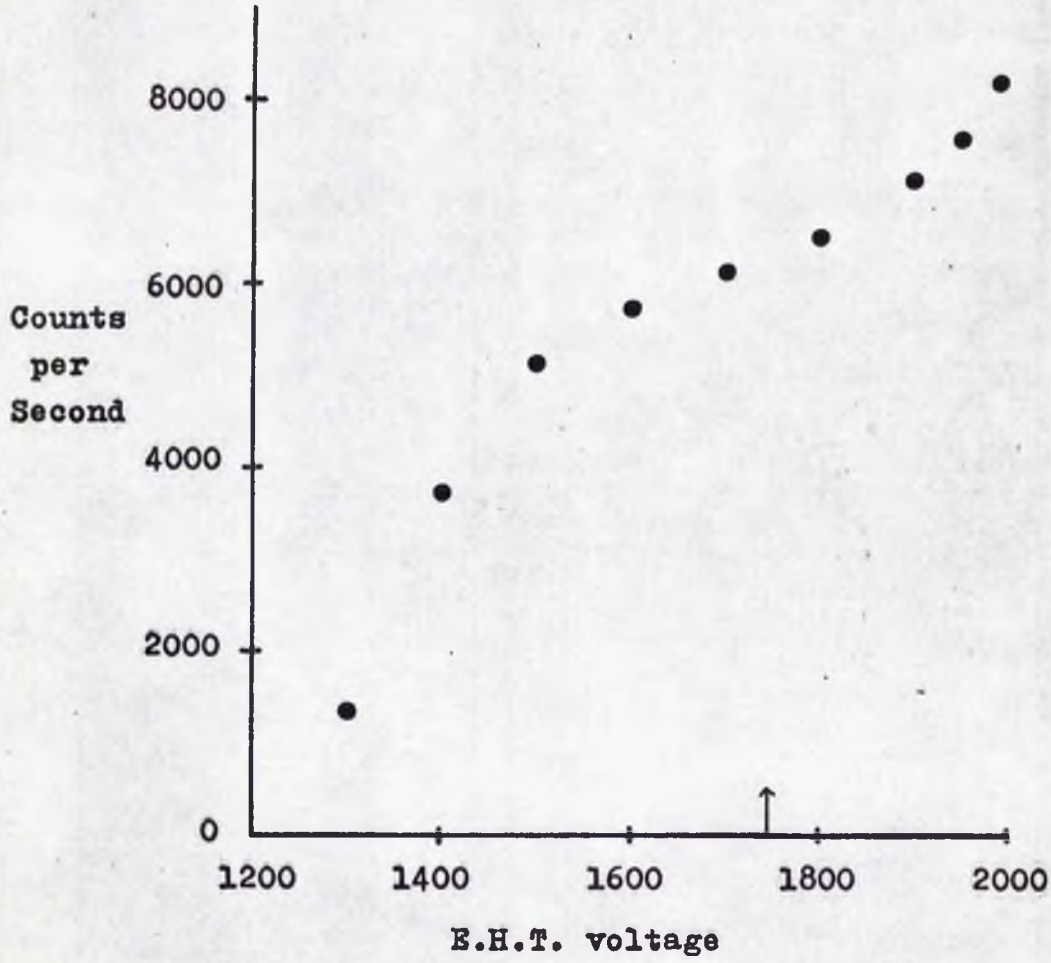

Under these circumstances, the overall gain of the photomultiplier depends on the value of the E.H.T. voltage applied. Reconsidering fig. 22, it is clear that altering the gain of the photomultiplier changes the size of any given pulse, and so is equivalent to changing the scale of the abscissa. Clearly, if one wishes to accept only those pulses belonging to a specific part of the pulse height distribution, one must specify both the discriminator setting and the value of the E.H.T. In practice, one sets the discriminator level such that the amplifier-discriminator operates satisfactorily, and then adjusts the E.H.T. to obtain the optimum result. Fig. 25 shows how the number of counts detected by the system varies with E.H.T. for the FW-118 with 0.35 inch diameter cathode, when the discriminator setting is held constant. The optimum operating voltage is indicated. This voltage was determined for all three photomultipliers once the equipment was finally set up at S. A. A. O., and the deduced operating voltages were:-

FW-118	(0.1 in. cathode)	1850 v
FW-118	(0.35 in. cathode)	1750 v
EMI 6256		1000 v.

The photomultipliers were always operated at these voltages irrespective of whether photon counting or charge integration techniques were being used.

An important property shown by fig. 25 is the relative insensitivity of pulse counting measurements to drift in the E.H.T. voltage. If the signal is S, then for pulse counting

$$\frac{\delta S}{S} \approx \frac{\delta V}{V}$$

that is, the fractional change in the measured signal is equal to the fractional voltage change. In the case of D.C. measurements, the signal is proportional to the gain of the multiplier, and typically

$$Gs \propto Vs$$

where Gs = gain of single stage of multiplier

Vs = voltage applied to that stage.

The overall gain of an m-stage multiplier is then

$$G = Gs^m \propto Vs^m$$

$$\therefore \quad \frac{\delta G}{G} = m \frac{\delta Gs}{Gs} \propto m \frac{\delta Vs}{Vs} = m \frac{\delta V}{V}$$

since $Vs \propto V$ (EMI Photomultiplier Catalogue, 1967). m is typically in the range 13 to 19, and so D.C. methods are much more sensitive to E.H.T. drift than pulse counting.

In the present investigation, the UBV measurements, obtained with the EMI 6256, were carried out using the integrator, whilst the R, I and narrow band measurements were made with the pulse counter. This distinction was made because the UBV signals were typically quite large, whereas the low quantum efficiency of the FW-118 gave rise to the small signals best handled by the pulse counter.

An instrument such as the St. Andrews Photometer gives rise to possibilities such as mixing pulse counter and integrator measurements; in other words, using the pulse counter as if it were just the most sensitive gain step of the integrator. However, there is a theoretical objection to this, since the

size of a pulse produced by an electron emitted from the photocathode depends on the velocity with which that electron reaches the first stage of the multiplier. This velocity depends primarily on the voltage difference through which the electron has been accelerated, but it obviously also depends slightly on the velocity with which the electron was emitted from the cathode. This latter velocity should depend, on average, on the wavelength of the photon which caused the emission of the electron. These circumstances lead one to expect longer wavelength photons to give rise to slightly smaller pulses than shorter wavelength photons. This effect should be negligible using pulse counting techniques, but should lead to D.C. methods being slightly more sensitive to light of shorter wavelength. Broad band filters may have a bandwidth, typically, of 1000 Å, and so when one is observing with such a filter, one may expect the effective wavelength of the observation to be shorter when one is using D.C. methods as opposed to pulse counting. The implication is that one would have to introduce a correction for this colour effect if it was desired to mix, say, observations in U obtained with both pulse counting and D.C. methods.

The size of the above effect has to be determined observationally, and during the present investigation some data were obtained accidentally. On 8/9 August 1973, the amplifier-discriminator failed in the middle of the night, and so the FW-118 observations had to be continued using the integrator. The above-mentioned colour effect would imply that the (R - I) measurements obtained during the first half of this night should

differ systematically from those obtained later. In fact, no such difference could be detected (the (R - I) zero point was constant), and so one deduces that for (R - I), at least, the effect is negligible. T. G. Hawarden subsequently did a deliberate test using UBV photometry with both the integrator and the pulse counter. He found a difference of $0^{m}.01$ in the zero point of the (B - V) scale, and this would seem to confirm that, in practice, one could mix integrator and pulse counter measurements.

Photometry of Mira Variables

(I) Photometric Aims

When the project was initiated in 1968, it was considered that information on the UBVRI photometry of Mira variables was lacking, although a significant amount of UBV photometry had been carried out (Smak, 1966), and Mendoza V (1967) had published some UBVRI. It was also thought that broad band photometry could usefully be supplemented by measurements of TiO blanketing using narrow band filters. Obviously, it would have been desirable to follow the magnitude and colour variations of individual variables throughout their cycles, but in practice the long periods of the variables mean that the achievement of such an aim would demand, say, one observation of each star per week. This would not only require quite a large amount of telescope time, but, more problematically, a very unusual distribution of the time. The only alternative was to observe a sizeable number of Miras at various phases, obtaining typically six observations of each individual variable spread around its light curve.

(II) Photometric Characteristics of Miras

The complexity of the spectra of Miras means that the results of the broad band measurements are functions of three variables. These are effective temperature, blanketing (mainly molecular) and the strength of the emission lines. For stars of earlier spectral type, UBV photometry primarily depends on effective temperature, with (U - B) additionally being affected by the Balmer discontinuity. Blanketing, as reflecting gravity

and abundance effects, is a secondary phenomenon about which useful information can be gained because it is secondary. For Mira variables, in particular those of types M and S, UBV photometry gives no information about the gradient of the continuum. V is extremely sensitive to TiO, and B slightly less so, hence (B - V) is almost constant for M stars. B is also slightly affected by emission, and U encompasses many strong emission lines whilst being relatively free from TiO. Hence at certain phases of the light cycles of M type Miras one may obtain colours like (B - V) = +1.5; (U - B) = -0.2.

This means that UBV colours alone do not generate useful parameters for the largest group of Miras, namely those of type M. The S stars are in a basically similar situation, although the principal culprit is now ZrO rather than TiO. The Carbon stars are fundamentally different. They have more normal (B - V) behaviour, but U is often too faint to measure due to obliteration by SiC_2 and C_3.

R and I measurements of the M types are affected much less by molecular blanketing, and as Hα shows only weakly in emission, they are not emission sensitive. Hence (R - I) should be a reflection of effective temperature. One therefore concludes that it should be possible to obtain effective temperatures, TiO strengths and emission strengths for M type Miras from UBVRI photometry. The project was conceived with a view to taking a first step towards this by investigating the characteristics of a variety of Miras, and how these characteristics change with time. The importance of the narrow band indices is to confirm and clarify the information obtained

from the broad bands. For example, does the changing TiO strength indicated by the narrow bands correlate with the temperature changes shown by the broad bands?

(III) Choice of Filters

The UBV filters were chosen so as to conform with those listed by Cousins (1973), and so are:

U : 1 mm Schott UG2 + 1.3 mm glass

B : 1 mm BG12 + 4 mm GG 385

V : 2 mm CMAG 302

The R filter was supplied by Sir Howard Grubb Parsons Ltd., and the I filter is 3 mm Schott RGN 9. The latter filter has a long wavelength cut-off, making the effective wavelength of I insensitive to the tail of the S - 1 response curve. This property enables replacement of the S - 1 photomultiplier with minimal changes in the photometric system. It was considered that this property cancelled the disadvantages of having a shorter effective I wavelength than that in Johnson's system.

The narrow band system was based initially on the work of Eggen (1967), which made use of filters at 6200 Å, 6500 Å and 10,200 Å, (62 - 65) measuring TiO strength and (65 - 102) being a colour index. The work of Wing (1966), however, revealed that the best continuum point lies at 10,400 Å, since VO bands appear longward of 10,450 Å and TiO bands between 9900 Å and 10,300 Å. I (104) is centred on 10,400 Å and is 30 Å wide. Unfortunately, for the purposes of this investigation, a band 30 Å wide would result in too bright a limiting magnitude. Inspection of a trace of the spectrum of the Taurus infrared

The Photometric Bands

Band	$\lambda(\mu)$	Features
U	0.36	Emission
B	0.45	Emission + TiO
V	0.55	TiO
R	0.68	TiO
I	0.85	TiO
63	0.63	TiO
65	0.65	Continuum + TiO
81	0.81	CN
103	1.03	Continuum
105	1.05	VO

Fig.26. Sensitivity Curves of the R, I and Narrow Bands.

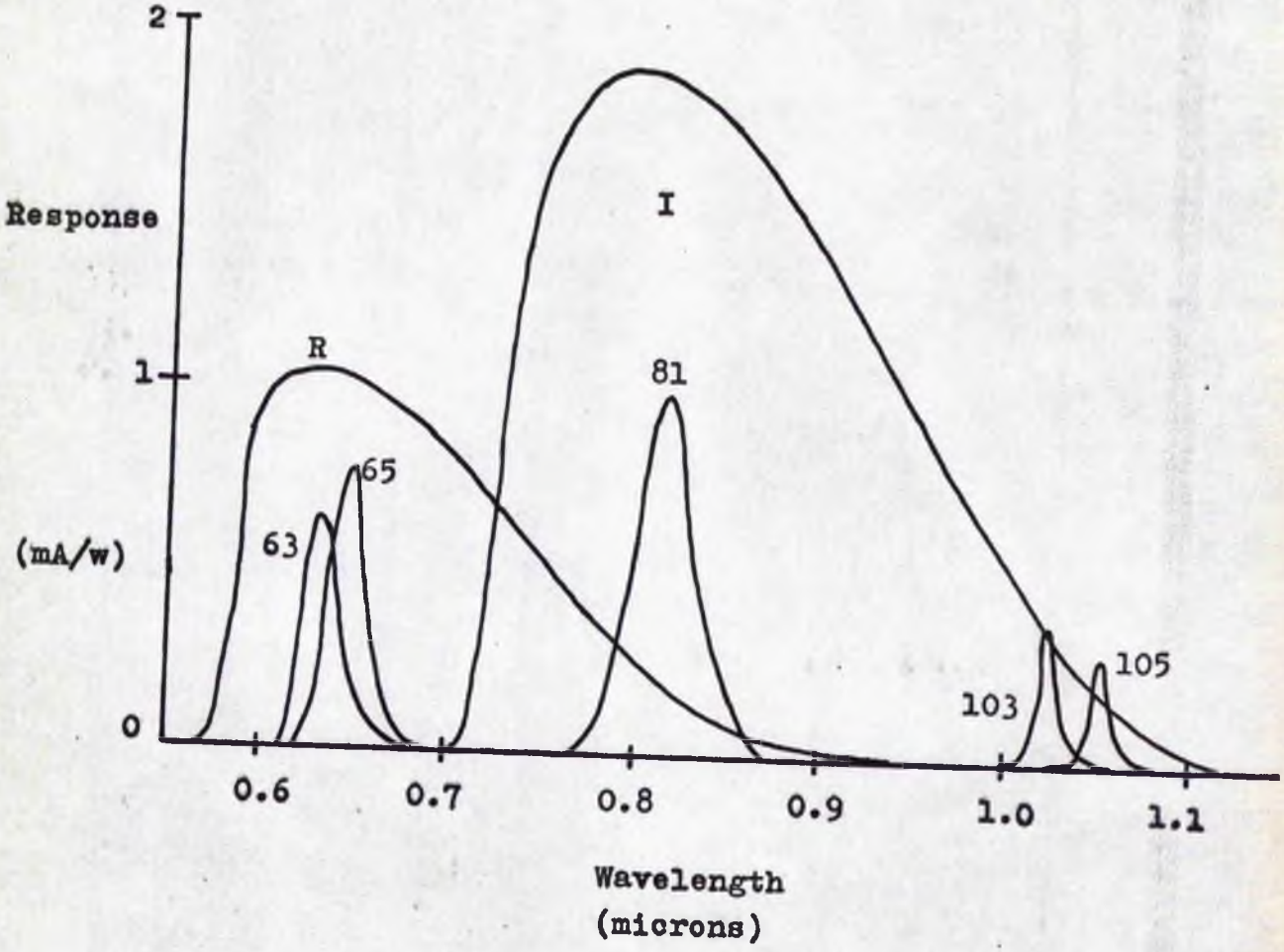

Fig.27. (R-I) Transformations.

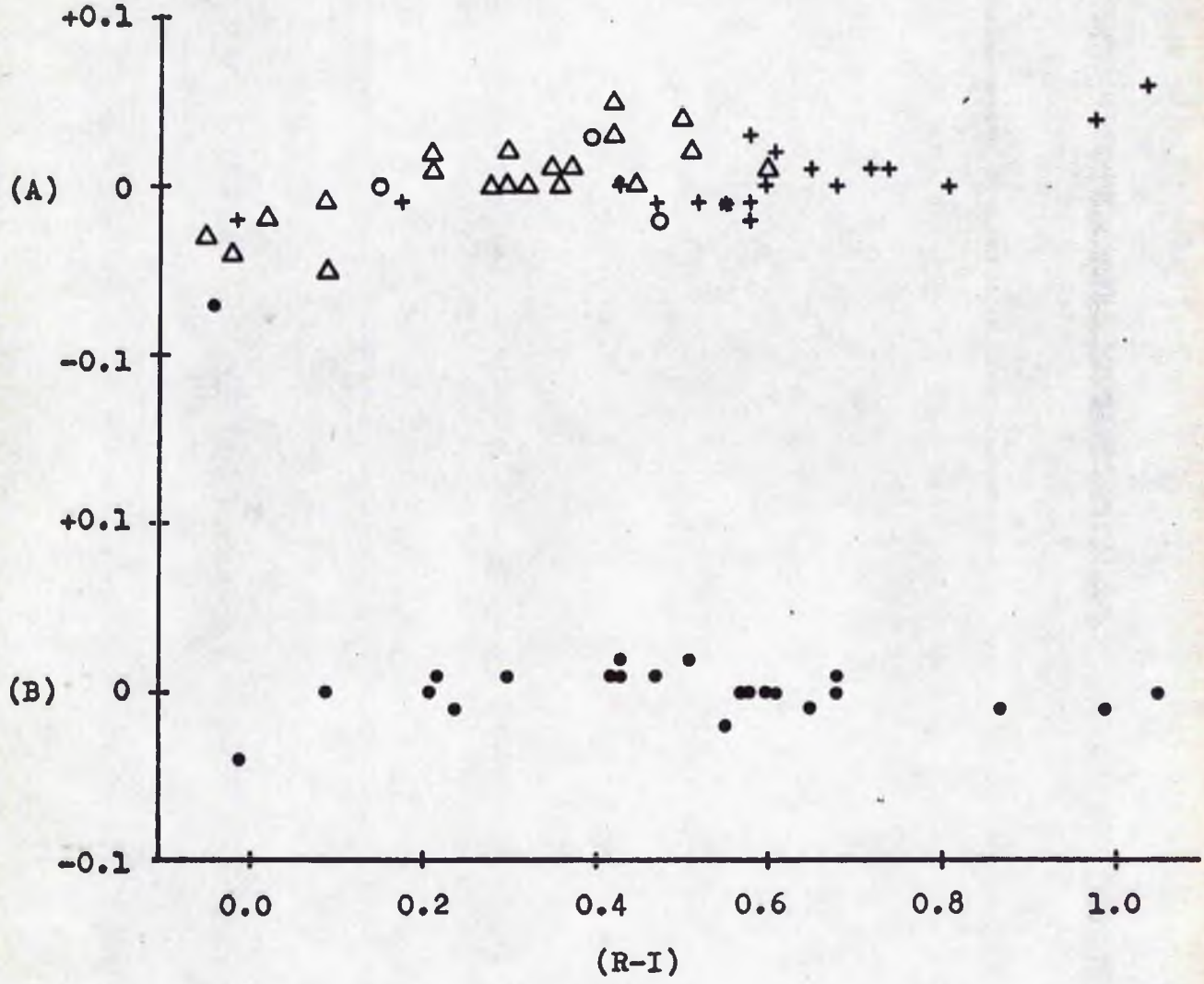

(A) Differences are present work minus Johnson et al. (1966).

+	Class III	*	Two class III
o	Class IV	●	Unknown
△	Class V		
*	Pec		

(B) Differences S-20 minus S-1.

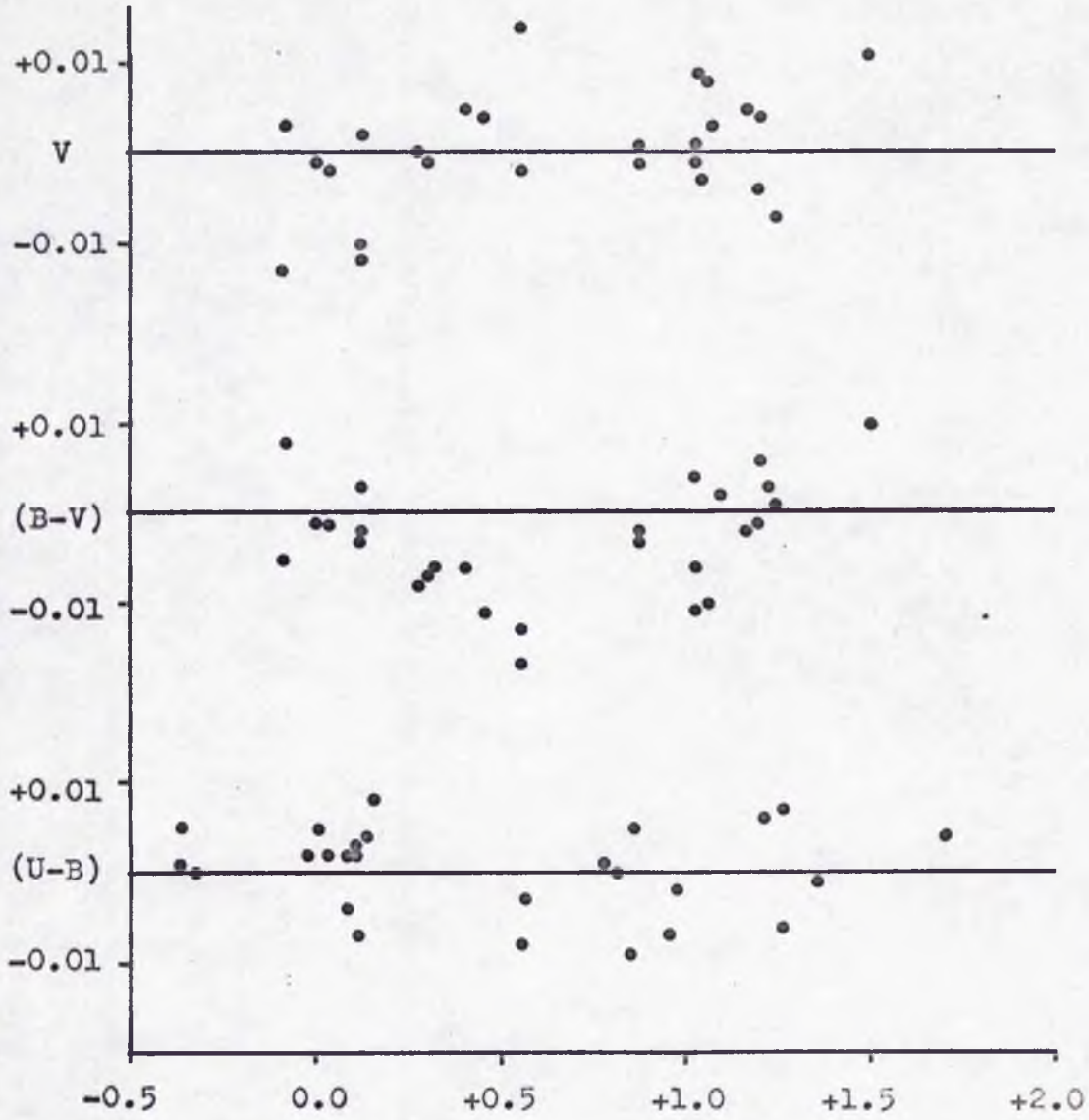

Fig. 27a Residuals in V, (B-V), (U-B), plotted against (B-V), (B-V) and (U-B) respectively. The second order correction required for (B-V) has been ignored in the present work. The residuals are in the sense present work minus Cousins (1973), and each represents a single observation.

object (Wing, Spinrad and Kuhi, 1967) shows it to be fairly flat between 10,400 Å and 10,250 Å, although the shortward section of this region may be affected by the tail of the TiO band at 10,150 Å (Lockwood, 1973). It was decided, therefore, to adopt a bandwidth of 150 Å centred at 10,350 Å, whilst retaining filters comparable to Eggen's 62 and 65. In practice, the filters actually received differed slightly from these specifications.

In addition filters were obtained centred on 10,540 Å thereby measuring VO, and 8150 Å which is the site of a strong CN band in carbon stars. The properties of the various bands are summarized in the table, and the sensitivity curves of the R, I and narrow bands are shown in fig. 26.

(IV) Observational Procedures

(a) Choice of Comparison Stars

Each variable was allotted a nearby K-type comparison star, selected from the Photoelectric Catalogue to reduce the probability of choosing an undetected variable. The comparison stars were tied onto Johnson's VRI system using stars F5 < Sp < K5 (Johnson et al. 1966), a linear colour transformation being adopted. Strictly, this merely serves to define an instrumental VRI system with values of the colour indices similar to those which would be obtained by Johnson et al. for the same star. The two sets of values might easily differ by $0^m.02$ due to luminosity effects (Fig. 27).

In UBV, the comparison stars were tied together, and then tied as a group to the system of the E-regions (Cousins, 1973).

The comparison stars were chosen so as to provide a convenient means of determining the zero points and checking on any variation in them. The difficulties described in "Photometer Operating Problems" persisted through most of the observing programme, revealing how necessary the adoption of nearby comparison stars had been.

A typical observing sequence was:-

Comparison Star 1	:	All colours
Sky	:	All colours
Mira 1	:	All colours
Sky	:	All colours
Comparison Star 2	:	All colours
Sky	:	All colours
Mira 2	:	All colours
Sky	:	All colours

This sequence is not optimum from the point of view of photometric accuracy, since it makes no provision for determining extinction coefficients and zero points from standards (e.g. E-region stars), nor for repeat measurements. It is, however, efficient in the use of telescope time when the photometer is an automated one. Where, as in our case, we are making measurements in ten colours, typically using 60 second integrations for the Miras and 30 second integrations for the comparison stars, a single combined Mira-comparison observation can imply 30 minutes in integration times alone. Under these circumstances it is necessary to neglect the above-mentioned precautions in the interest of observing a reasonable number of variables in a night. In addition, this implies that a night with less than about five consecutive photometric hours is not useful.

(b) The Broad Band Systems

In addition to the observations made using the St. Andrews Photometer on the S. A. A. O. 100 cm telescope, some observations were made using a "People's" photometer attached to the S. A. A. O. 50 cm telescope. The latter were obtained in VRI only, with an EMI 9659 (extended S-20) tube and the following filters:

V : 3 mm Schott GG 495 + 4mm BG 38

R : 2mm OG 570

I : Wratten 88 A

These observations were made for the purpose of tying the comparison stars onto the Johnson system and to each other. This series of observations provided the basic (V - R) data for the comparisons as well as adding to the V and (R - I) data obtained with the 100 cm. In addition, a few observations were made of Miras on this VRI (S-20) system.

Further measurements were obtained by fitting an FW-118 and corresponding R and I filters onto the "People's" photometer, enabling additional comparisons to be made between the systems. These were extended on one occasion to enable transformations between the S-1 and S-20 systems to be determined for the Miras themselves. These proved to be highly non-linear, as might be expected.

The transformations finally adopted for the K stars were:

St. Andrews Photometer

$$U - B = 1.04\,(u - b)$$

$$B - V = 0.995\,(b - v)$$

$$V = v$$

$$V - R = 1.15\ (v - r)$$

$$R - I = 1.20\ (r - i)$$

"People's" Photometer

$$V = v$$

$$V - R = 1.365\ (v - r)$$

$$R - I = 1.372\ (r - i)$$

It is noteworthy that both V magnitudes coincide with the system of the E-regions. Study of the comparison stars alone, however, revealed the existence of a difference between the two systems. The "People's" photometer results were therefore modified by

$$V = v + 0.005 \quad ; \quad (R - I) > + 0.62$$

$$V = v + 0.111\ (R - I) - 0.064 \quad ; \quad (R - I) < + 0.62$$

It should be noted that the final values of (V - R) determined for the comparison stars are inevitably less reliable than the values for the other colours. More problematically, the S-1 (V - R) colour equation cannot be considered accurately determined, and this is perhaps the greatest error factor affecting the Mira data.

(c) The Narrow Band System

The narrow band measurements were combined producing the following indices:

$$(63, 65) = \text{Zero point} - (2.5\ \log I(63) - 2.5\ \log I(65)) - 0.38$$

$$(65, 103) = \text{Zero point} - (2.5\ \log I(65) - 2.5\ \log I(103)) + 2.5$$

$$(103, 105) = \text{Zero point} - (2.5\ \log I(103) - 2.5\ \log I(105)) + 0.95$$

$$81c = \text{Zero point} - 0.5\ (2.5\ \log I(65) + 2.5\ \log I(103)) - 2.5\ \log I(81)$$

The respective zero points were chosen to be equal to 0.0 on the night of 13/14 November 1973. The numerical constants were introduced for convenience, resulting in (65, 103) $\simeq$ 0.0 at spectral type A0, whereas the remaining indices are approximately zero at K0. For black bodies, all the indices would become more positive with decreasing temperature. When TiO is present, (63, 65) becomes relatively more positive. (103, 105)and 81c, on the other hand, become relatively more negative in the presence of VO and CN respectively.

(d) Reduction Procedures

The reductions were carried out using the Data General NOVA 1220 computer at S. A. A. O. After editing the paper tape output of the photometer, each night was reduced routinely using programmes developed for the purpose. At this stage mean zero points and extinction corrections were applied, along with the previously discussed colour corrections. The extinction coefficients per air mass were:

U - B	:	0.25
B - V	:	0.11
V	:	0.12
V - R	:	0.05
R - I	:	0.03
(65, 103)	:	0.04

The UBVRI residuals were then plotted against colour enabling a visual check to be made on the acceptability of the adopted colour and extinction coefficients. The night

was then further processed, the V and (V - R) measurements of each Mira being corrected by the residual shown by the corresponding comparison star. The Mira data, therefore, were processed such that (U - B), (B - V), (R - I) and the narrow band indices were given mean nightly zero points, whereas V and (V - R) were obtained differentially.

The measurements made using the "People's" photometer were reduced using the S. A. A. O. standard reduction programmes written by A. J. Penny.

(e) Errors

The table summarising the values obtained for the comparison stars also lists the number of observations made in each colour and the corresponding internal errors. For the UBV photometry, these values should also be representative of the total errors, although it is to be understood that for these red stars the colour equation cannot be determined with the degree of reliability expected for stars of intermediate colour. The errors quoted in (V - R) and (R - I) must be interpreted as internal errors only, since the scatter shown when comparisons are made with the list of Johnson et al. (1966) is much larger and probably contains systematic effects.

The errors in the variable star data are very difficult to estimate, except by analogy with the comparison stars on the one hand, and by scrutiny of the photon statistics on the other. An additional difficulty arises when (V - R) is considered, since this colour is defined by the S-20 measurements, and the S-1 to S-20 transformation is, unfortunately, not terribly well defined because of the equipment problems :

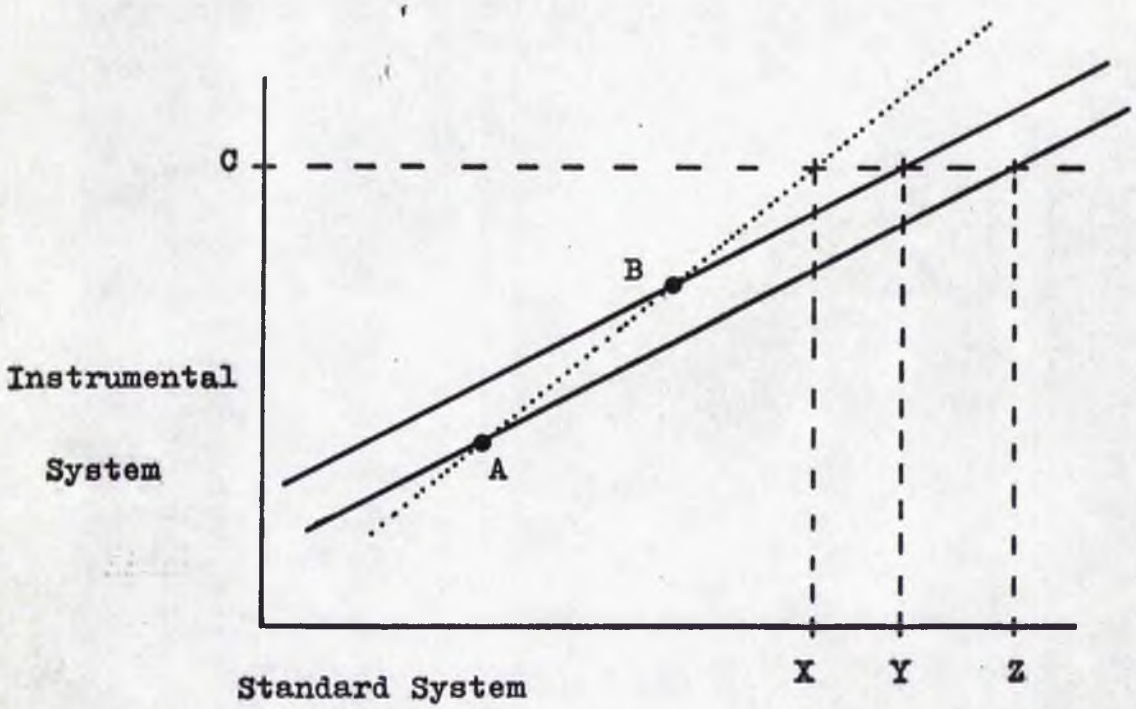

Fig.28. The Effect of Incorrect Colour Equation Upon Differential Photometry.

X = True value of C
Y = C relative to B
Z = C relative to A

In addition it was not possible to determine a direct transformation between $(V - R)_{S-1}$ and $(V - R)_{Johnson}$ because the majority of the high weight stars in the latter's list were too bright for observation on the 100 cm.

Fig. 28 shows the effect of an incorrectly determined colour equation upon differential photometry. The dotted line is the true relationship between the new measurements and the standard system. The slope of this line defines the colour correction between the systems, and the position of the line defines the zero point. Suppose that the colour correction between the systems has been determined wrongly, then the adopted calibration line may have the slope indicated by the solid lines. Let the star C give the instrumental measurement marked, and reduce it firstly relative to standard star A and then relative to B. Clearly one obtains a transformed value of C dependent upon the colour of the standard star used.

Suppose that

$$V - R = m_1(v - r)$$

is the true transformation from the S-1 measurements to the system defined by the comparison star values determined using the S-20. Suppose additionally that the adopted transformation is

$$V - R = m_2(v - r)$$

This error will not affect the observations of an individual variable when compared with itself, but since different variables are tied to different comparison stars, the above effect will introduce a scatter into any diagram combining the (V - R) measurements of all the variables. If the difference

Fig.29. Differences between S-1 and S-20 (R-I) Measurements of Miras.

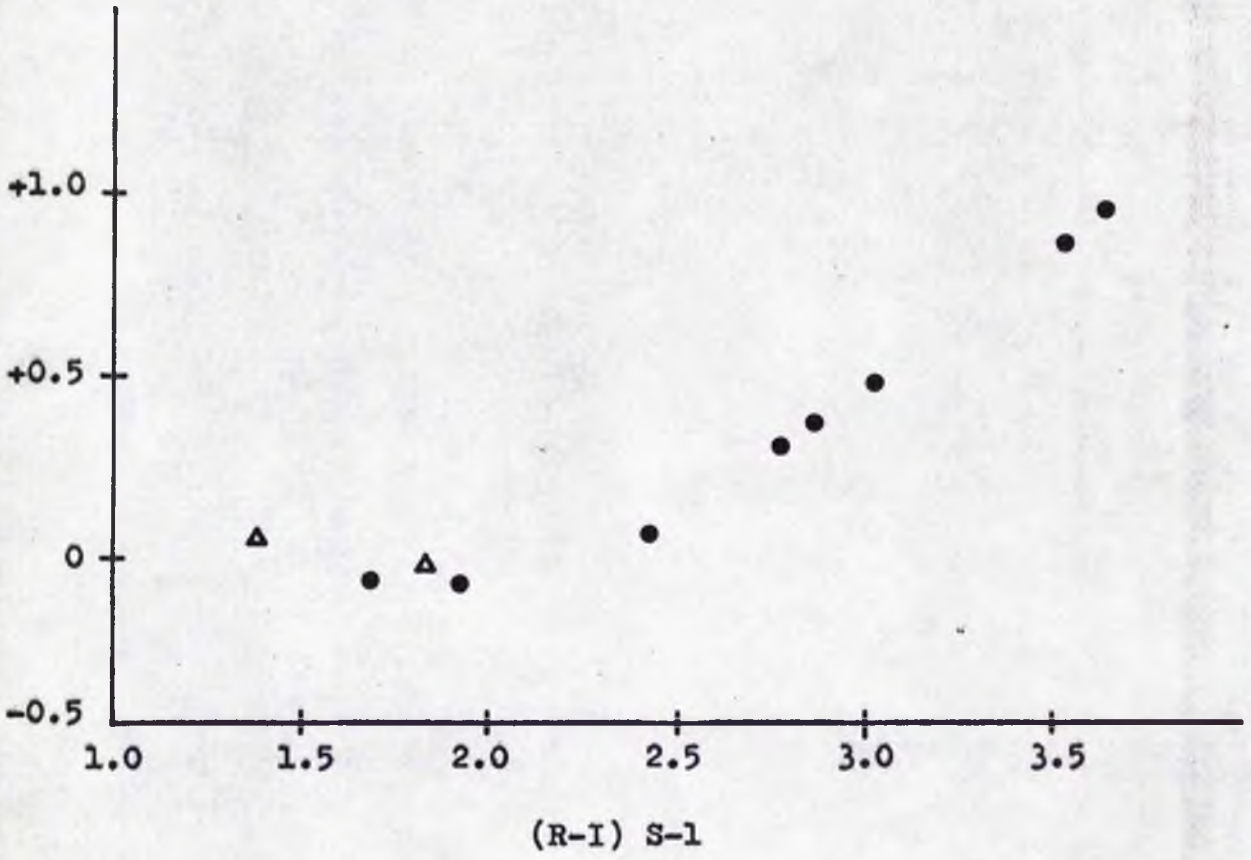

The vertical axis is the difference S-1 minus.S-20 in magnitudes after the linear colour correction has been applied. Circles and triangles are Me and Ce stars respectively.

in (V - R) between the reddest and bluest comparison star is Δ, then this effect will introduce a scatter of total amplitude

$$\varepsilon = \Delta \left(1 - \frac{m_2}{m_1}\right)$$

Given that $m_2 = 1.15 \pm 0.05$

$\Delta = 0.8$

then $\varepsilon = 0.035$

Hence one may have an extra scatter in (V - R) of up to $\pm$ 0.02.

So far only internal errors have been considered for the Mira data. Discussion of external errors is unfortunately impossible since the variable stars are redder than any standard stars, and so there is no way of defining a transformation to, say, the system of Mendoza's (1967) measurements. Barnes (1973) attempted to make his VRI results compatible with Mendoza's by demanding that the two colour diagrams produced by the two sets of data should be similar, but it was decided not to attempt such corrections for the present data. Fig. 29 shows the results of comparing S-20 and S-1 VRI measurements of Miras and indicates the sort of transformation problems which can occur. The present results are, then, merely corrected by an extrapolation of the linear correction applied to the K star data.

As a consequence of the above considerations the Mira observations are listed with an indication of their "error group" rather than individual probable errors. The error groups are:

1	:	$\pm$ 0.01
2	:	$\pm$ 0.02
3	:	$\pm$ 0.04
4	:	$\pm$ 0.1
5	:	$>\pm$ 0.1

Fig.30.

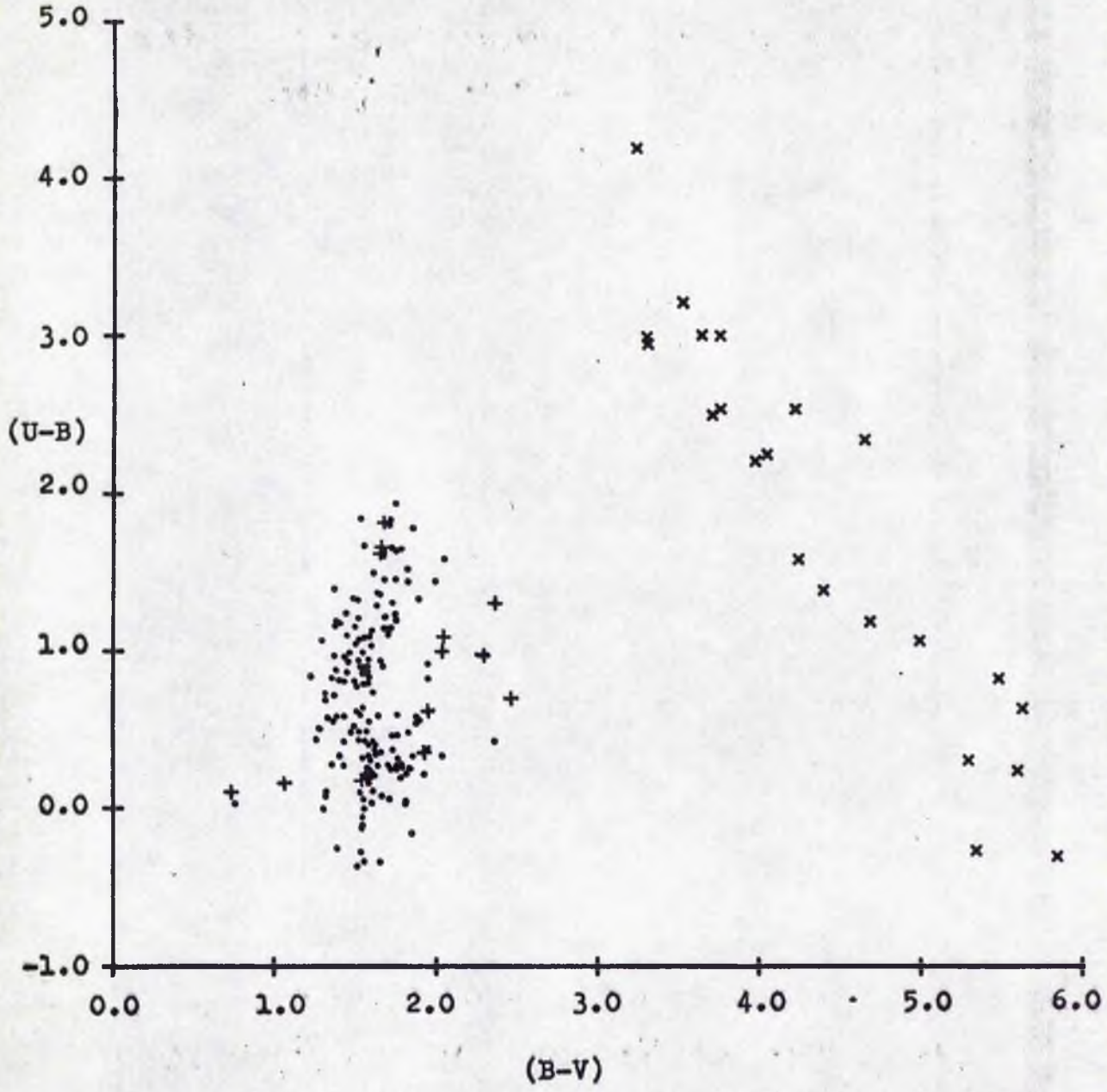

. Me Stars
+ Se Stars
x Ce Stars

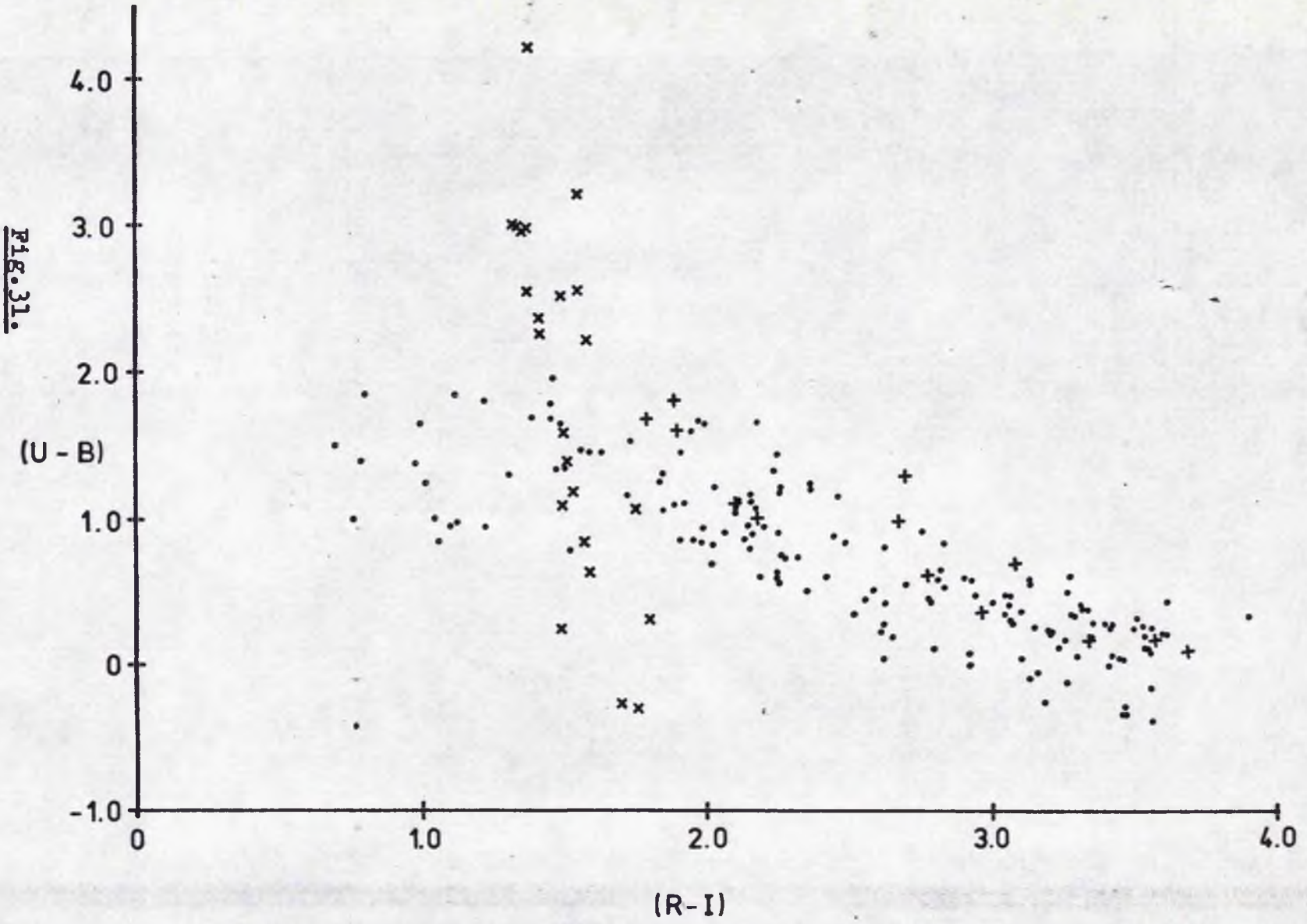

Fig.31.

Analysis of Results

The fully reduced measurements of the Miras were collected together for all the nights, and grouped by star using the S.A. A. O. Nova computer, the final list then being stored on magnetic disk. This enabled the computer to be used in plotting out light curves and two colour diagrams, either for individual stars or for the stars as a whole; a useful facility allowing initial scrutiny of all the possible combinations of the ten colours. In this section the more relevant two colour diagrams are briefly described, and then particular points of interest are discussed at greater length.

Observations in error group 5 are neglected.

(I) The Colour-Magnitude and Two-Colour Diagrams

(a) (U - B), (B - V) (fig. 30)

The two colour diagram shows all the observations of the variables irrespective of phase. There are two widely separated zones in this diagram corresponding to the Me and Ce variables respectively, with the Se stars clustering around the redder parts of the Me region. The Ce zone shows that (B - V) and (U - B) are related, for these stars, such that bluer (B - V) corresponds to redder (U - B), although with a large ($\sim 1^m$) scatter.

(b) (U - B), (R - I) (fig. 31)

In this diagram the Me and Ce stars practically change places as compared with the (U - B), (B - V) diagram. Here (R - I) changes very little for the Ce stars, but the Me and Se stars show a strong correlation in the sense that bluer

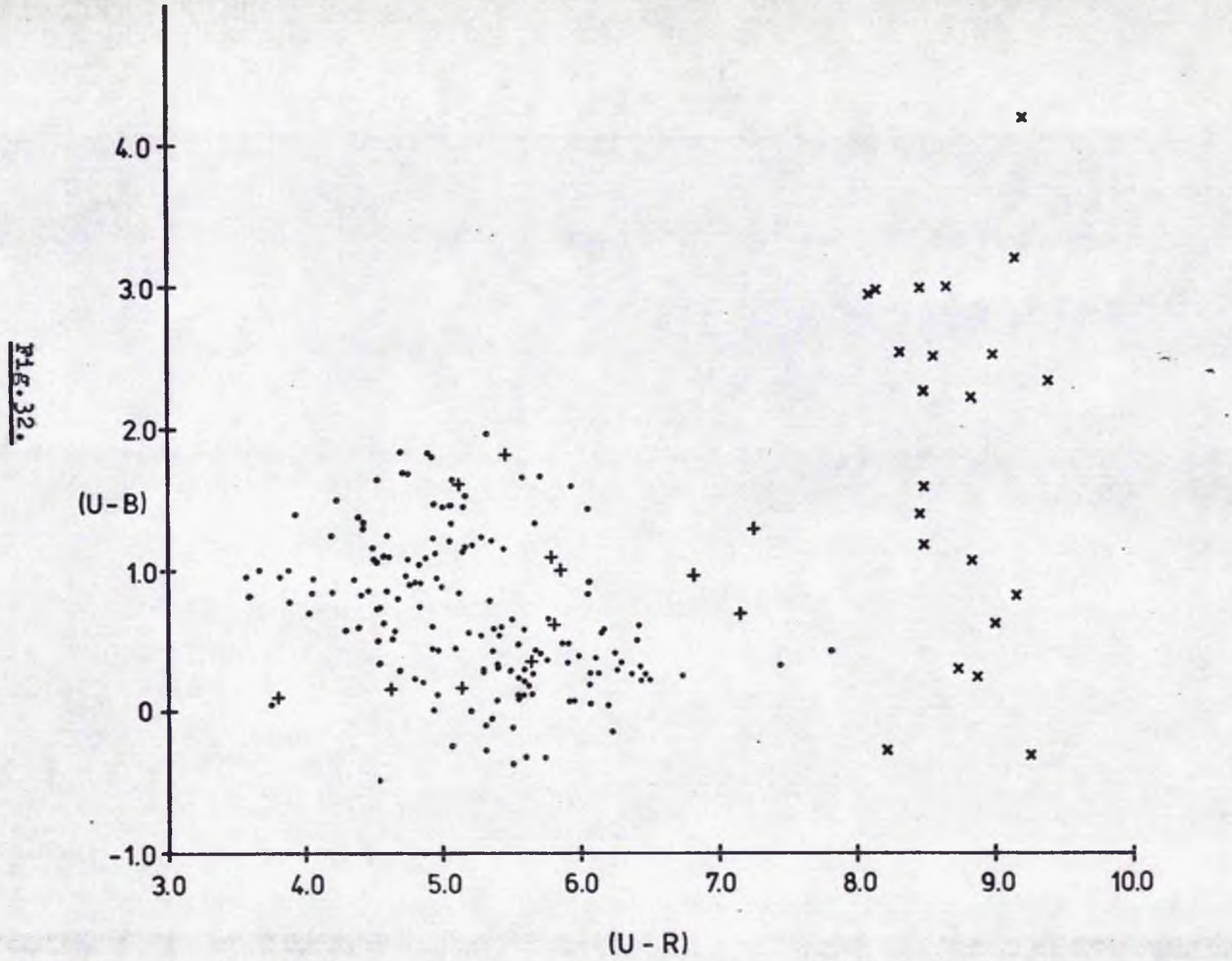

Fig. 32.

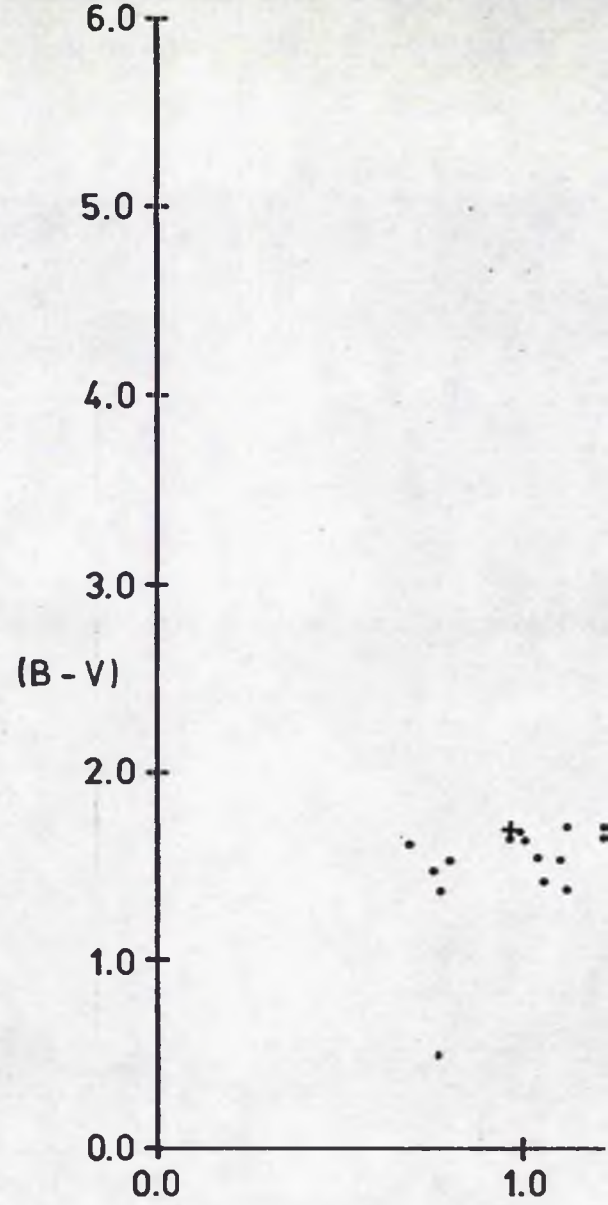

Fig.33.

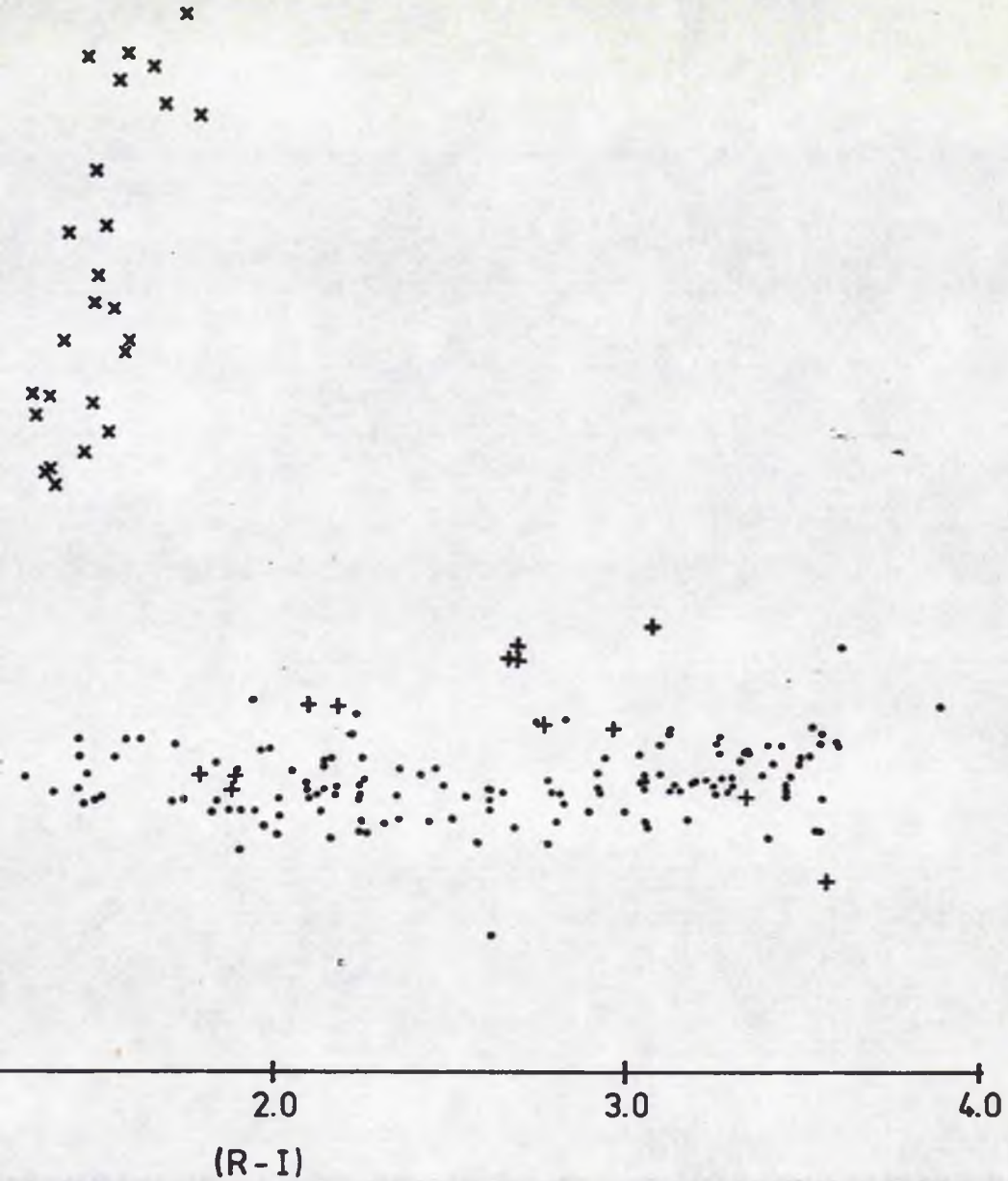
2.0
3.0
4.0
(R - I)

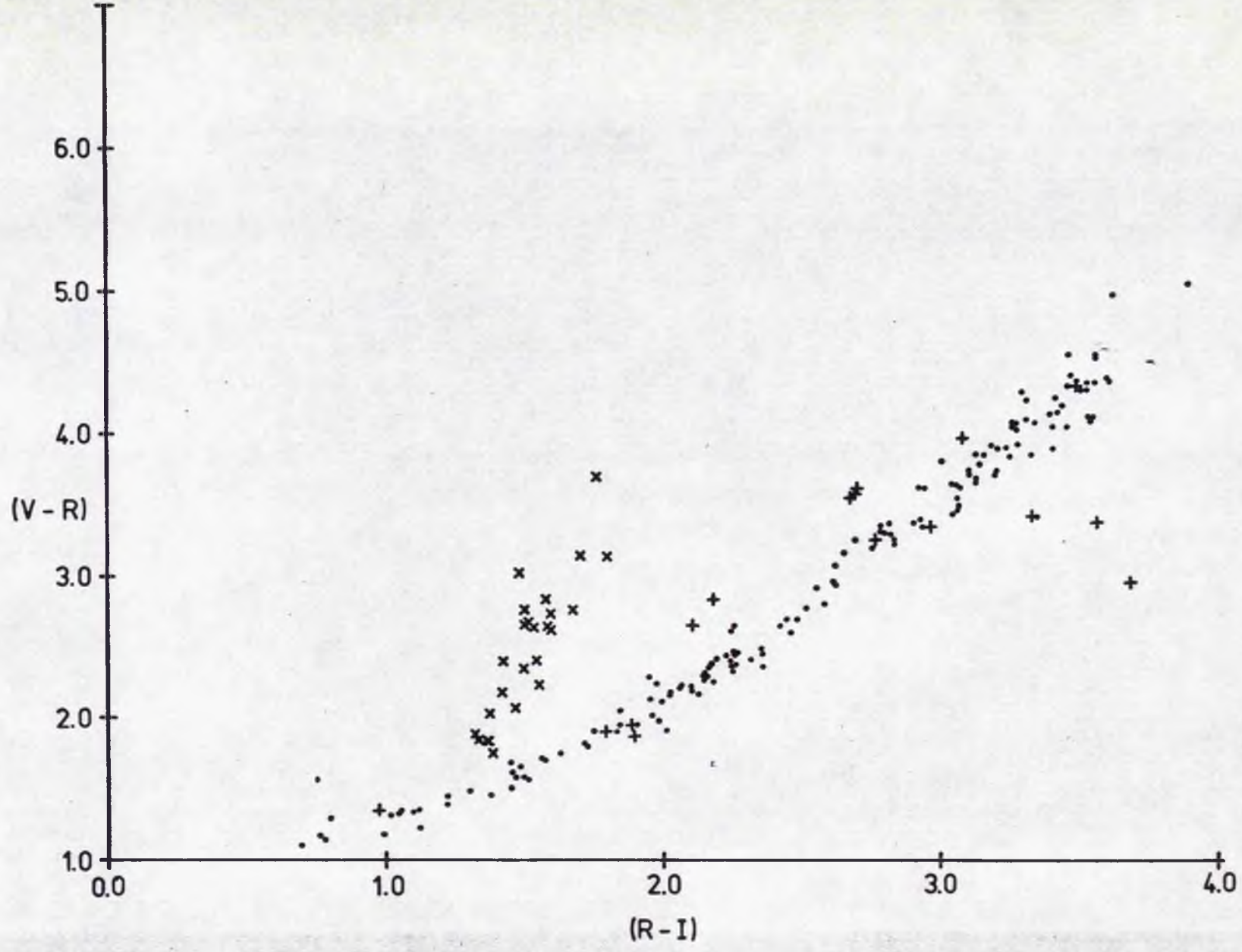

Fig.34.

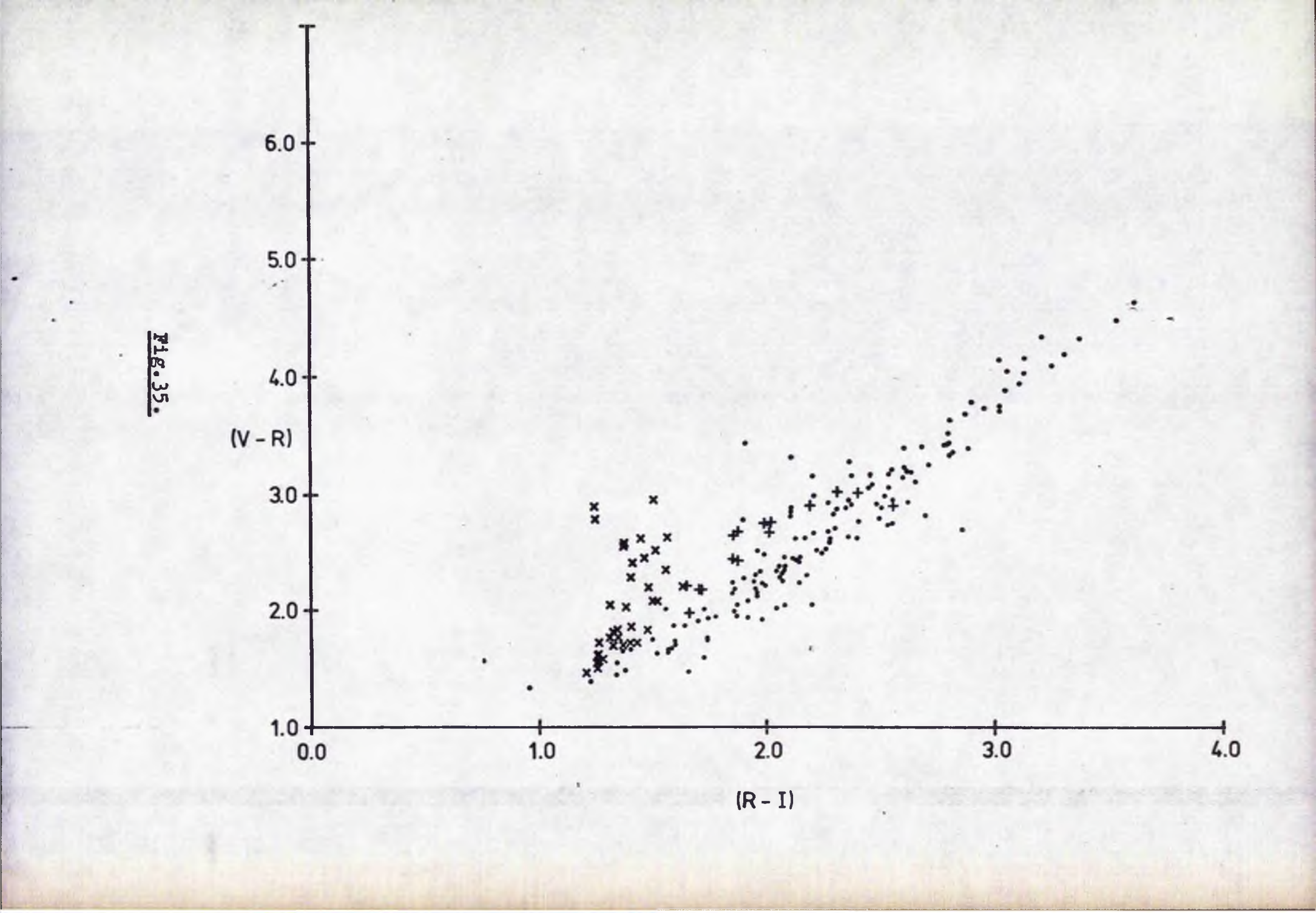

Fig.35.

(R - I) corresponds to redder (U - B), the scatter being $\sim 1^m$. This scatter ought to be due to the presence of emission lines.

(c) (U - B), (U - R) (fig. 32)

This diagram is interesting in that for some reason these two colours show remarkably little correlation with one another.

(d) (B - V), (R - I) (fig. 33)

This shows a clear separation of the Ce stars from the others. If (R - I) correlates well with temperature, this diagram illustrates the poor temperature dependence of (B - V) for M stars.

(e) (V - R), (R - I) (fig 34)

This diagram has been discussed by Barnes (1973) and also in an earlier section (fig. 12). As for all the two colour diagrams in the present section, fig. 34 contains all the reliable observations made and so combines measurements taken at assorted phases of the stars' variations. Fig. 35 shows the equivalent diagram prepared from Barnes' data. The distribution of points in figs. 34 and 35 is different because Barnes attempted to concentrate his observations around phase 0.0, and so has very few observations at the reddest colours. Notwithstanding this selection effect, fig. 34 shows a sequence for the Me stars with far less scatter than does fig. 35. No explanation has been found for this effect which is far too large to be caused by differences in the random errors associated with the two lots of photometry. A possible

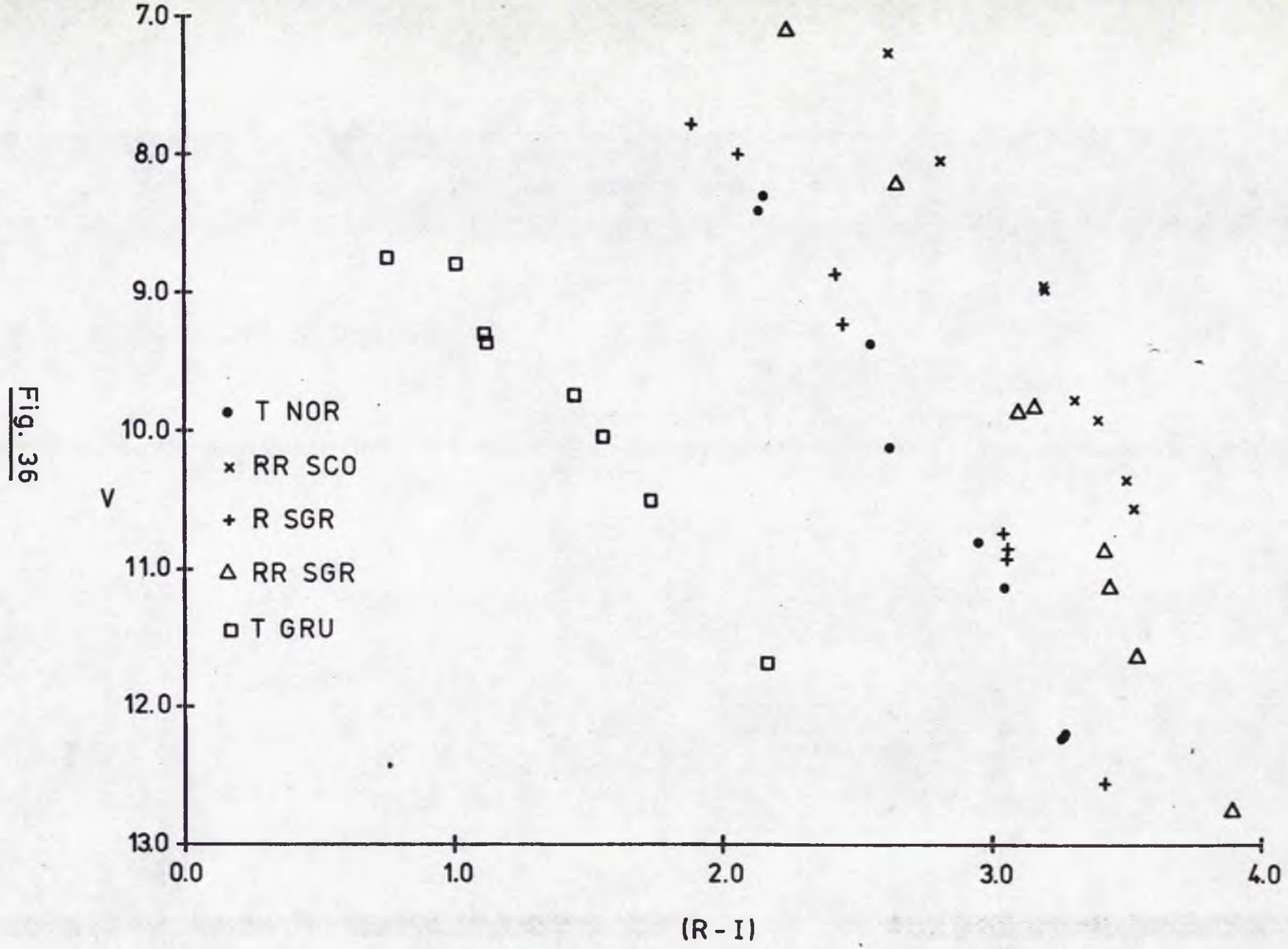
7.0
8.0
9.0
10.0
11.0
12.0
13.0
V
0.0
1.0
2.0
3.0
4.0
(R - I)
T NOR
RR SCO
R SGR
RR SGR
T GRU

Fig. 36

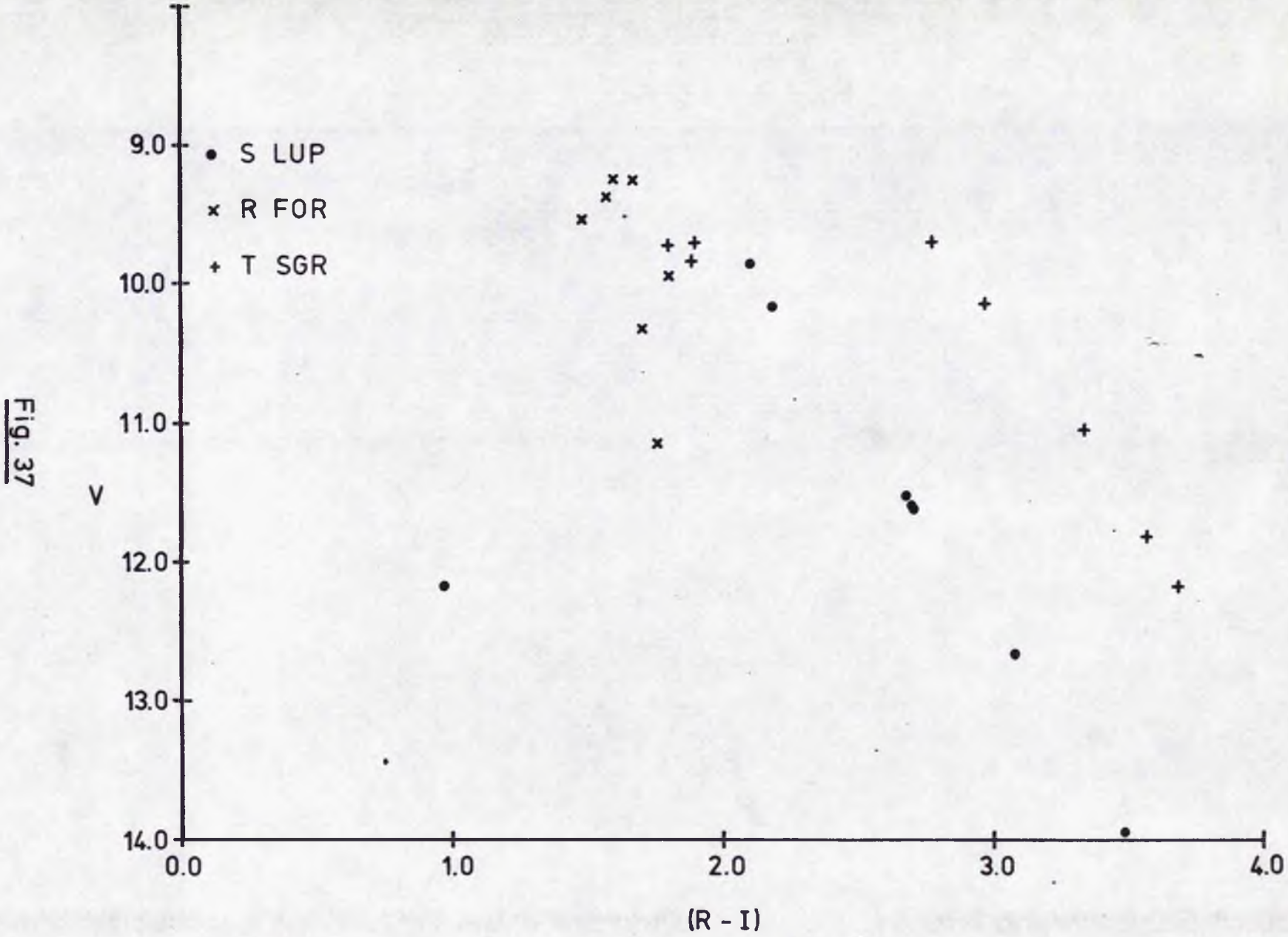

Fig. 37

explanation may lie in some odd property associated with the exact wavelengths of the filters used.

Fig. 34 shows an Me sequence with a scatter of the order of $0^m.2$ for $(V - R) < +4$. In the region redder than this there is a marked increase of the scatter, but at least part of this may be due to the influence of faint blue companions, since when the variables are reddest in (V -R) and (R - I) they are near minimum V. Any companion of a Mira will be bluer than the Mira itself, and so double stars tend to appear with too small a value of (V - R) for their (R - I). This effect is quite clear in the case of R Aqr, (see later section), although, surprisingly, not in that of Mira Ceti.

(f) V, (R - I) (figs. 36 and 37)

Fig. 36 is the (V, R - I) diagram for the five best-observed Me stars, and it reveals that the measurements of any individual variable always occupy a narrow zone such that brightest V coincides with bluest (R - I), and faintest V coincides with reddest (R -I). This is an unexpected result since it was assumed that a given variable would describe a large loop in this diagram as it ran through its cycle. Instead, one can say, approximately, that a star moves forwards and backwards along a single smooth curve in the diagram. Furthermore, at a given (R - I) the curves for different stars appear to have similar shapes and slopes, and in a later section an attempt is made to derive a composite curve describing the behaviour of all the Me stars in the (V, R - I) diagram.

Fig. 37 shows the behaviour of the Se stars S Lup and T Sgr, and the Ce star R For. The coverage of the light cycles

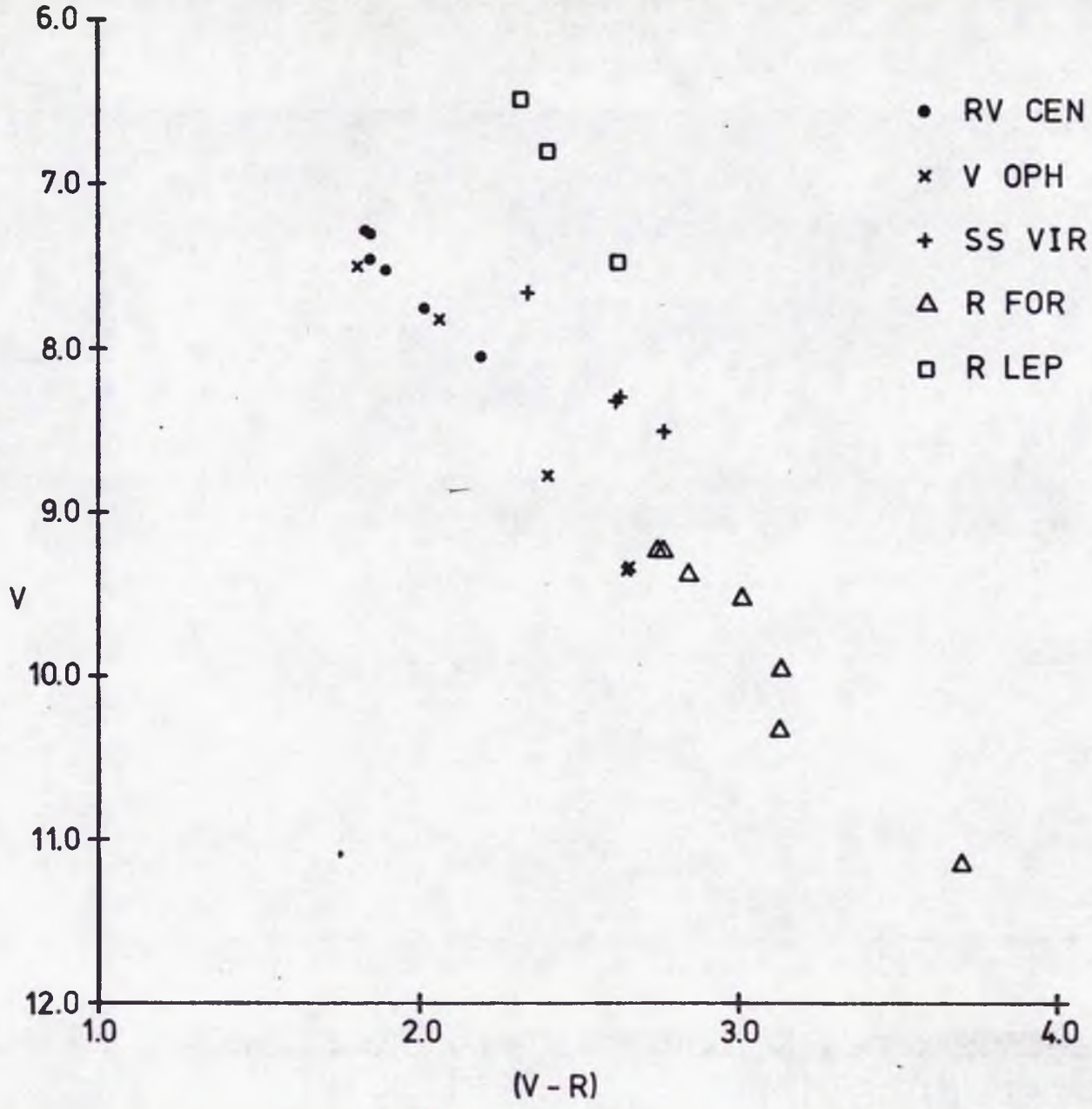
6.0
7.0
8.0
9.0
10.0
11.0
12.0
V
1.0
2.0
3.0
4.0
(V - R)
RV CEN
V OPH
SS VIR
R FOR
R LEP

Fig. 38

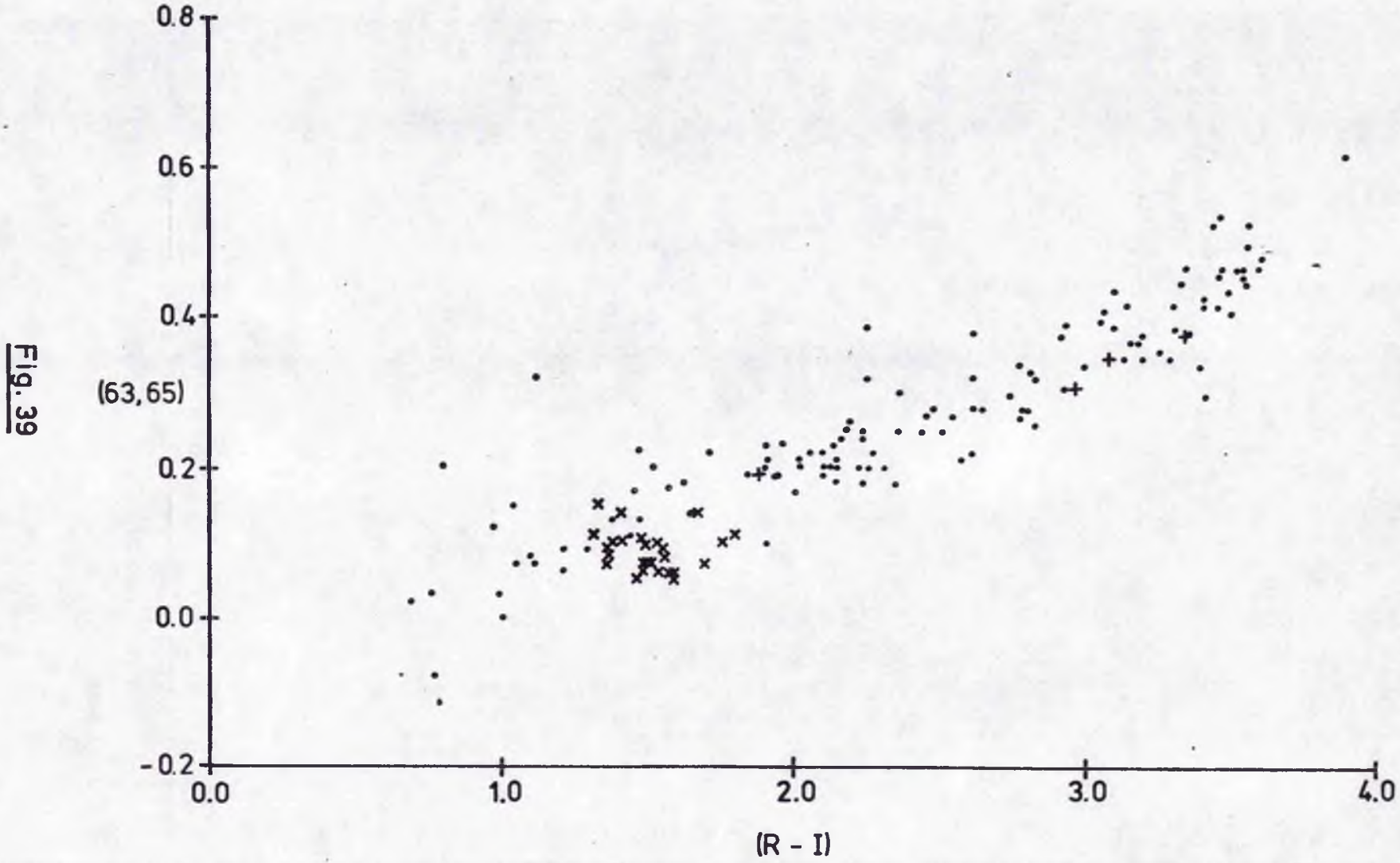

Fig. 39

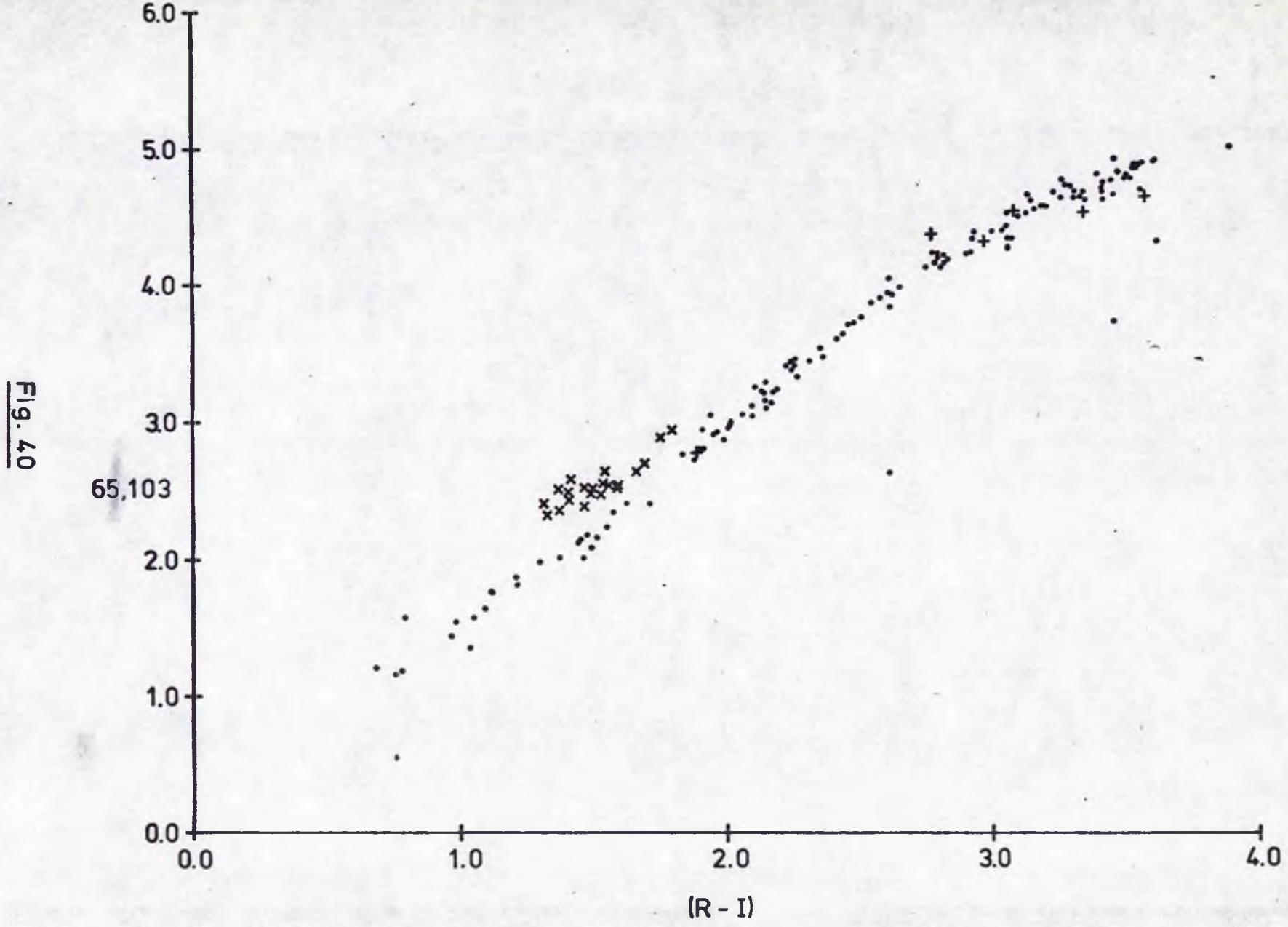

Fig. 40

65,103

is insufficient for one to say more than that all three stars probably trace complicated paths. It should be noted that the measurements of T Sgr include the light from a companion of magnitude V $\approx$ 12.5, whose influence is also seen in fig. 34.

(g) V, (V - R) (fig. 38)

This diagram is plotted for the Ce stars only. It would seem that the relationship between V and (V - R) for the Ce stars is analogous to that between V and (R - I) for the Me stars.

(h) (63, 65), (R - I) (fig. 39)

This diagram shows that TiO strength is well correlated with (R - I) for the Me stars, and also that (63, 65) does not show signs of saturation even for the reddest Miras. On the contrary, the diagram behaves as though there were a "saturation" effect occurring in (R - I). The 6300 Å band of TiO is caused by a complex mixture of subordinate transitions, unlike the (0,0) band at 7100 Å chosen by Lockwood and Wing (1971), which saturates at about spectral type M7.

(i) (65, 103), (R - I) (fig. 40)

An extremely tight correlation exists in this diagram. Essentially it would seem superfluous to measure both (R - I) and a narrow band continuum index, and since the former can be measured more accurately, it makes sense to discontinue measurements of the latter type.

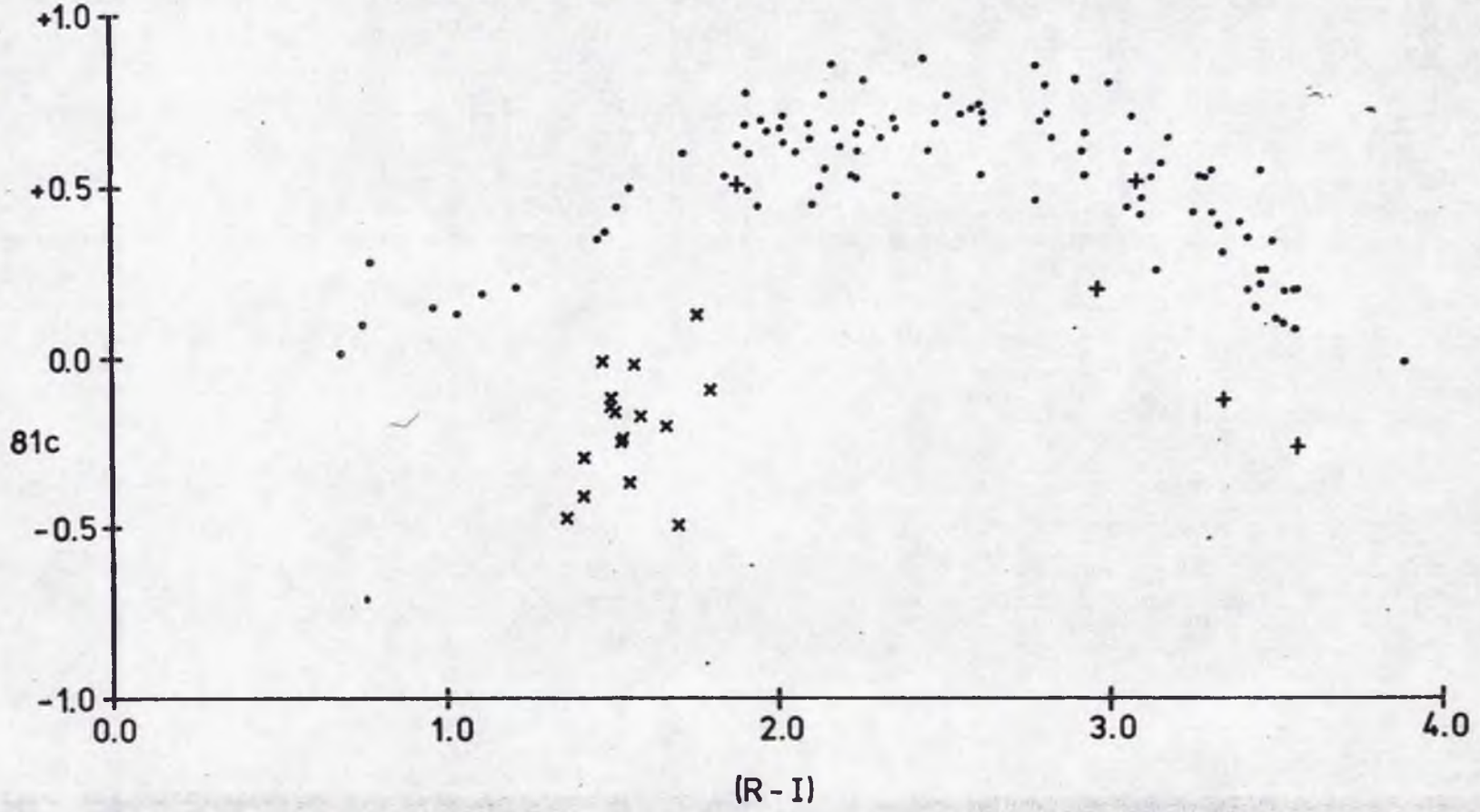

Fig. 41

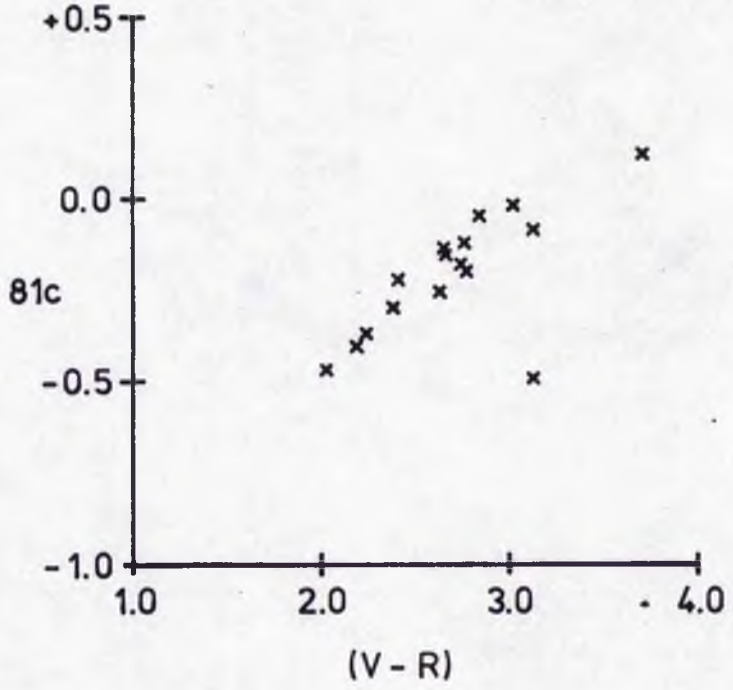

Fig. 42

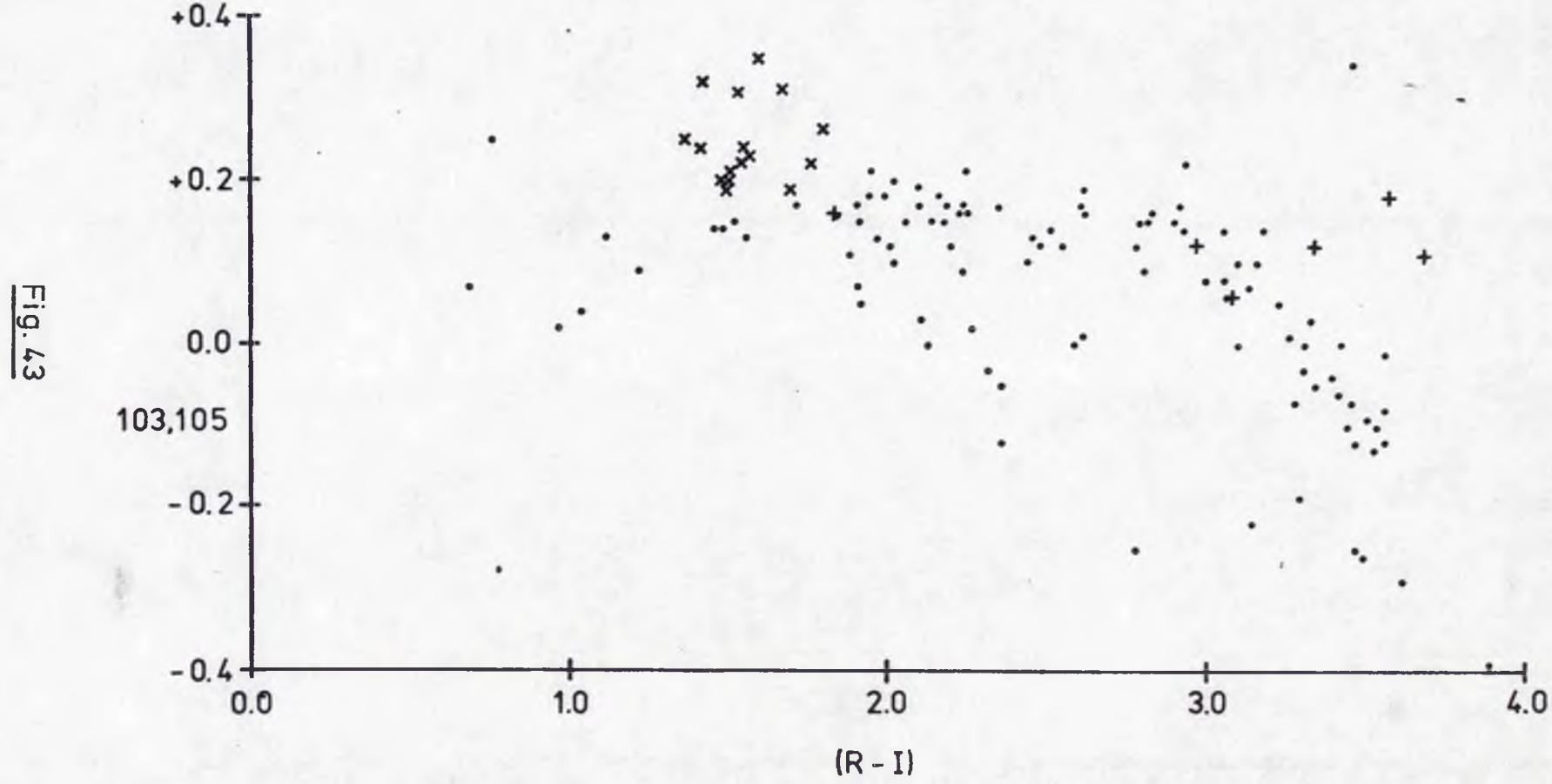

Fig. 43

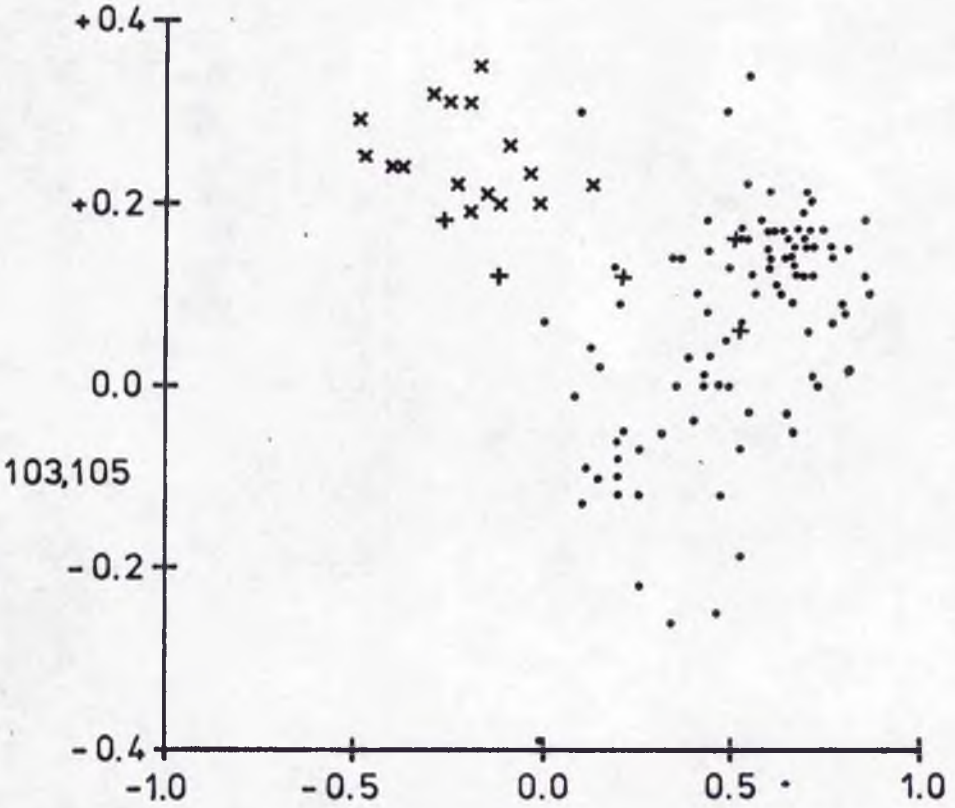

Fig. 44

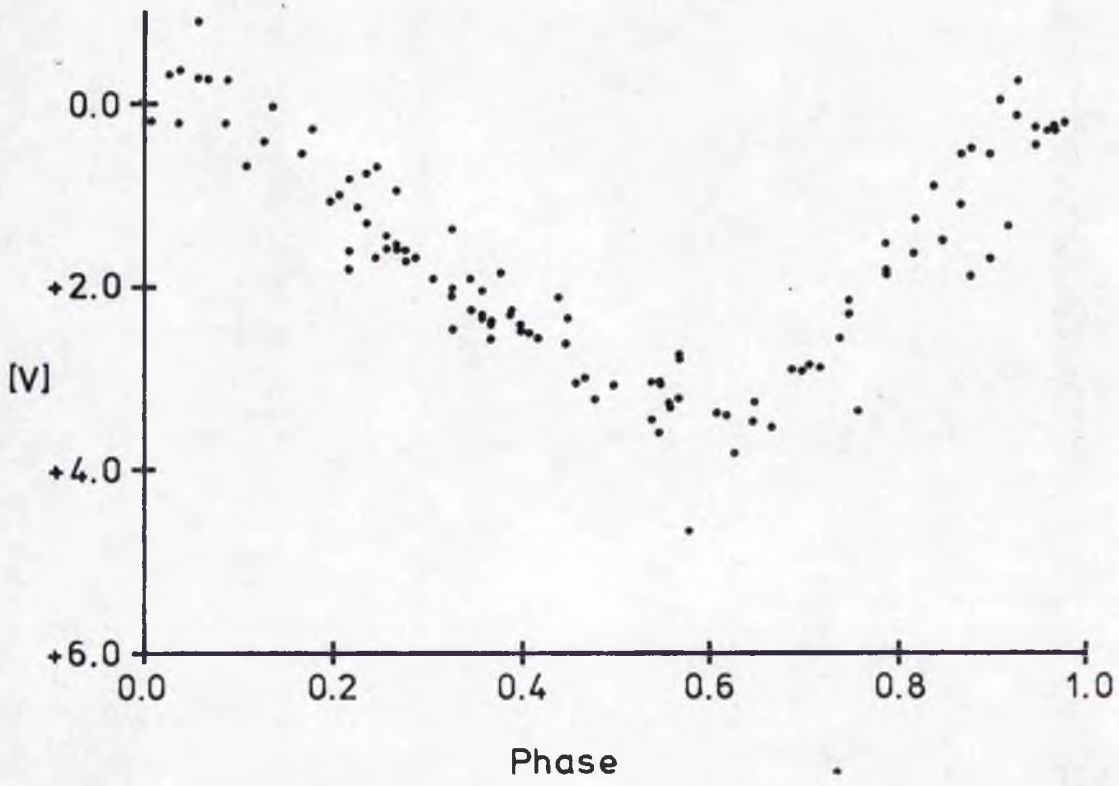

Fig. 45

(j) 81c (figs. 41 and 42)

The correlation between 81c and (R - I) seems remarkably poor for Ce stars, considering that 81c is supposed to measure CN strength. The sequence of Me and Se stars shows 81c increasing with (R- I) until strong blanketing appears in the 8000 Å region, whereupon the trend reverses.

Fig. 42 contains only the observations of the Ce stars, and it shows that (V - R) correlates far better with 81c than does (R - I). This would seem to imply that (V - R) is the more significant broad band index where Ce stars are concerned.

(k) (103, 105), (R - I) (fig. 43)

As expected (103, 105) is almost constant until (R - I) becomes greater than +3, and thereafter increases quite rapidly as the VO band at 10,540 grows in strength. The numerous points lying below the most populated part of the diagram imply that the Me stars probably describe loops in it, but the coverage of the light cycles is not sufficient to clarify this point.

(l) 81c, (103, 105) (fig. 44)

Predictably, the diagram separates the Ce and Me stars. The Se stars appear in intermediate positions but, as so often, they cannot be distinguished unequivocably from the other types.

(m) V, Phase (fig. 45)

The visual light curves of Miras have been observed for many years, a good selection of them being collected in

Campbell (1955). The quantity of data obtained in the present investigation is, of course, insufficient to define light curves for the individual variables observed. Nonetheless, an attempt has been made to deduce a mean curve for the Me variables as a group, and this is shown in fig. 45.

The procedure adopted was as follows. Firstly, periods and epochs were taken from G. C. V. S., and the magnitudes at mean maxima and minima from Campbell (1955). These were used as initial scaling factors and the resultant diagram of 'V' against Phase was plotted. This diagram appeared almost random due to numerous phase discrepancies. These were corrected for the obvious cases and the diagram re-plotted. It now became possible to draw a mean curve of sorts through the data. This curve was expressed in tabular form and the points for the individual stars were shifted relative to it in phase and magnitude until the sums of the squares of the differences (observed point - mean curve) were minimized. This produced a new mean curve considerably different in shape from the original. Further processing reduced the scatter about this mean curve but did not lead to any further gross alterations in shape.

The final diagram shows a light curve with equally sharp maxima and minima and a rising branch steeper than the falling branch. It also shows a scatter of about 1^m, which is to be expected but is rather disappointing since it had been hoped to use the mean curve in investigating the possible existence of loops in the colour-magnitude diagrams.

(II) Extended Discussions

In this section, ideas generated by the results are considered at length, along with the observations of individual variables of interest.

(a) V, (R - I)

This diagram was initially inspected for the stars individually, expecting that it would reveal sizeable loops. In fact, for the Me stars, these 'loops' proved to be too narrow to be distinguished from a simple curve along which the individual stars move backwards and forwards. Visual inspection led to the conclusion that different variables of similar (R - I) show similar V, (R - I) diagrams, and that, further, these diagrams change systematically with (R - I). This can be summarized by saying that, approximately,

$$V + K = F(R - I),$$

where K changes from star to star, but F (R - I) is the same for all Me variables.

One can try to produce a composite V, (R - I) diagram for the stars observed by superimposing their individual diagrams and allowing movement in the V co-ordinate. However, it was thought more satisfactory to use an alternative approach.

Differentiating we have

$$\frac{dV}{d(R - I)} = F^1 (R - I)$$

The slopes of the individual diagrams were determined by

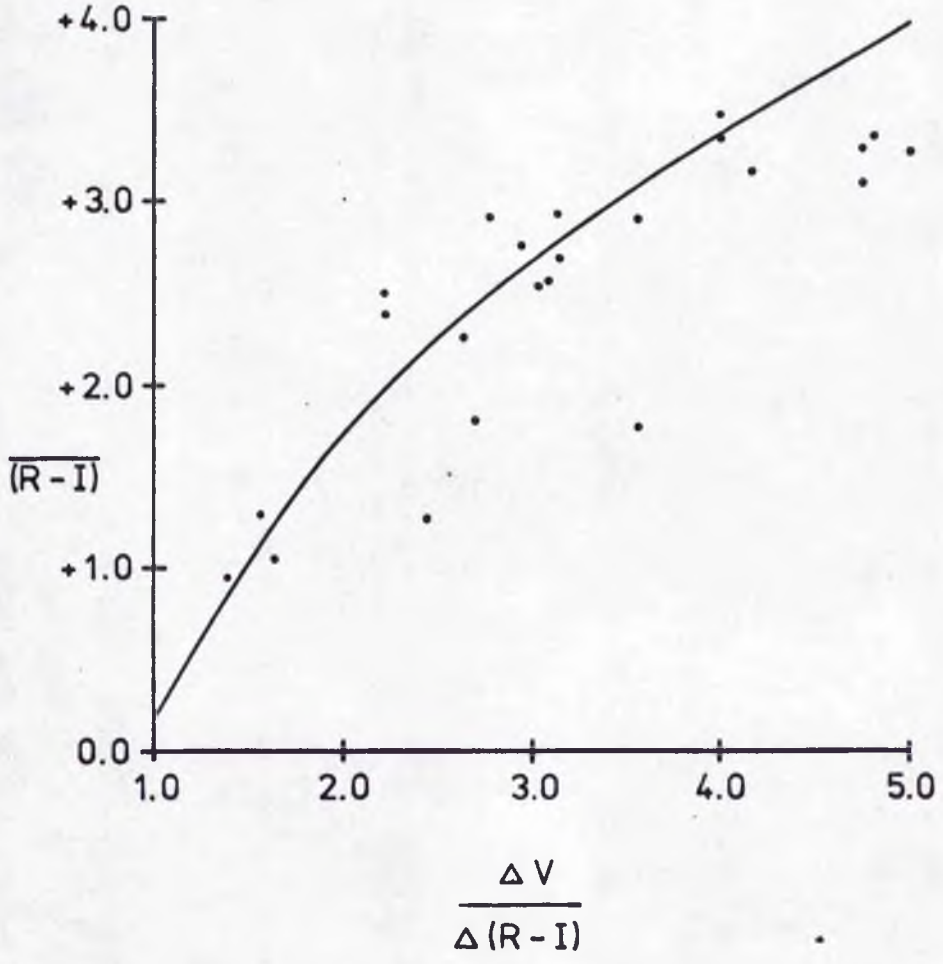

Fig. 46

simply drawing a straight line through the data points and also determining their median (R - I). Hence a series of values of $\frac{\Delta V}{\Delta(R - I)}$ and $\overline{(R - I)}$ were obtained, and these are shown plotted for the Me stars with six or more observations (fig. 46). In cases where there were sufficient observations covering a large (R - I) range, the measurements were separated into two groups by colour enabling two determinations of $\frac{\Delta V}{\Delta(R - I)}$ and $\overline{(R - I)}$.

Despite the scatter in fig. 46, it is clearly possible to draw a mean curve through the data by eye. Several such attempts to define a mean relation were made, and equations describing the deduced curves were determined graphically. The curve finally adopted is shown in fig. 46, and it is a compromise between accuracy and mathematical simplicity. Its equation is

$$\frac{\Delta V}{\Delta(R - I)} = 0.97 \exp [0.42 (R - I)]$$

An example of a better fit to the data is

$$\frac{\Delta V}{\Delta(R - I)} = 1.27 \exp [0.8 (R-I) + 0.8 (R-I)^2],$$

but describing the relationship in this form gives little advantage over expressing it purely numerically.

Integrating the adopted equation gives the form

$$V + K = f (R - I) + C = F (R - I),$$

where C is a constant and K varies from star to star. Clearly, if one assigns an arbitrary value of K to some chosen

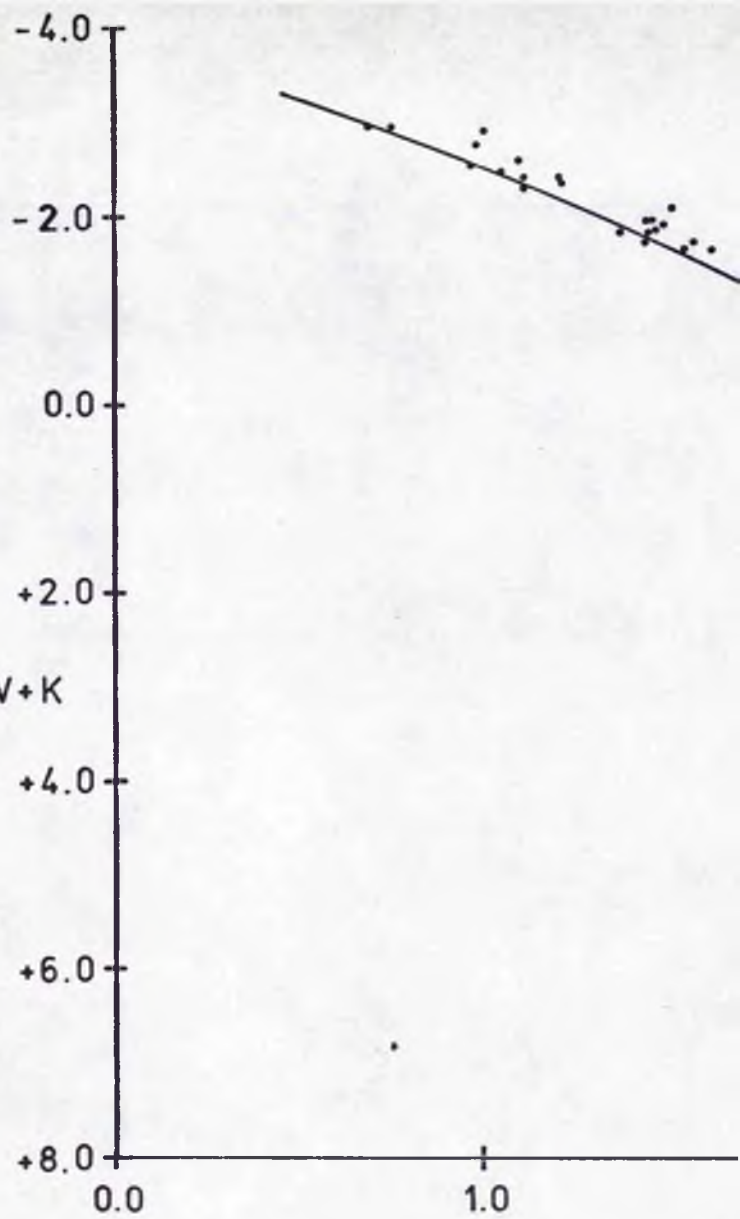

Fig. 47

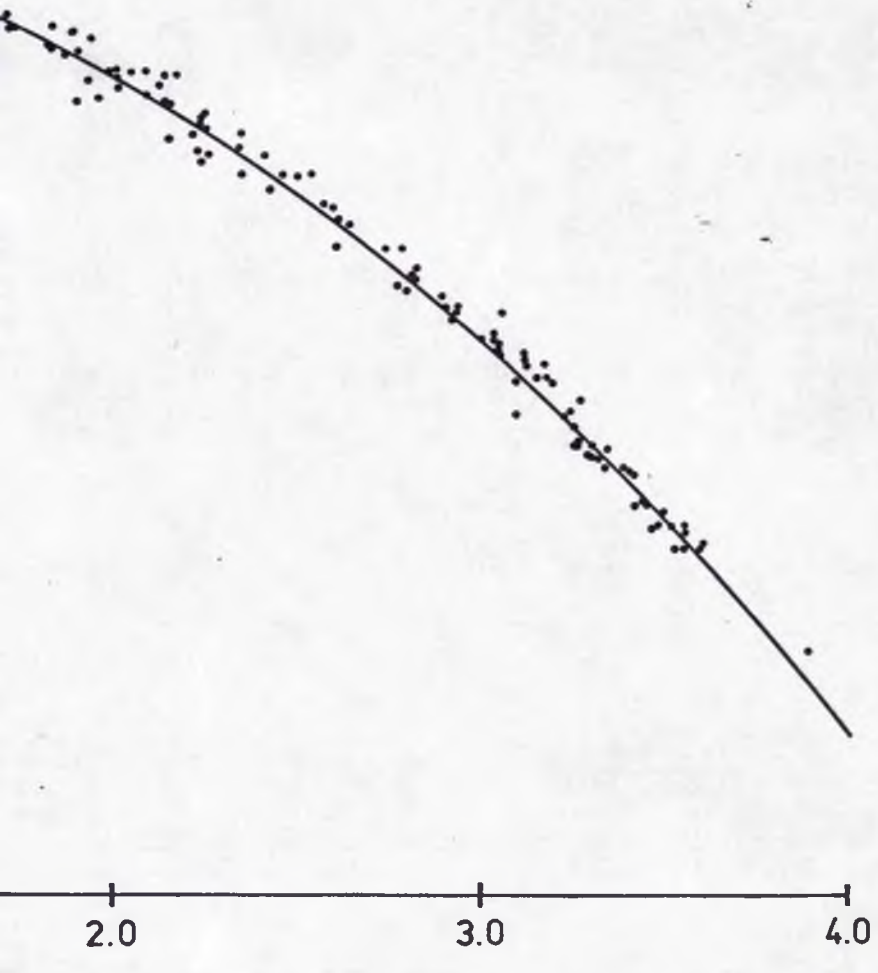
2.0
3.0
4.0
(R-I)

variable star, then one can determine the corresponding K value for any other variable, having calculated the value of C.

Choosing for Mira Ceti

$$V + K = M_V$$

$$\therefore \quad K = -4.2$$

(assuming $\overline{M}_V(\max) = -0.5$, $\overline{V}(\max) = +3.7$), gives

$$V + K = 2.31 \exp [\, 0.42\ (R - I)] - 6.11.$$

This differs from the relation determined previously (Kelly, 1974) because of the availability of extra data.

The observations of a particular Me star give a set of values of V and (R - I) and so a series of values of K is obtained. The adopted value of K for that star is taken to be the arithmetical mean of these calculated values, and fig. 47 shows the resulting (V + K), (R - I) diagram for all the Me variables with more than one observation, except for those discussed individually in a later section.

(b) Value of the (V + K), (R - I) Diagram

Mean V light curves are available for many Me variables because of the accumulated visual data. The properties of the individual stars are normally compared at some representative point on their light curves, for example mean maximum or mean minimum. Given $\overline{V}(\max)$ for an Me variable, plus a small number of VRI observations at random phases of the variable, one can determine K and hence the value of (R -I) corresponding to $\overline{V}(\max)$ (or any other chosen point on the mean light curve). Given that (R - I) is a significant

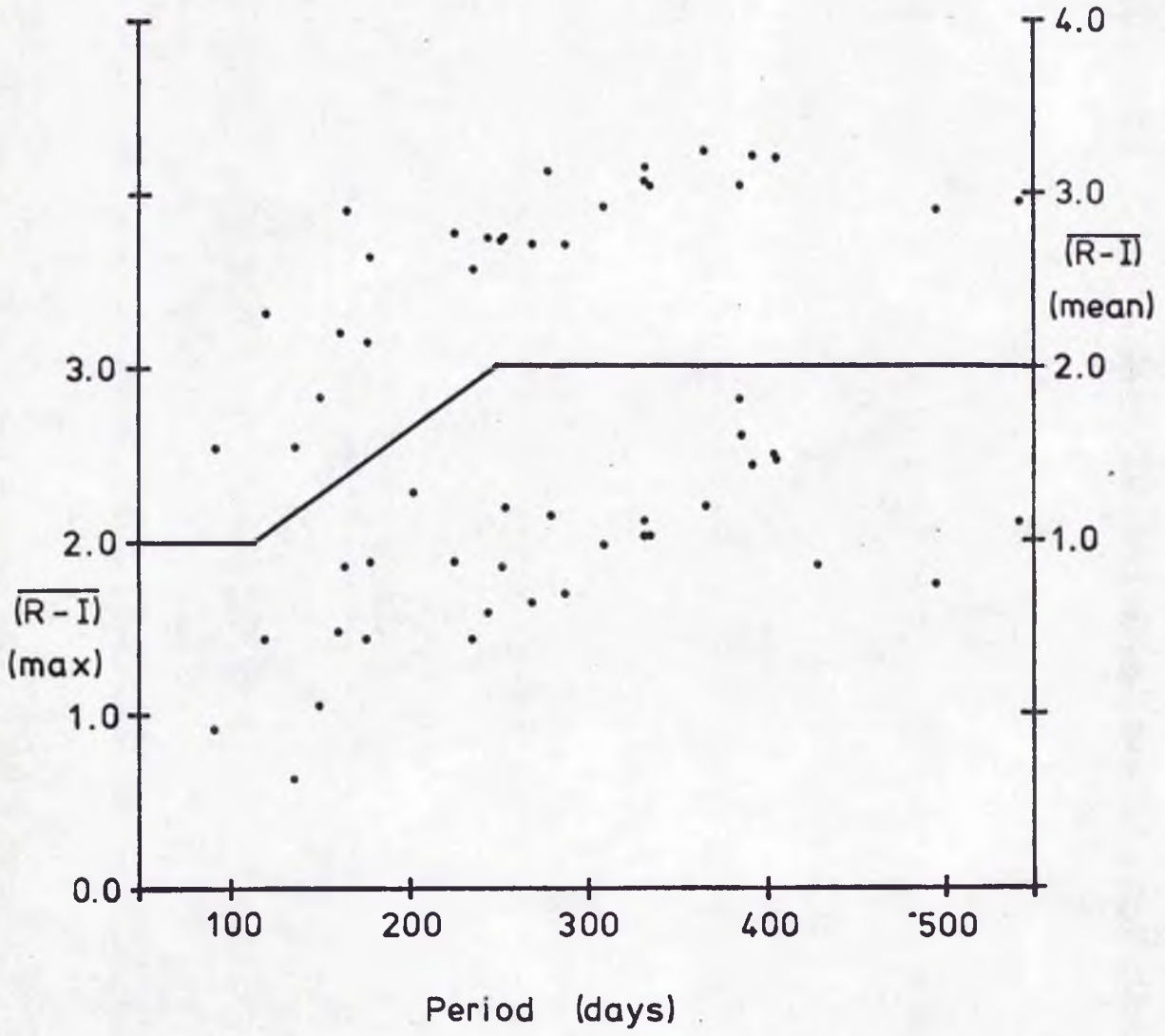
4.0
3.0
(R-I)
(mean)
2.0
1.0
3.0
2.0
(R-I)
(max)
1.0
0.0
100
200
300
400
500
Period (days)

Fig. 48

indicator of the star's physical condition, this means of obtaining estimates of (R - I) at specified phases should be useful in investigations concerned with the trends discernible in the variables as a group.

Fig. 48 is the Period -$(\overline{R - I})$diagram constructed by combining the present data with that listed in Campbell (1955), and it shows the values of R - I corresponding to $\overline{V}$(max) and $\overline{V}$(mean). An interesting feature of this diagram, shown especially by the $\overline{R - I}$(mean) points, is the relatively orderly sequence for 220 $<$ Period $<$ 410 as opposed to the relatively too 'blue' points at the longest periods, and the increased scatter at the shortest periods.

(c) <u>The interpretation of V + K as M_V</u> (Table 4)

It is noted that the composite (V + K), (R - I) diagram is dimensionally equivalent to an M_v, (R - I) diagram (Kelly, 1974).

The distance modulus $d = V - M_v$,

therefore $M_v + d + K = f(R - I) + C$

where d and K vary from star to star.

Clearly $M_v \equiv V + K$

if $d + K =$ constant for all Me Miras. This hypothesis is rather difficult to test since it requires the availability of a list of Me Miras of various periods, with well-determined distances, and such a list does not exist. The procedure selected, therefore, is to determine $\overline{V}$(max) + K for the variables observed and compare the results with statistical investigations of the relationship between $\overline{M}_v$(max) and Period. In addition, observations were made

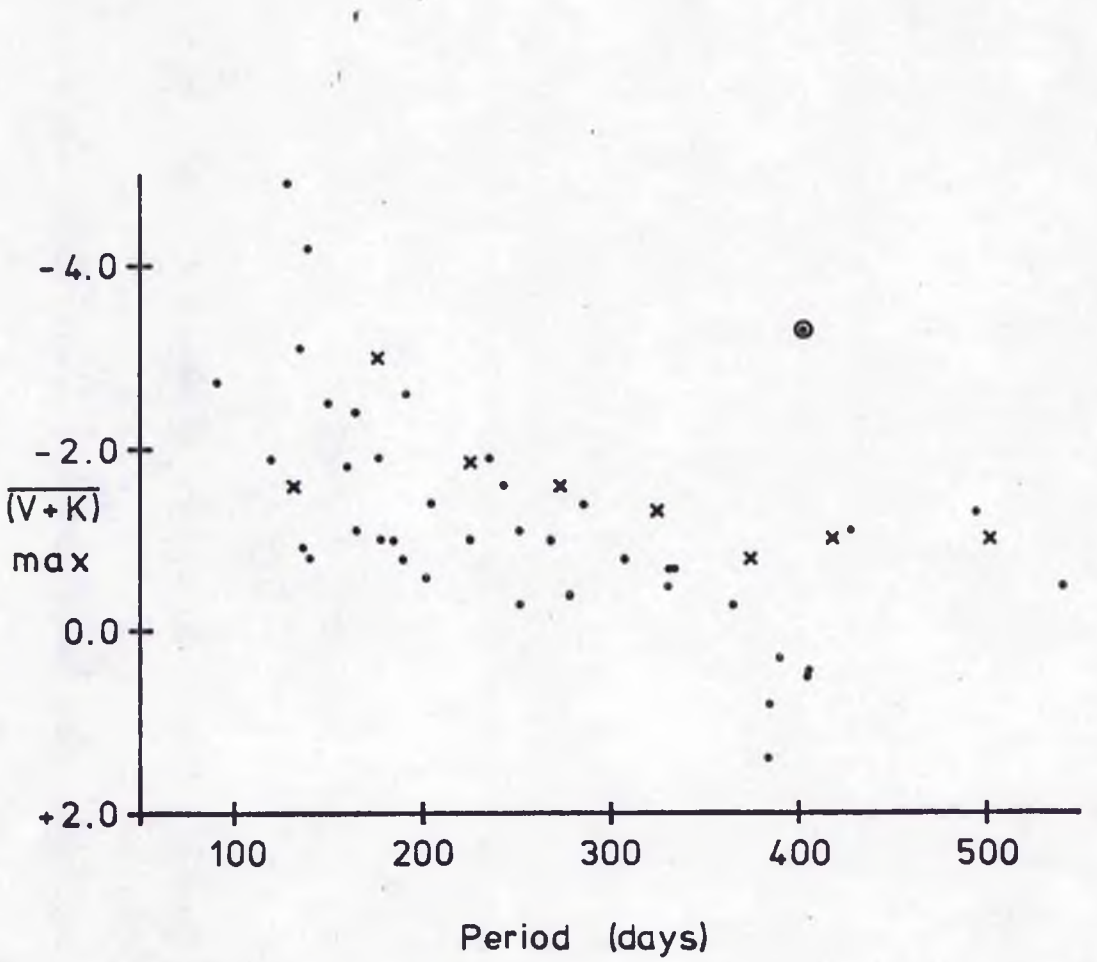

× statistical parallaxes

⊙ BM Sgr. V(max) used, as $\overline{V(max)}$ is not available.

Fig. 49

of the variables in the globular clusters 47 Tuc and M69 (NGC 6637).

The determinations of K for individual variables of particular interest, but with few VRI (S-1) measurements, have been augmented by observations made in VRI (S-20) and transformed with the help of fig. 29. These are listed in table 3, but it should be noted that they may not correspond with the S-1 photometric system to an accuracy better than $0^m.1$.

Fig. 49 shows $\overline{V}(max) + K$ plotted against period, along with the mean absolute magnitudes of sets of Miras grouped by period obtained from statistical parallaxes (Clayton and Feast, 1969). It is convenient to discuss this diagram in three sections.

(i) $200d < \text{Period} < 400d$

Over this range of periods one sees a monotonic relationship between $\overline{V}(max) + K$ and period, with a slope slightly greater than that of $\overline{M}_V(max)$ given by the statistical investigation. Broadly, one can say that in this region $\overline{V}(max) + K$ and $\overline{M}_V(max)$ do not have vastly different characteristics, although it must be recalled that the former has a zero point which is determined by an adopted distance modulus for Mira Ceti of $4^m.2$.

(ii) $\text{Period} > 400d$

Here we have a glimpse of a potentially very interesting phenomenon, represented, unfortunately, by only a small sample of stars. Instead of a smooth continuation of the sequence of 200 to 400 day stars, there is a group of stars lying considerably higher in the diagram. These are BM Sgr,

KS Sco, R Nor and R Cen, and they are also distinguished by an anomalous position in the (Period, A - E) diagram, which is concerned with the radial velocities shown by the absorption and emission lines in the stars' spectra (Feast 1963).

In addition R Nor and R Cen have light curves with double maxima, suggesting that they may have an affinity with stars of half the period: but in this context, S Pav also sometimes shows a double maximum and has an anomalous (A -E) yet lies at $\overline{V}(max) + K = +1.3$.

If $\overline{V}(max) + K$ is equivalent to $\overline{M}_v(max)$, then one is tempted to see a split occurring in the sequence of Miras for the stars of long period, some lying on a continuation of the sequence of shorter period stars, while others are considerably more luminous. This would affect the statistical results by reducing the overall slope of the ($\overline{M}_v(max)$, Period) relationship and raising it at the longest periods, as well as making the results heavily dependent upon the precise sample of stars chosen.

(iii) Period $<$ 200d

It has long been suggested that the shorter period stars are a mixture of groups of differing luminosities (e.g. Feast 1963). Specifically, the statistical investigations show a break in the otherwise smooth ($\overline{M}_v(max)$, Period) relationship, the shortest period group being faint. Feast (1963) suggested that there may be a mixture of fundamental and overtone pulsators here, but later invest-

igators (Barnes, 1973; Keeley, 1970a), have contested this.

The VRI measurements produce a straightforward continuation of the principal sequence of the Me variables to shorter periods, with only a hint of the increased dispersion expected. Ultimately, of course, the only way of making a strict comparison with the statistical studies would be to make observations of the same sample of stars.

(iv) The Values of K for the Globular Cluster Miras

V4 in M69 and the three Miras in 47 Tuc were measured and K determined for each of them, the results being included in table 4. These give an "apparent distance modulus" of - K = 13.0 $\pm$ 0.3, which compares favourably with $(m - M)_o$ = 13.03, E_{B-V} = 0.04, implying (m - M) = 13.15 (Hartwick and Hesser, 1974). This is a surprisingly close agreement, given the method by which the (V + K), (R - I) relationship was determined and the uncertainties in the distance modulus of Mira Ceti.

For M69, - K = 15.0 $\pm$ 0.3 was obtained, compared with 15.8 given by Hartwick and Sandage (1968). This comparison is inherently inconclusive since Lloyd Evans and Menzies (1971) have criticized Hartwick and Sandage's photometry, and the photometry here for JD 2442197 looks unreliable, possibly caused by contamination of the sky measurements. The problems of measuring individual stars in globular clusters also apply to 47 Tuc, where V1 could only be measured by offsetting it considerably in the diaphragm to eliminate a nearby (~ 5 arcsec.) star.

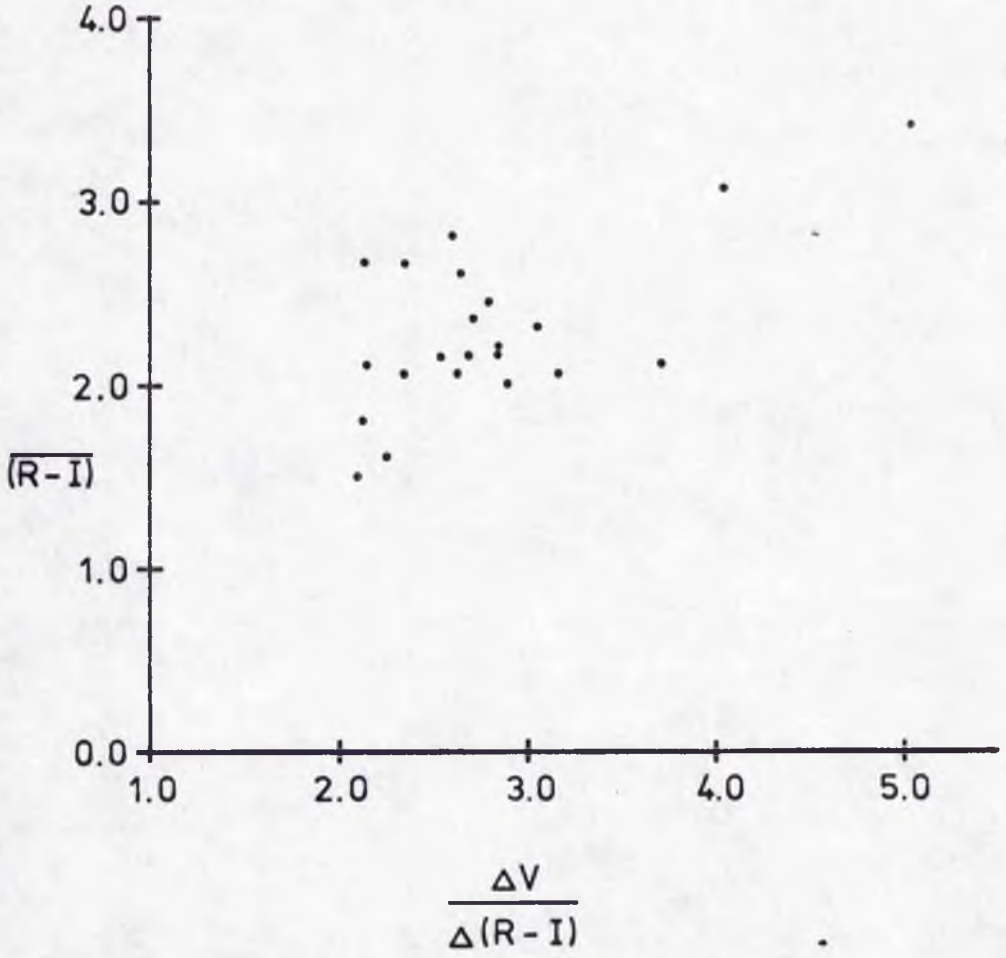

Fig. 50

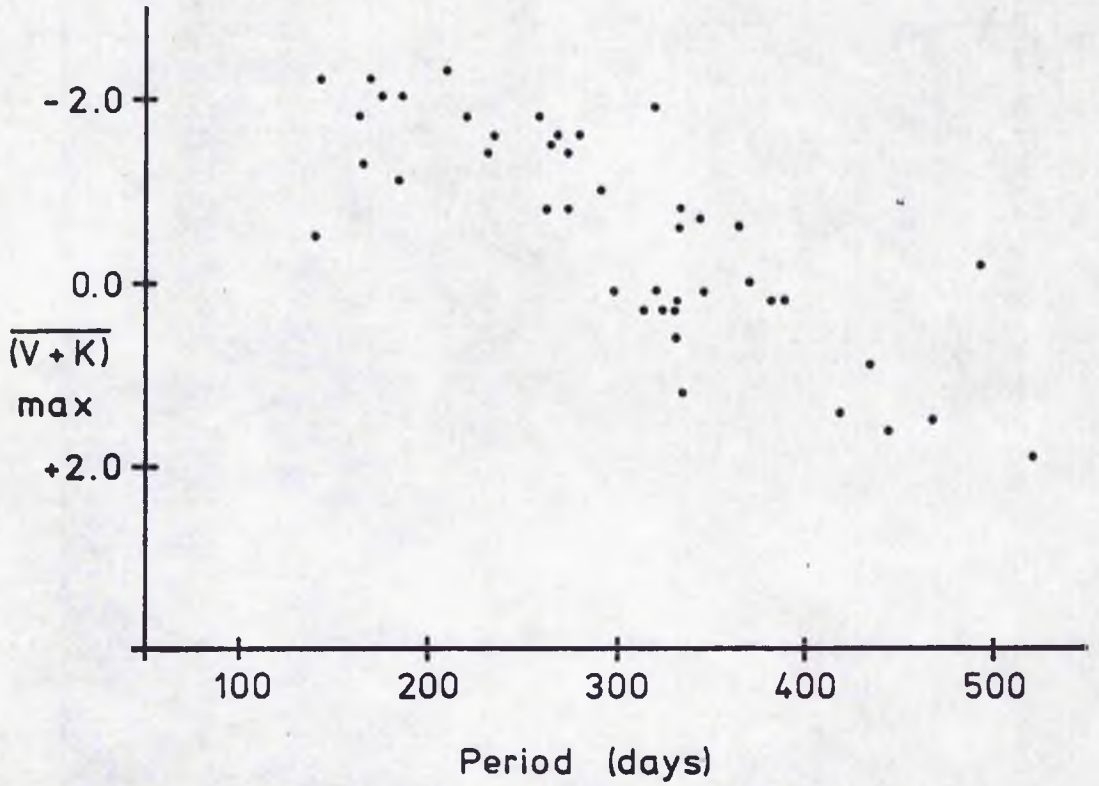

Fig. 51

(v) Barnes' Photometry

Barnes (1973) has published a considerable number of VRI observations of Miras, mainly concentrated around maximum. It has previously been noted that Barnes' (V - R), (R -I) diagram shows more scatter than that from the present measurements. A similar effect was found when a $\frac{\Delta V}{\Delta(R-I)}$, (R - I) diagram was constructed from his Me data (fig. 50), and this makes it impossible to deduce a mean (V, R - I) diagram specifically for his photometric system. An attempt was made, therefore, to analyse his results using the present relationship.

The $\overline{V}$(max) + K, P diagram (fig. 51) shows one 494 day star (Z Tau) lying well above the principal sequence, which here stretches beyond 500 days. Among the short period stars, some lie along the principal sequence while others are somewhat below it. The meaning of this has, of course, to be interpreted with caution, and Barnes states in his paper that his measurements show no hint of the suggested overtone pulsators.

(vi) Summary of the ($\overline{V}$(max) + K, P) Diagra m

Firstly, one recalls that $\overline{V}$(max) + K = F (R - I), and so this diagram is analogous to the ($\overline{R - I}$ (max), P) diagram. However, the effect of the transformation is to exaggerate somewhat the differences in (R - I).

It is tempting to distinguish three different groups of Me Miras.

Group I : A monotonic sequence running from P = 150 days, $\overline{V}(max) + K = -3$, to P = 500 days, $\overline{V}(max) + K = +2$.

Group II : A number of long period Miras lying above Group I.

Group III : Feast's overtone pulsators.

Theoretical models (Keeley, 1970a,b) have tended to show fundamental periods much longer than the periods of typical Miras, and in addition these models are rather unstable with respect to the first overtone. Perhaps one should extend Feast's idea of Miras pulsating in different harmonics to give:-

Group II : Fundamental pulsators

Group I : First overtonee pulsators

Group III : Second overtone pulsators

Stars such as R Cen and R Nor would then be regarded as having incipient first overtone effects in their light curves.

(d) <u>The Behaviour of I</u>

It has been suggested that the I magnitude should be very important for Miras (Barnes, 1973; Eggen, 1971). One expects that colour-magnitude diagrams involving I should show sizeable loops, because I will be relatively more sensitive to a red star's radius variations than will

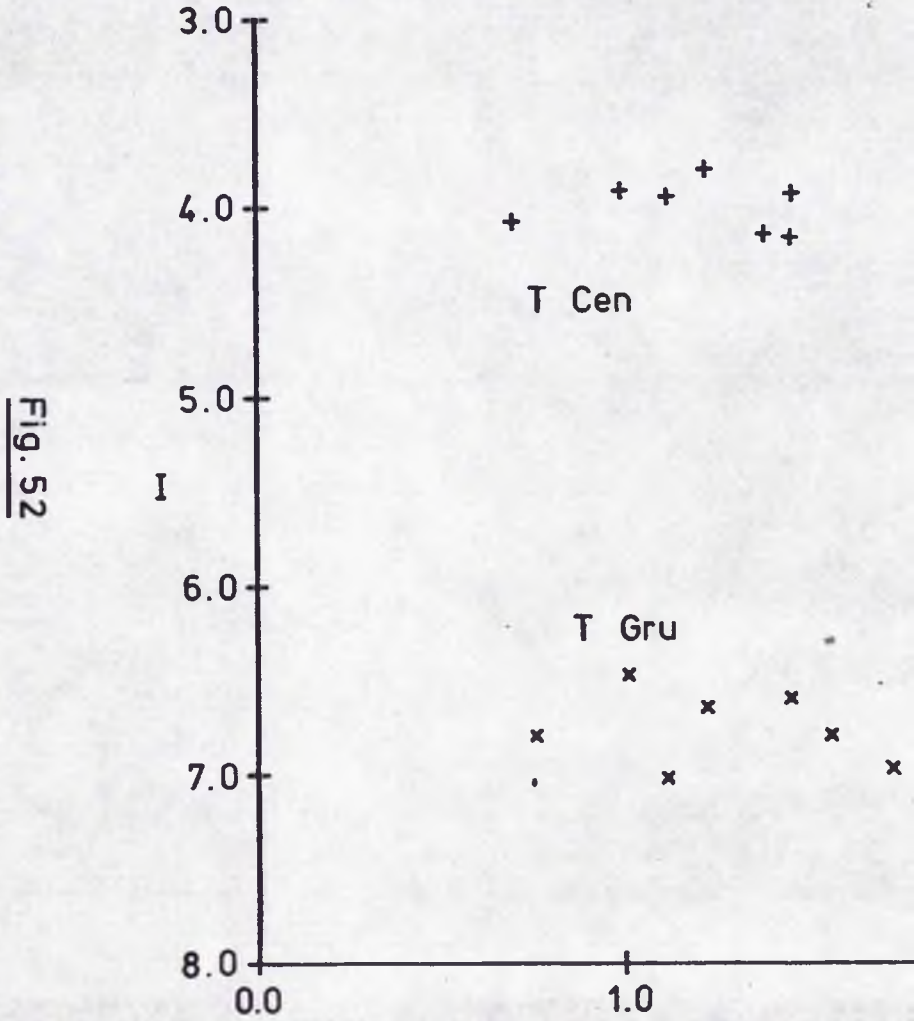

Fig. 52

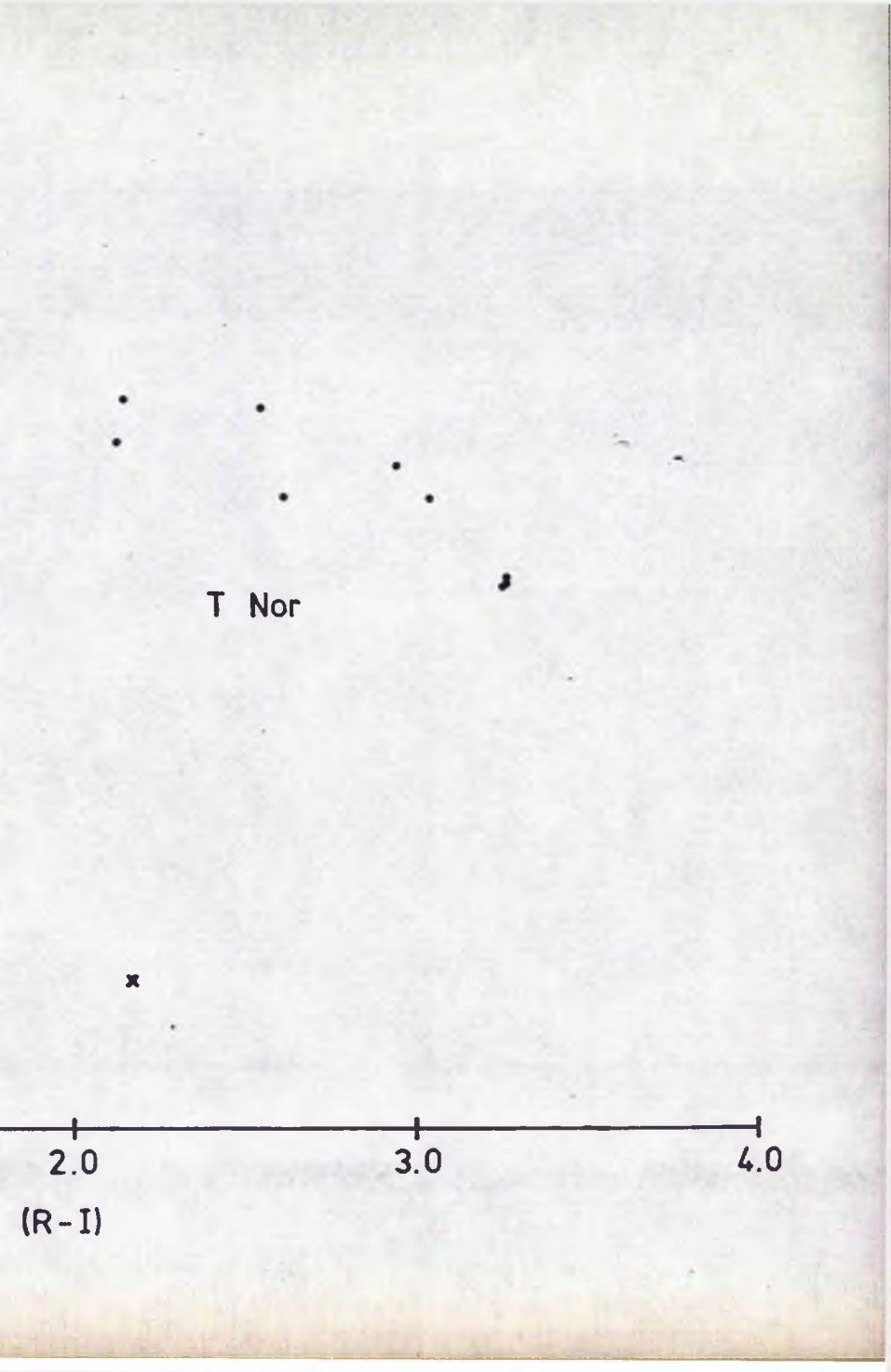
T Nor
2.0
3.0
4.0
(R-I)

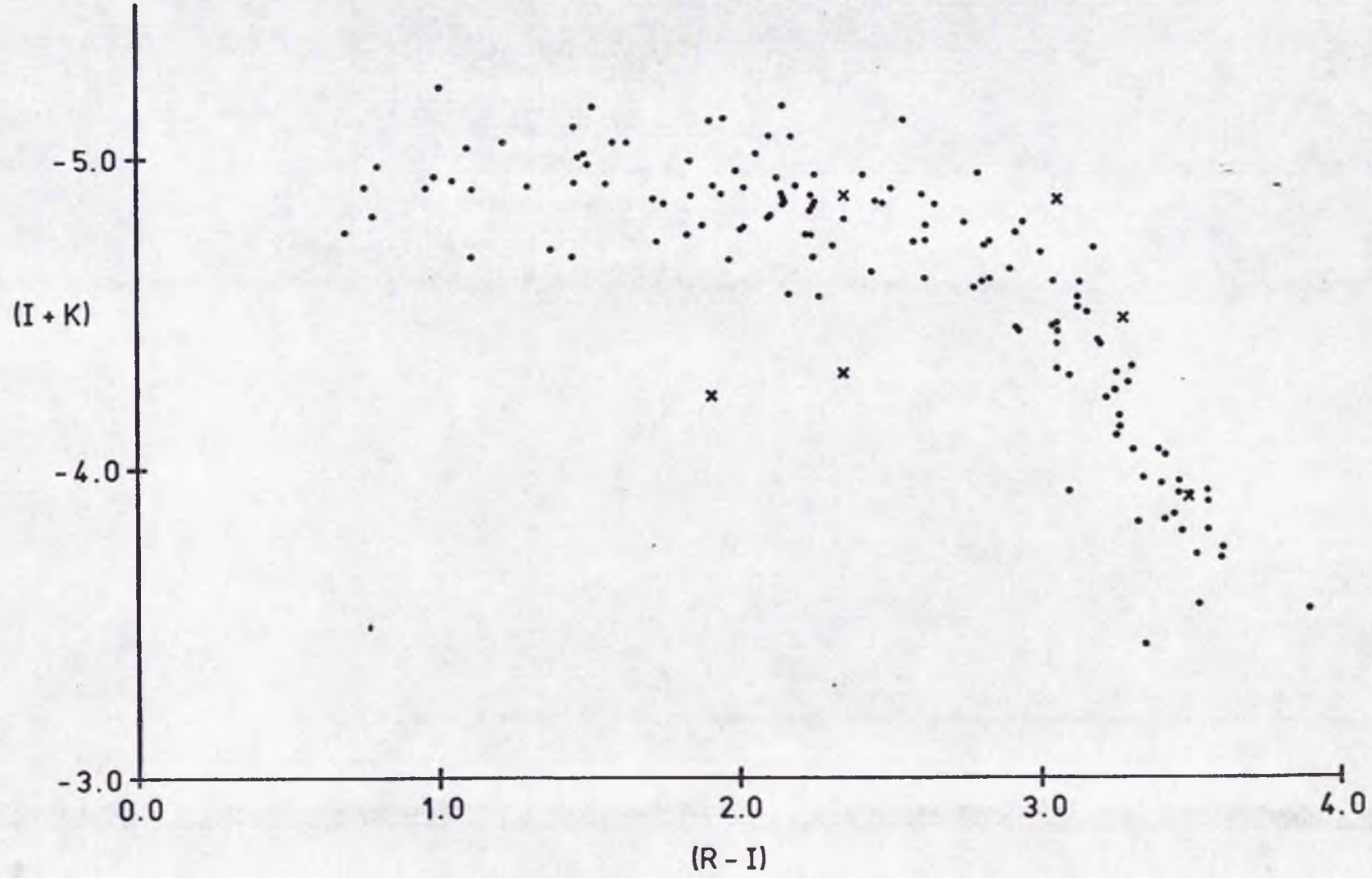

Fig. 53

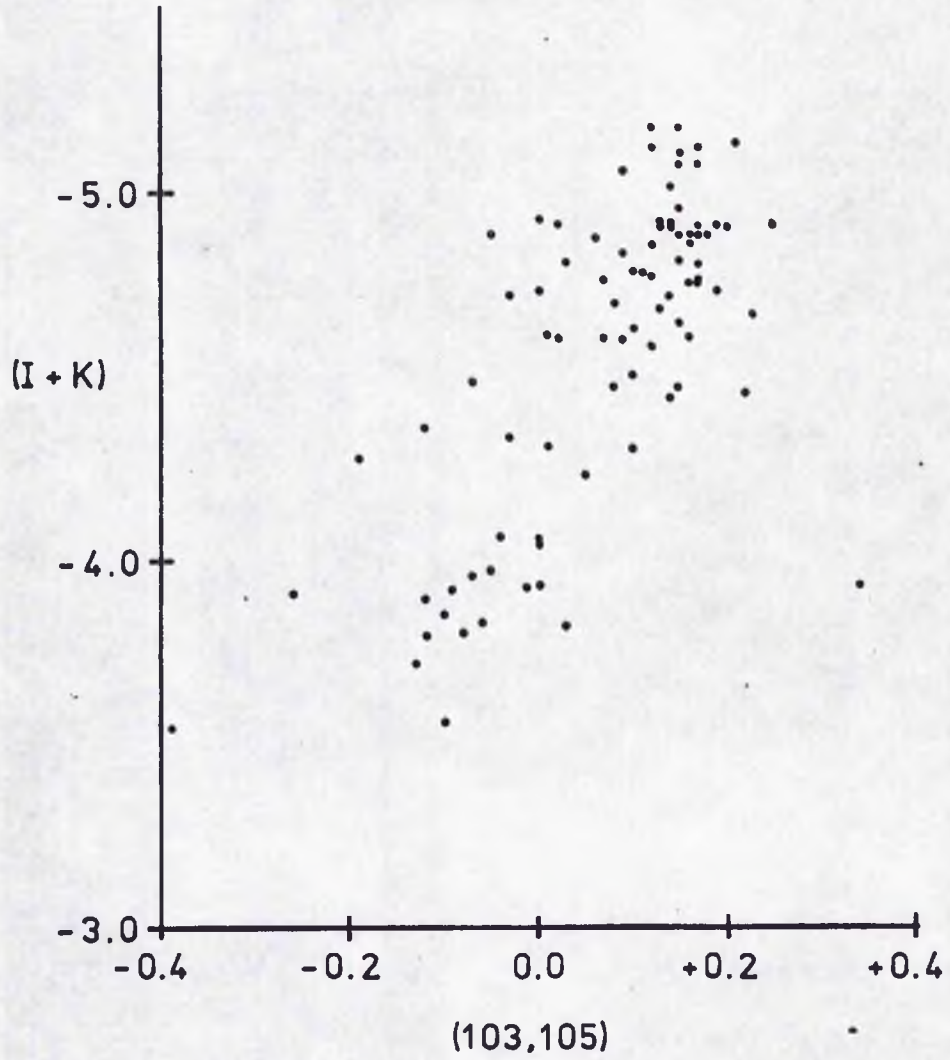

Fig. 54

V, due to I's smaller amplitude. Fig. 52 shows I plotted against (R - I) for three Me stars, T Cen (P = 91 days), T Gru (136d.) and T Nor (244d.), and it confirms this expectation.

The dependence of I on (R - I) for the Me variables as a group can be investigated by using the (I + K), (R -I) diagram. Fig. 53 shows this for all the observations of all the Me variables except R Aqr. The crosses mark the observations of R Cet, some of whose points are unexpectedly discrepant. Given that the scatter in this diagram will be mainly due to effects associated with a phase shift between the (R - I) and radius variations, the main feature displayed is the slow decrease in I with increasing (R - I) up to (R - I) $\approx$ 3.0, followed by the much more rapid decrease in I. This is an interesting and unexpected effect, and one must associate it with the similar phenomenon shown by the (103, 105), (R - I) relation (fig. 43). In fig. 54, (I + K) is plotted against (103, 105). Unfortunately, there is considerable scatter in this diagram, but one is led to the conclusion that for (R - I) $>$ + 3.0, the R and I magnitudes are both subject to blanketing by VO, such that (R - I) is not significantly affected.

(e) <u>(U - B) and Emission Line Strength</u>

The scatter in the (U - B), (R - I) diagram (fig. 31) should be due to the varying strength of the emission lines present in U. To investigate this, a straight line was drawn through the Me data shown in fig. 31, and its equation

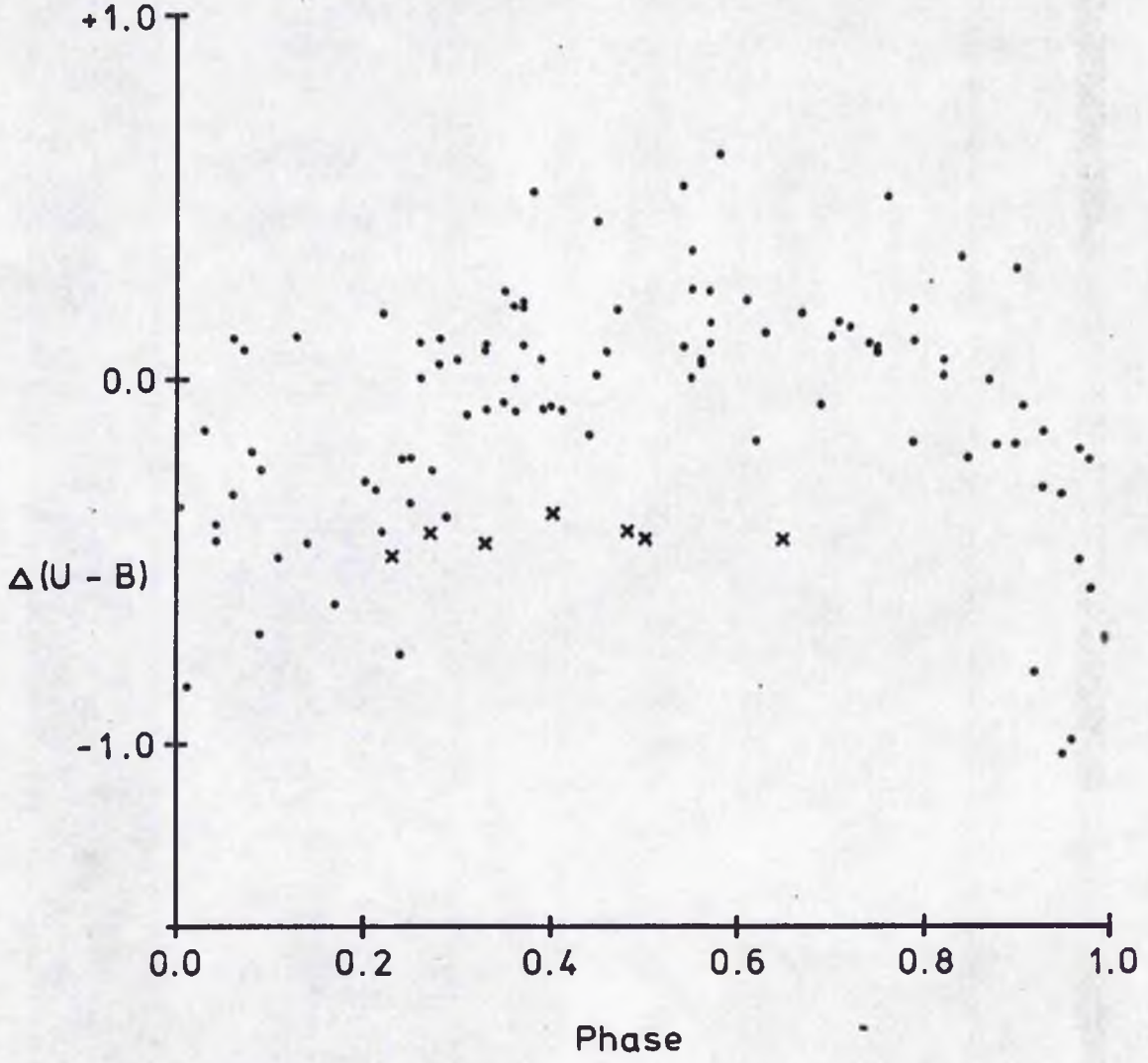

Fig. 55

determined as

$$(U - B) = 2.57 - 0.71\,(R - I).$$

This was then used to calculate the difference $\Delta(U - B)$ between each individual observation and the average $(U - B)$ value at the observed $(R - I)$. The results are shown in fig. 55, plotted against the phases determined during the production of the (V, Phase) diagram. $\Delta(U - B)$ is defined in the sense that negative values correspond to emission in U, and R Nor and R Cen are eliminated from this diagram because of their unusual light curves. Mira Ceti is plotted with crosses, showing the influence of its blue companion.

Fig. 55 exhibits the inevitable large scatter, some of which will be due to differences in the variables' amplitudes, to errors in the phases determined, to interstellar reddening, and to the presence of double stars. It is clear, however, that $\Delta(U - B)$ reaches a flat-topped maximum around phase 0.6, and a rather sharper minimum in the region of phase 0.1 to 0.2. These phase relationships are reminiscent of those deduced as probable for the variables' velocities of expansion and contraction (Pettit and Nicholson, 1933, Scott, 1942), and one is led to the conclusion that greatest emission strength as indicated by $\Delta(U - B)$ probably coincides with the stars' maximum velocity of expansion.

The values of $\Delta(U - B)$ lying in the phase intervals 0.9 to 0.3 and 0.4 to 0.8 were averaged for each individual star, enabling estimates to be obtained of the amplitudes of the variation in $\Delta(U - B)$. These amplitudes were found to be poorly correlated with period and with visual amplitude ΔV.

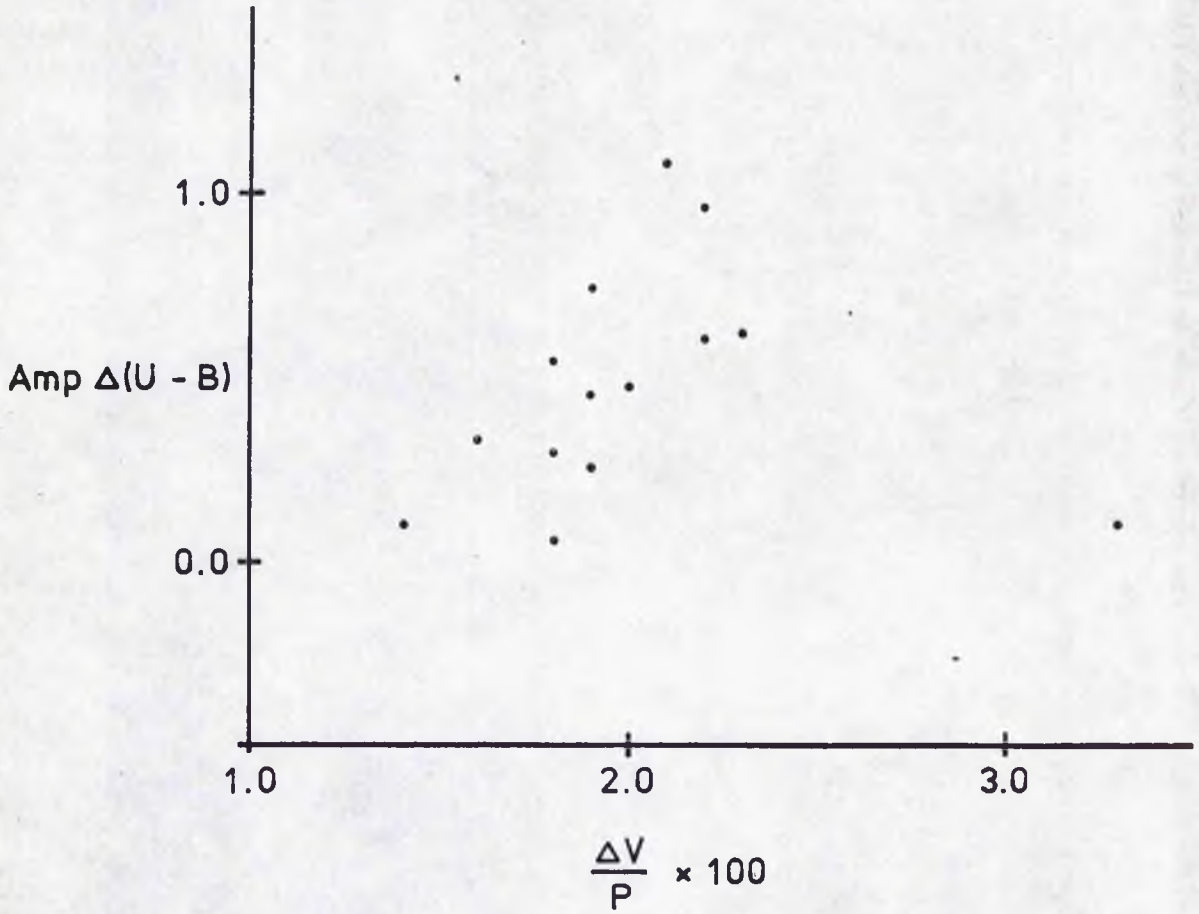

Fig. 56

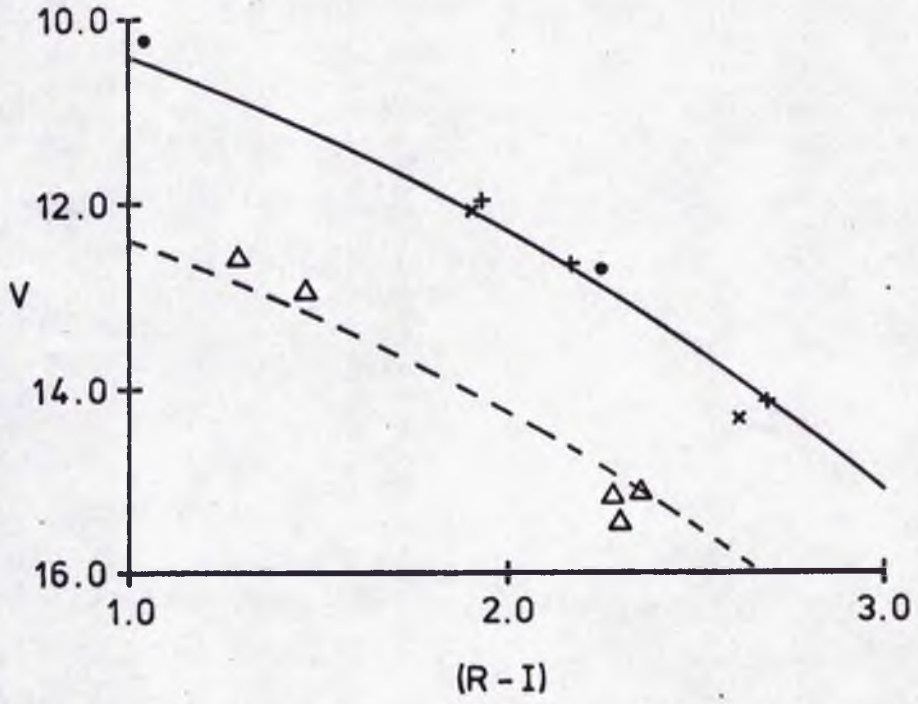

- V1 47 Tuc
× V2 ..
\+ V3 ..
△ V4 M69

Fig. 57

However, fig. 56 shows the $\Delta(U - B)$ amplitudes plotted against $\Delta V/P$, and these quantities appear to be related in the sense that a steeper light curve (large $\Delta V/P$) corresponds to stronger emission (large $\Delta(U - B)$ amplitude). Assuming that the emission lines are generated by a shock wave travelling outwards through the stellar atmosphere (e.g. Willson, 1976), then fig. 56 is consistent with the idea that stronger emission in U is associated with a stronger shock, which in turn corresponds to a steeper light curve.

The star lying away from the rest in fig. 56 is R Cet, which has a large amplitude ($5^m.5$) for its 166 day period, and has been mentioned as slightly odd with respect to the (I + K), (R - I) diagram.

(f) Particular Variables of Interest

(i) The Globular Cluster Members

The three variables in 47 Tuc and the one in M69 were mentioned in connection with testing the relationship between V + K and M_V, and fig. 57 shows the V, (R - I) diagram for these observations. The solid line indicates the function

$$V - 13.0 = 2.31 \exp(0.42 (R - I)) - 6.11,$$

in other words, the mean adopted (V + K), (R - I) relationship, assuming that K = - 13.0. The most discrepant points for the 47 Tuc variables are those for V2, observed on J.D. 2442256, when its (B - V) of 0.76 makes the measurement suspect, and of V_1 when its (R - I) of 1.04 puts it into

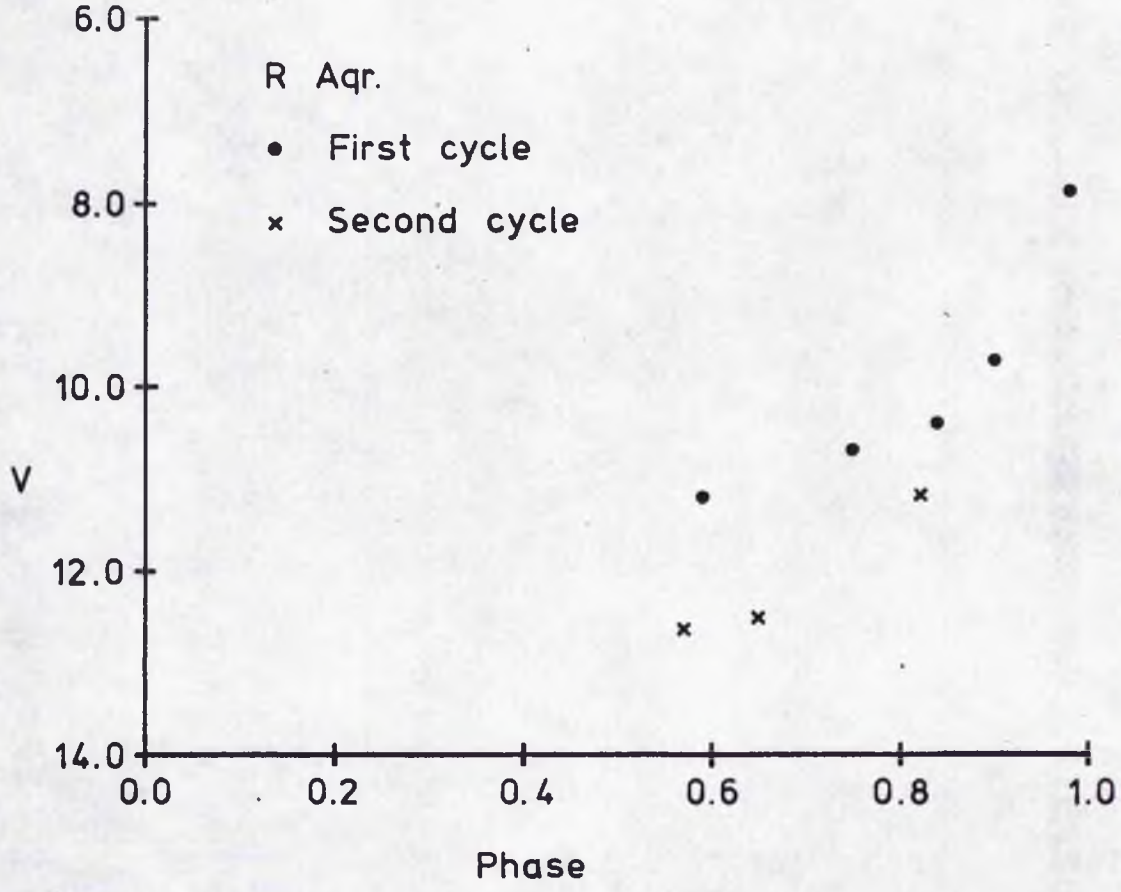
R Aqr.
First cycle
Second cycle
6.0
8.0
10.0
12.0
14.0
V
0.0
0.2
0.4
0.6
0.8
1.0
Phase

Fig. 58

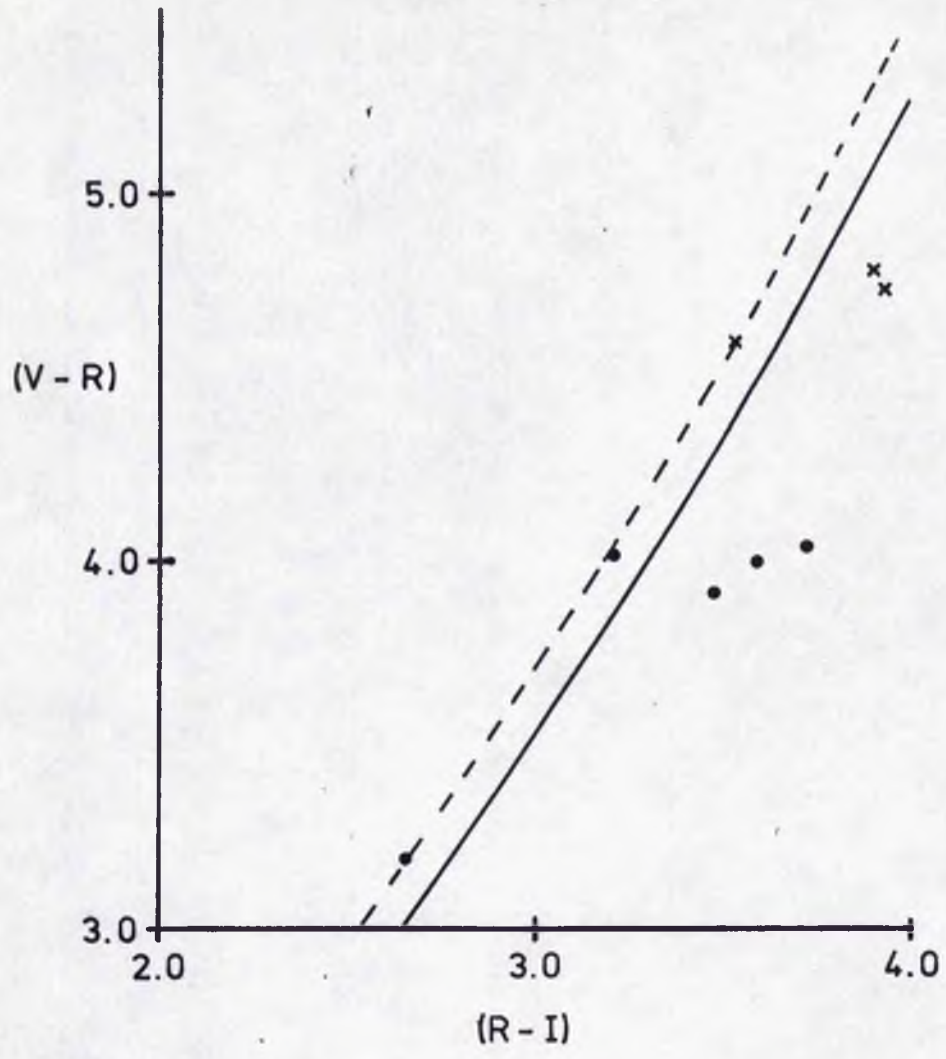

——— Mean relationship for Me stars

— — — Adopted relationship for R Aqr

Fig. 59

the region of the (V + K), (R - I) diagram where the adopted mean relation tends to fall below the observed points (fig. 47).

The observations of V4 in M69 are not a particularly good fit to the mean relation for K = - 15.0, which is indicated by the broken line. This difficulty is tentatively ascribed to the observations fainter than V = 15 being very sensitive to contamination of the sky measurements.

(ii) R Aqr P = 386 days. V = 7.3 to 10.1

R Aqr consists of an Me variable plus a Be subdwarf embedded in a nebula (Beals, 1951). Pettit and Nicholson (1933) estimated the magnitude of the blue companion by assuming their infrared measurements to be due to the Me star, and using them to predict its visual magnitude at minimum. This was then compared with the observed composite magnitude and m_v = 10 deduced for the blue star. The depth of the minima achieved by the composite object is known to vary, and this is attributed to variations in the B star.

The observations of R Aqr were spread over two cycles and are shown in fig. 58, which would indicate that the B star was unusually faint during the second minimum observed. This conclusion is supported by fig. 59, which shows the relevant portion of the (V - R), (R - I) diagram. When near minimum, the V magnitude is strongly affected by the B star, whereas R and I are mainly determined by the M star, and so the observations fall below the mean relation for the

Analysis of R Aqr

The subscripts 0, 1 and 2 refer to the observed values and those for the Mira and its companion respectively. In addition it is assumed that

$$(U-B)_1 = 0$$
$$(B-V)_1 = 1.7$$

JD	1847	1908	1943	2227	2255
V_o	11.20	10.67	10.40	12.61	12.48
B_o	12.26	11.88	11.59	13.35	13.38
U_o	11.88	11.60	11.36	12.55	12.57
V_1	12.28	11.36	10.90	13.21	12.95
B_1	14.0	13.1	12.6	14.9	14.7
U_1	14.0	13.1	12.6	14.9	14.7
V_2	11.70	11.49	11.48	13.54	13.62
B_2	12.5	12.3	12.1	13.6	13.8
U_2	12.0	11.9	11.8	12.7	12.7
$(B-V)_2$	0.8	0.8	0.6	0.1	0.2
$(U-B)_2$	-0.5	-0.4	-0.3	-0.9	-1.1

Me stars. The observations of the second cycle remain close to the mean relation for larger values of (R - I) than do those for the first cycle.

Assuming that the measured R and I are due to the Mira alone, one can calculate, with the aid of the (V - R), (R - I) diagram, the magnitudes V_1 and V_2 of the Me and Be stars separately. If one further assumes that the Me star has $(B_1 - V_1) \approx 1.7$, $(U_1 - B_1) \approx 0.0$ when it is faint, one can calculate B_2 and U_2 for the Be star. The table lists the results of this procedure, along with the Julian Date of the observations.

The values of V_2 must be considered to be fairly reliable, and although the amplitude of the variation seems rather large, it is comparable with that reported for the Be companion of Mira Ceti (Joy, 1954). The colours deduced are rather more surprising, particularly their change from one year to the next. The deduction of the values of U_2 and B_2 rests on the assumed colours of the Me star, which are made difficult to estimate because of its extreme redness ($R - I > 3.5$), but it is probably safe to assume that U_2 and B_2 are affected both by emission lines from the B star and also by radiation from the nebula. In other words, the U_2 B_2 V_2 values apply to the combination of the B star and the nebula, both of which probably vary.

This object is clearly worth an extended observational study.

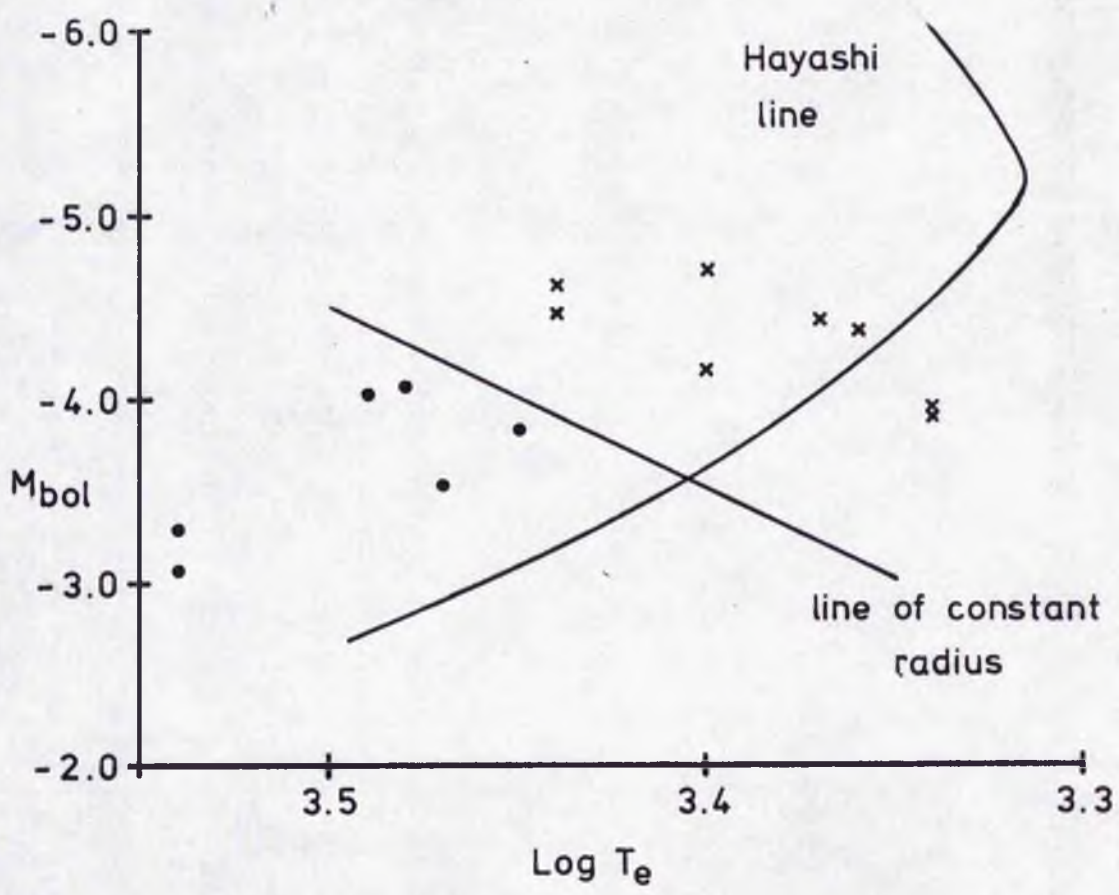
-6.0
-5.0
-4.0
-3.0
-2.0
M_{bol}
Hayashi
line
line of constant
radius
3.5
3.4
3.3
Log T_e

Fig. 60

Applications of the VRI Photometry to Theory

(I) The (M_{bol}, log Te) Diagram

Mendoza V's (1966) results can be used to calibrate log Te and (M_{bol} - V), for the Me stars, in terms of (R - I) (fig. 9), although with the reservation that the (R - I), log Te diagram shows a large scatter and few points.

The relationships obtained were

$$\log Te = 3.63 - 0.088\ (R - I)$$

and

$$M_{bol} - M_v = m_{bol} - V = 2.31 - 2.89\ (R - I)$$

Additionally assuming

$$V - M_v = - K$$

gives

$$M_{bol} = 2.31 - 2.89\ (R - I) + V + K$$

(a) Radius Variations

Fig. 60 shows the positions of two representative Me stars in the (M_{bol}, log Te) diagram, along with the supposed Hayashi line from fig. 15. The behaviour of any individual star in this diagram is, of course, independent of the assumption concerning K, and so we consider this behaviour first.

By the definition of effective temperature, the surface brightness of a star is proportional to Te^4, and so a star of luminosity L will have

$$\begin{aligned} M_{bol} &= - 2.5 \log (L/Lo) \\ &= \text{const.} - 2.5 \log Te^4 - 2.5 \log \pi r^2 \\ &= \text{const.} - 10 \log Te - 5 \log r. \end{aligned}$$

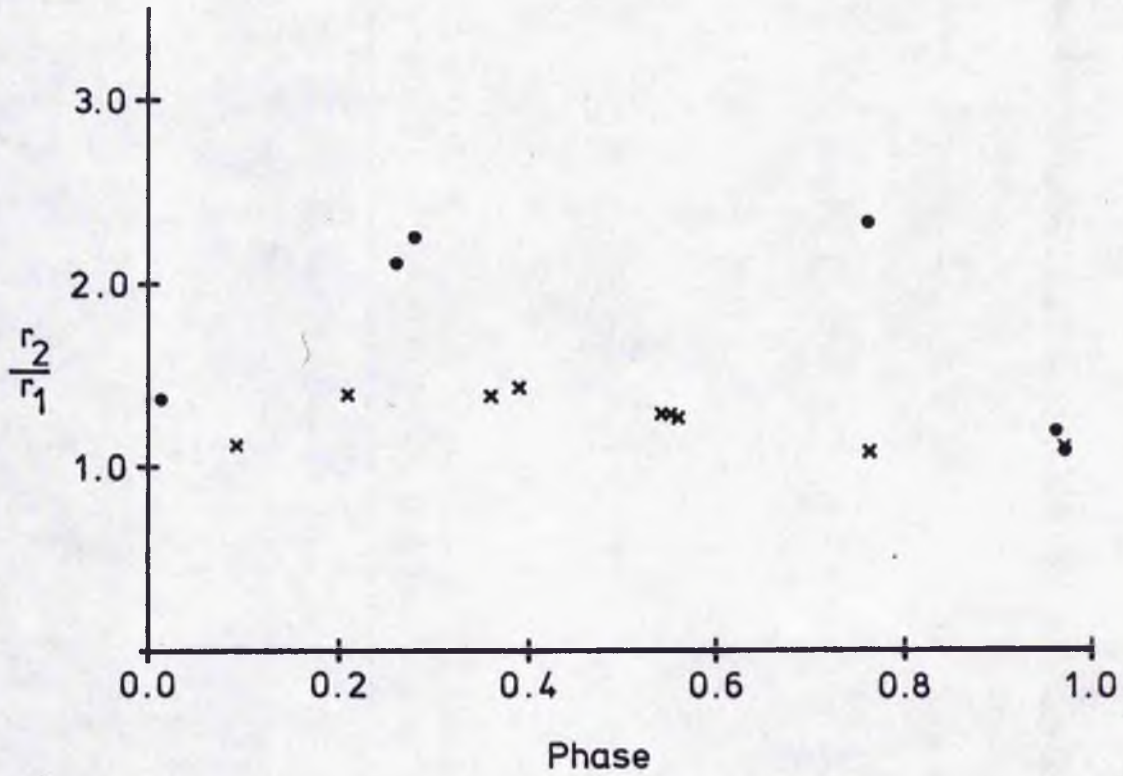

Fig. 61

Suppose the star varies from (T_1, r_1) to (T_2, r_2), then

$$\Delta M_{bol} = -10 \log \frac{T_1}{T_2} - 5 \log \frac{r_1}{r_2}$$

Fig. 61 shows the deduced radii for S Car and T Nor, computed relative to the point of minimum radius inferred from fig. 60, and plotted against the phases obtained during the production of the mean (V, Phase) diagram. The interesting feature in fig. 61 is that whereas T Nor (P = 286d.) shows a 40% change in radius, which is similar to Pettit and Nicholson's (1933) result, S Car seems to change its radius by a factor of two. This is very surprising, but it is consistent with the orientation of S Carinae's loop in the (M_{bol}, log Te) diagram, relative to the line of constant radius.

The behaviour of T Nor and S Car is typical of the other Me stars observed, and so one is led to the conclusion that the shorter period stars show larger radius variations, and this general conclusion is only invalidated if the (M_{bol} - V) and log Te calibrations are wildly out.

(b) The Me sequence in the (M_{bol}, log Te) Diagram

The mean (V + K), (R - I) relation cannot be used when considering the movement of an individual variable in the (M_{bol}, log Te) diagram. This is because the mean (V + K), (R - I) relation specifically ignores the effect of the stars' radius variations when those variations are out of

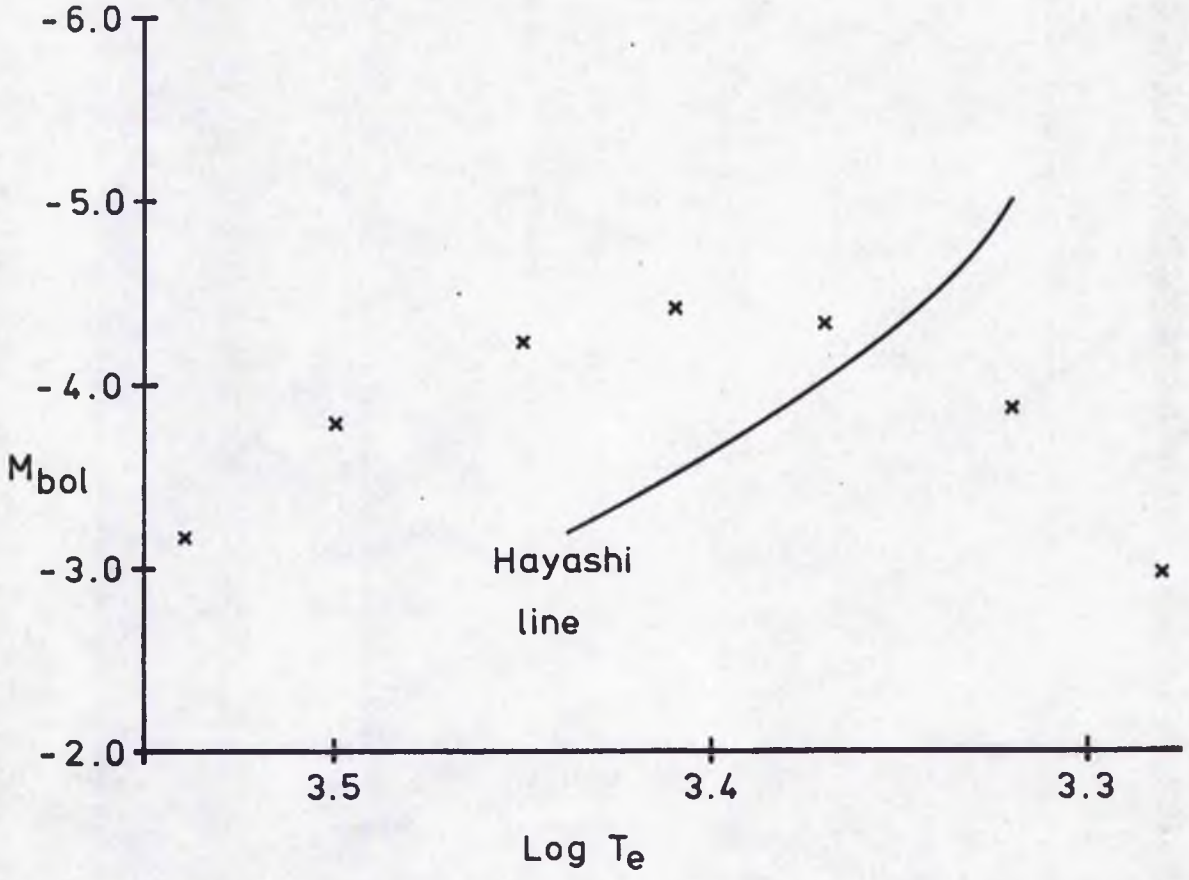

Fig. 62

phase with (R - I), and so its use would eliminate one of the main features of the (M_{bol}, log Te) diagram. However, if one wishes to compare the sequence of Me variables with theoretical models, one is interested only in the characteristic positions of the stars, for example the centroids of their loops in the (M_{bol}, log Te) diagram.

For this purpose we put

$$M_v = V + K = 2.31 \exp (0.42 (R - I)) - 6.11$$

Therefore

$$M_{bol} = 2.31 \exp (0.42 (R - I)) - 2.89 (R - I) - 3.8$$

and

$$\log Te = 3.61 - 0.088 (R - I)$$

Fig. 62 shows the points for $\overline{R - I}$ = 1.0 to 4.0 in steps of 0.5. Disappointingly the shape of this sequence does not follow the shape of the probable Hayashi line. However, the two loci do not cross until $\overline{R - I} \approx +3.2$, which is approximately the colour of the reddest star observed during the present programme. The conclusion must be that Mendoza's scales of M_{bol} and Te greatly reduce the discrepancy between theory and observation noted by Keeley (1970a).

(II) <u>The Pulsation Constant, Q</u>

(a) <u>The Computation of Q</u>

(i) <u>The basic formulae</u>

By definition,

$$Q = P \sqrt{\frac{\overline{\varrho}}{\overline{\varrho_\odot}}}$$

where $\overline{\rho_\odot}$ = mean solar density.

Introducing the stellar mass $\mathcal{M}$ and radius r,

$$Q = P \left(\frac{\mathcal{M}}{\mathcal{M}_\odot}\right)^{\frac{1}{2}} \left(\frac{r_\odot}{\bar{r}}\right)^{3/2}$$

Also $$\frac{L}{L_\odot} = \left(\frac{r}{r_\odot}\right)^2 \left(\frac{T}{T_\odot}\right)^4$$

where T and $T_\odot$ are effective temperatures.

Therefore

$$Q = P \left(\frac{\mathcal{M}}{\mathcal{M}_\odot}\right)^{\frac{1}{2}} \left(\frac{L_\odot}{\bar{L}}\right)^{\frac{3}{4}} \left(\frac{\bar{T}}{T_\odot}\right)^3$$

In addition

$$M_{bol} - M_{bol0} = -2.5 \log \left(\frac{L}{L_\odot}\right) ;$$

and using

$$M_{bol0} = 4.72$$

$$T_\odot = 5800$$

$$\mathcal{M}_\odot = 1$$

gives

$$\log Q = \log P + 0.5 \log \mathcal{M} + 0.3\bar{M}_{bol} + 3\log \bar{T} - 12.71$$

(ii) The dependence on mass

Feast (1963) has shown that the kinematic characteristics of Miras as a function of period are consistent with there being a relationship between mass and period. He deduced

that Me stars of short period (200d.) have $\mathcal{M} \approx 1$, whereas the longer period variables have $\mathcal{M} \approx 2$. We can conveniently indicate this dependence by setting

$$\log \mathcal{M} = \log P - 2.30$$

Hence

$$\log Q = 1.5 \log P + 0.3\bar{M}_{bol} + 3 \log\bar{T} - 13.86.$$

(iii) The dependence on M_v and $(R - I)$

Using

$$M_{bol} - M_v = 2,31 - 2,89\ (R - I)$$

$$\log T = 3.63 - 0.088\ (R - I)$$

gives

$$\log Q = 1.5 \log P + 0.3\bar{M}_v - 1.13\ \overline{(R - I)} - 2.28$$

Given the value of Q, this equation represents a period - luminosity - colour (P - L - C) relationship and so provides a means of computing absolute magnitudes. Some implications of this are considered in the next section. Here we assume

$$M_v = V + K = 2.31 \exp(0.42(R - I)) - 6.11$$

Hence

$$\log Q = 1.5 \log P + 0.69 \exp(0.42\ (R - I)) - 1.13\ \overline{(R - I)} - 4.11$$

It has been mentioned previously that a choice has to be made concerning which values of the stars' periodically varying characteristics have to be used in the calculation

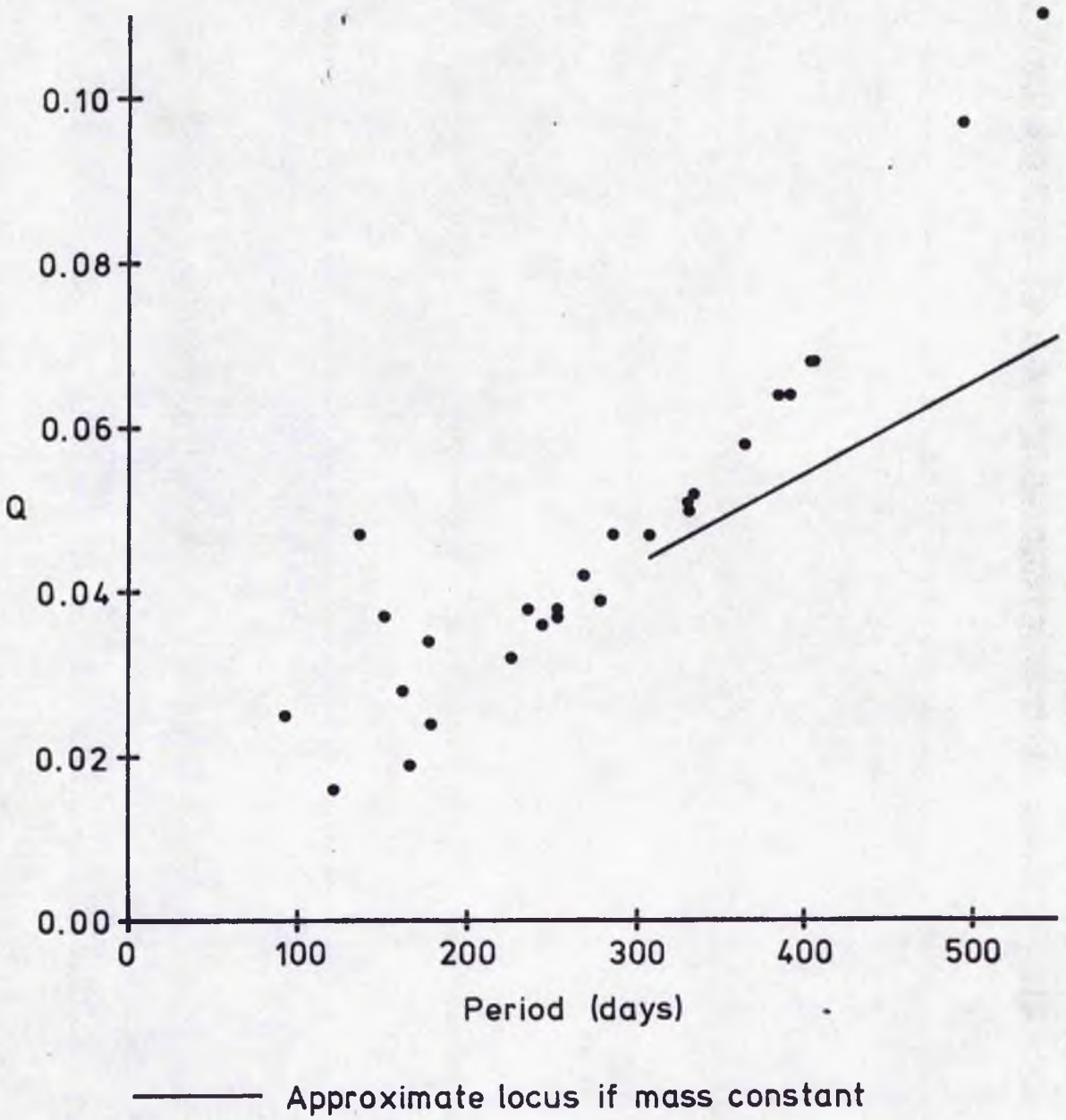
0.10
0.08
0.06
Q
0.04
0.02
0.00
0
100
200
300
400
500
Period (days)
Approximate locus if mass constant

Fig. 63

Keeley's Model Calculations for Fundamental and Overtone Pulsators

M_{bol}	Fractional Core Mass	R (10^{13} cm)	P_o	Q_o	P_1	Q_1
-3.75	0.94	1.15	180	0.098	70	0.038
-3.75	0.88	1.31	220	0.098	81	0.036
-3.75	0.57	1.65	310	0.098	125	0.039
-4.55	0.93	1.86	434	0.114	-	-
-4.55	0.85	2.22	640	0.129	175	0.035
-4.55	0.64	2.65	865	0.160	250	0.046
-4.55	0.40	3.07	1600	0.198	330	0.041
-4.55	0.20	3.37	>2500	>0.27	-	-
-4.95	0.73	3.26	1190	0.135	290	0.033

of Q. In the present case we have eliminated all the periodic quantities in terms of (R - I), and so we choose $\overline{(R - I)}$ to be that value, computed from the mean value of V reached by any variable during its cycle.

Fig. 63 shows the values of Q obtained for the better observed Me stars in the present programme, plotted against period. The actual values fall in the same range as those produced by Keeley's (1970a) calculations (shown in the table), but the very strong dependence of Q on period is rather worrying. An interesting feature of fig. 63 is the large scatter which appears at shorter periods, with some stars lying at higher Q values than the bulk of the remainder. The position of these stars is not consistent with their pulsating in a higher mode of vibration.

The apparent strong dependence of Q on period could be spurious due to two possible causes. Firstly, the masses assumed are tied to the mass of the stars at the main sequence turn-off of groups of stars with similar kinematic characteristics. In other words, these masses are estimates of those the variables had when they left the main sequence, and so take no account of the mass probably lost by these stars. Assuming that $\mathcal{M}$ = const. $\simeq$ 1 shifts the values of Q to the region of the line shown in the (Q, P) diagram.

Changing the mass dependence still leaves a very inconstant Q, which ultimately can only be made constant by discarding the present M_v, (R - I) relationship.

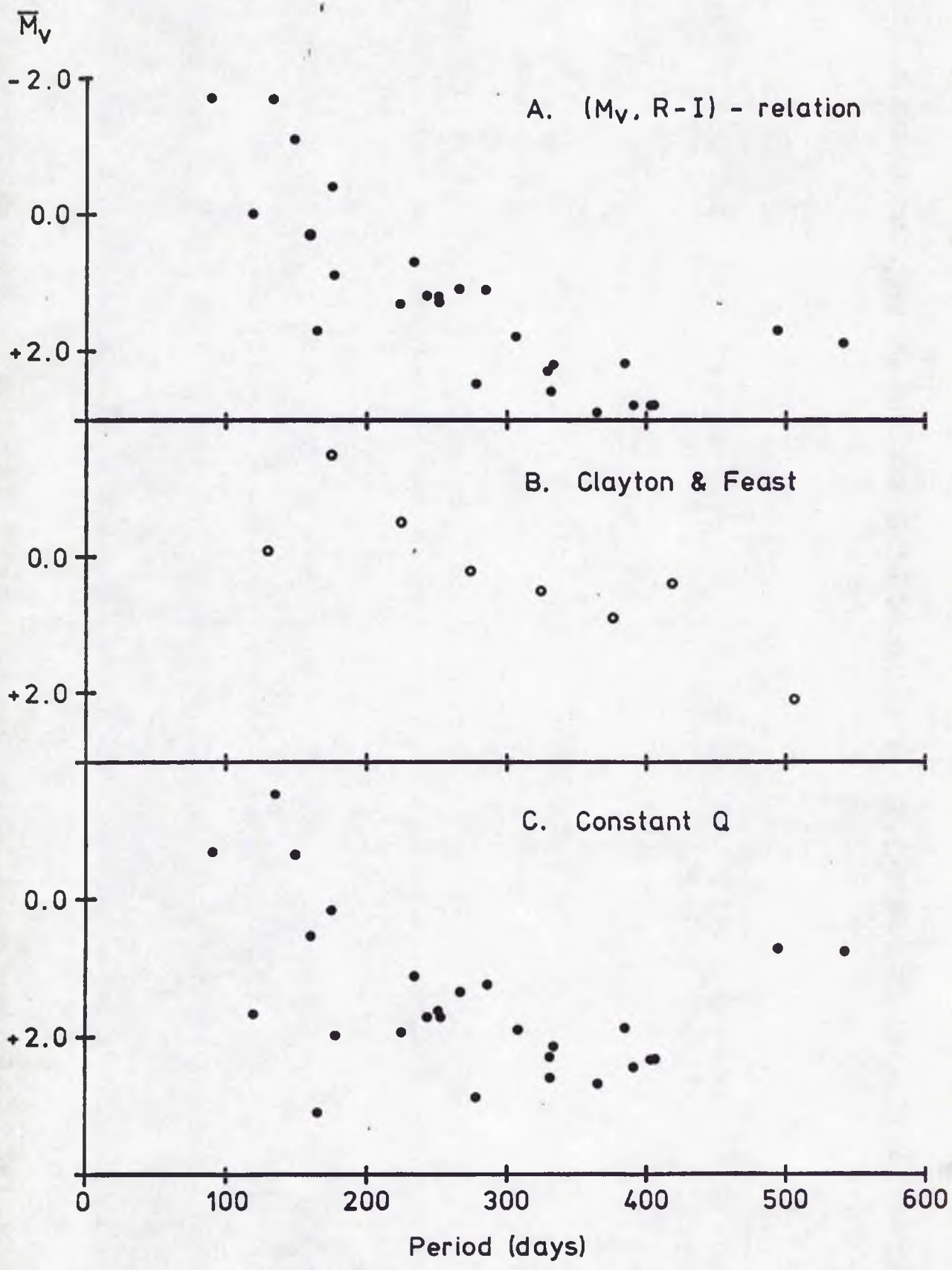
$\overline{M}_V$
-2.0
0.0
+2.0
A. (M_V, R-I) - relation
B. Clayton & Feast
C. Constant Q
0
100
200
300
400
500
600
Period (days)

Fig. 64

(b) Q and Absolute Magnitudes

Recalling that

$$\log Q = 1.5 \log P + 0.3 \bar{M}_v - 1.13 (\overline{R - I}) - 2.28$$

provided

$$\log \mathfrak{M} = \log P - 2.30,$$

then if Q is a constant, $\bar{M}_v$ is calculable. By assuming $V - M_v = 4.2$ for Mira Ceti, we find that

$$Q = 0.051$$

Therefore

$$\bar{M}_v = 3.3 + 3.77 (\overline{R - I}) - 5 \log P.$$

Fig. 64 shows the three ($\bar{M}_v$, P) diagrams obtained from assuming the (M_v, R - I) relation, from Clayton and Feast's (1969) kinematical studies and from assuming the constancy of Q.

It is interesting to look at the third of these diagrams, with a view to explaining the outstanding long and short period stars in terms of different modes of vibration. For Mira variables it is a useful rule-of-thumb to apply the analogy of an organ pipe closed at one end. The air in such a pipe will have modes of vibration whose frequencies have the ratios 1 : 3 : 5 : 7 ..., and we are probably interested in trying to explain the data in terms of the lowest possible modes. Keeley (1970a) and Langer (1971) have calculated theoretical values of the ratios for Miras, and the results are

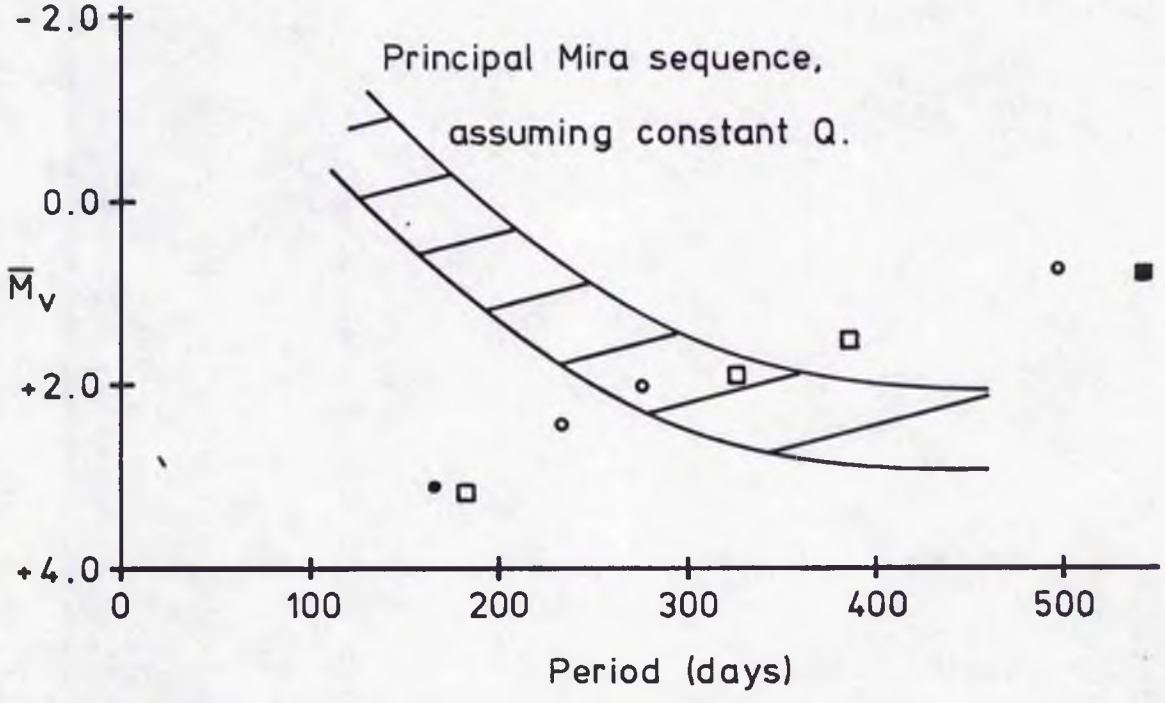

- • R Cet, observed.
- ○ R Cet, period multiplied by 7/5, 5/3 and 3.
- ■ R Cen, observed.
- □ R Cen, period multiplied by 5/7, 3/5 and 1/3.

Fig. 65

$$\frac{P_o}{P_1} = 2.5 \text{ to } 4$$

$$\frac{P_1}{P_2} = 1.2 \text{ to } 1.4$$

Two exceptional stars in fig. 64c are R Cet ($166^d, 3^m.1$), and R Cen (542^d, $0^m.8$), and fig. 65 shows the consequences of assuming that they are stars harmonically related to the principal sequence of Miras. Adopting the 1 : 3 ratio improves the calculated position of neither star, and in fact they merely exchange places. Both give potentially convincing results when their periods are corrected by the factors 3 : 5 or 5 : 7. Summarizing, the positions of R Cet and R Cen in fig. 64c are best explained if the ratios of the frequencies of variation R Cen : typical Miras : R Cet are 3 : 5 : 7.

(c) <u>The Accuracy of the Determination of Q</u>

Reintroducing the mass into the P - L - C relation gives

$$\log Q = \log P + 0.5 \log \mathfrak{M} + 0.3\bar{M}_v - 1.13(\overline{R - I}) - 1.13$$

Assume that P, $\overline{R - I}$ and the bolometric correction and effective temperature calibrations are error-free, and that $\bar{M}_v$ and $\mathfrak{M}$ have been wrongly estimated, the true values being $\bar{M}_v^{\,1}$ and $\mathfrak{M}^1$

Set $\bar{M}_v^{\,1} = \bar{M}_v + m$

$\mathfrak{M}^1 = \alpha \mathfrak{M}$

then $\log Q^1 = \log Q + 0.5 \log a + 0.3m.$

m is essentially the error in the distance modulus, and this could be of the order of $0^m.5$.

Setting

$$m = 0.5$$

$$a = 1.2$$

gives

$$\log Q^1 = \log Q + .04 + .15$$

$$\frac{Q^1}{Q} = 1.5$$

It can be seen that a 50% error in Q determinations is not at all unlikely, even neglecting the problem of choosing the correct phase at which to make the computation.

Summary: The State of the Photometry of Mira Variables

The spectra of Mira variables have been studied extensively for a long time. Merrill's (1940) monograph still provides an adequate coverage of the subject when combined with Merrill (1960) and Merrill and Deutsch (1959). The kinematics of the stars have also been investigated a number of times, a general discussion of the kinematic properties, as well as an attempt at luminosity classification of the spectra, being presented by Feast (1963).

In contrast, the photometry of Miras has been mainly restricted to the visual estimates by amateurs (Campbell, 1955). Smak (1966) demonstrated the properties of Miras with respect to UBV photometry, but the obscure nature of those properties meant that Mendoza V's (1967) multicolour photometry must mark the starting point of attempts to extract the astrophysical data photometrically. Since then, Barnes (1973) in VRI, and Eggen (1975) in UBVRI, have begun building a body of photoelectric data which must soon become voluminous enough to warrant extensive cross-comparisons. Future photoelectric work should be slanted, firstly, towards obtaining complete VRI light curves of some Miras, in other words, following their variations through individual cycles. Secondly, UBVRI photometry should continue, given that R and I introduce the possibility of interpreting the UBV results. Finally, an attempt should be made to extend and improve Mendoza V's bolometric corrections and effective temperatures.

Table 1. Comparison Stars for Mira Variables

The first column lists the HD numbers of the comparison stars, along with their associated variables. The main body of the table gives the results of the ten colour photometry, and underneath each figure are listed the number of observations in that colour and its probable error in units of $0^m.001$.

HD	U-B	B-V	V	V-R	R-I	63,65	65,103	81c	103,105
1187	1.564	1.352	5.647	1.010	0.689	0.012	1.212	0.017	0.080
S Scl	11	11	13	6	14	11	11	10	10
	2	2	8	5	4	5	5	5	5
12642	1.956	1.589	5.618	1.313	1.055	0.087	1.646	0.153	0.126
o Cet	14	14	19	10	19	13	13	13	13
R Cet	3	3	5	3	3	5	5	5	5
15220	1.393	1.244	5.882	0.906	0.611	0.007	1.090	-0.001	0.069
R For	10	10	15	9	15	9	9	9	9
	2	2	7	3	4	5	5	5	5
16074	1.643	1.394	5.731	1.050	0.730	0.013	1.277	0.057	0.103
U Cet	7	7	10	5	10	6	6	6	6
	3	3	8	5	5	7	7	7	7
20559	0.827	1.031	5.395	0.805	0.556	0.008	0.980	0.012	0.086
X Cet	5	5	10	7	10	4	4	4	4
	4	4	8	5	5	20	20	20	20
25803	1.173	1.158	6.111	0.850	0.577	0.005	1.042	0.028	0.058
T Eri	7	7	11	7	11	6	6	6	6
	3	3	8	5	5	10	10	10	10
30202	1.820	1.478	6.229	1.129	0.814	0.065	1.357	0.125	0.110
R Cae	3	3	6	5	6	2	2	2	2
	5	5	10	8	8	10	10	10	10

HD	U-B	B-V	V	V-R	R-I	63,65	65,103	81c	103,105
31414	0.711	0.938	5.691	0.700	0.485	-0.006	0.865	0.054	0.047
R Lep	4	4	8	4	8	4	4	4	4
	3	3	10	10	7	10	10	10	10
34642	0.796	0.993	4.819	0.773	0.534	-0.001	0.954	0.073	0.062
T Col	4	4	8	4	8	4	4	4	4
	5	5	8	10	7	8	8	8	8
37763	1.202	1.133	5.196	0.867	0.566	0.014	1.017	-0.022	0.088
R Oct	.2	2	4	4	6	2	2	2	2
	10	10	10	10	8	20	20	20	20
45433	1.592	1.385	5.546	1.043	0.726	0.026	1.245	0.050	0.109
V Mon	4	4	8	4	8	4	4	4	4
	5	5	8	10	7	5	5	5	5
76579	1.874	1.549	5.940	1.197	0.862	0.042	1.432	0.083	0.071
T Hya	4	4	6	3	7	4	4	3	3
	10	10	10	10	8	20	20	30	30
82858	1.412	1.345	6.266	1.033	0.736	0.018	1.289	0.018	0.071
R Car	6	6	7	4	9	6	6	3	3
	5	5	10	10	5	8	8	10	10
85656	1.321	1.311	5.566	0.961	0.680	0.011	1.234	-0.026	0.056
S Car	5	5	5	3	7	5	5	2	2
	5	5	10	10	8	10	10	20	20
105639	1.113	1.123	5.954	0.844	0.564	-0.006	1.053	0.019	0.061
SS Vir	4	4	4	3	6	4	4	1	1
	3	3	10	10	8	10	10	20	20
116292	0.741	0.984	5.346	0.732	0.494	-0.021	0.896	0.085	0.110
R Hya	5	5	3	2	6	5	5	1	1
	3	3	15	20	8	10	10	20	20
119971	1.415	1.360	5.459	1.061	0.759	0.009	1.306	0.070	0.073
RV Cen	5	5	4	2	6	5	5	2	2
	6	6	10	20	8	10	10	10	10

HD	U-B	B-V	V	V-R	R-I	63,65	65,103	81c	103,105
121056	0.868	1.011	6.174	0.769	0.519	-0.008	0.951	0.043	0.075
T Cen	7	7	6	2	8	7	7	4	4
	5	5	10	20	7	10	10	20	20
122210	1.285	1.265	6.112	0.952	0.676	0.001	1.186	0.040	0.070
RT Cen	5	5	4	2	6	5	5	2	2
	6	6	10	20	8	10	10	20	20
126241	1.771	1.504	5.850	1.096	0.776	0.028	1.388	-0.003	0.076
R Cen	5	5	4	2	6	5	5	2	2
	4	4	10	20	8	8	8	10	10
128068	1.716	1.493	5.532	1.134	0.799	0.025	1.376	0.031	0.063
S Lup	6	6	4	1	6	6	6	3	3
	5	5	10	20	8	10	10	20	20
141544	1.065	1.155	6.005	0.893	0.627	0.005	1.107	0.056	0.077
T Nor	7	7	6	2	8	7	7	4	4
	5	5	8	20	7	5	5	10	10
146850	1.508	1.537	5.989	1.254	0.906	0.026	1.548	0.055	0.109
V Oph	4	4	8	5	8	4	4	3	3
	10	10	8	10	8	10	10	20	20
147700	0.805	1.013	4.479	0.751	0.507	-0.001	0.935	0.002	0.112
RZ Sco	4	4	7	5	8	4	4	2	2
	4	4	10	10	7	10	10	10	10
152636	2.110	1.753	6.330	1.455	1.129	0.074	1.803	0.123	0.105
RR Sco	7	7	10	5	11	7	7	5	5
	5	5	8	10	5	10	10	10	10
182629	1.253	1.230	5.563	0.916	0.637	0.018	1.130	0.023	0.062
R Sgr	17	17	14	4	18	16	16	11	11
T Sgr	2	2	5	10	3	5	5	5	5
188603	1.555	1.465	4.526	1.063	0.738	0.028	1.318	0.006	0.082
RR Sgr	12	12	12	3	14	11	11	9	9
	2	2	5	15	5	5	5	5	5

HD	U-B	B-V	V	V-R	R-I	63,65	65,103	81e	103,105
212953	0.667	0.961	5.472	0.755	0.511	-0.010	0.932	0.048	0.035
T Gru	10	10	12	6	13	10	10	9	9
	3	3	5	8	5	8	8	10	10
223807	1.160	1.170	5.746	0.865	0.583	-0.007	1.051	0.035	0.078
R Aqr	11	11	14	7	15	11	11	10	10
	2	2	5	8	4	5	5	5	5

Table 2. Photometry of Mira Variables

Each block of data is headed by the name of the star, its period in days, and its spectral class. Each set of observations is headed by JD, which is the Julian Day Number minus 2440000. Each individual colour has its error group listed next to it, group 1 being the most accurate, whereas group 5 measurements have been ignored throughout the work.

	R Aqr		386d		Me + Pec			
JD	1847		1908		1943		1967	
U-B	-0.38	1	-0.28	1	-0.23	1	0.02	1
B-V	1.06	1	1.21	1	1.19	1	1.43	1
V	11.20	1	10.67	1	10.40	1	9.73	1
V-R	3.92	1	4.05	1	4.00	1	4.02	1
R-I	3.87	1	3.72	1	3.58	1	3.20	1
63,65	0.56	4	0.48	3	0.30	4	0.29	3
65,103	5.07	3	5.01	2	4.95	3	4.66	2
81c			-0.11	2	0.10	3	0.55	2
103,105			-0.34	2	-0.26	2	-0.11	2
JD	1999		2227		2255		2323	
U-B	0.45	1	-0.80	1	-0.81	1	-0.36	1
B-V	1.43	1	0.74	1	0.90	1	1.60	1
V	7.85	1	12.61	1	12.48	1	11.17	1
V-R	3.19	1	4.75	1	4.80	1	4.60	1
R-I	2.65	1	3.92	1	3.89	1	3.52	1
63,65	0.29	2	0.70	3	0.64	3	0.47	1
65,103	3.99	2	4.98	2	4.99	2	4.85	1
81c	0.75	2	-0.34	2	-0.28	2	0.32	1
103,105	0.10	1	-0.41	1	-0.36	1	-0.05	1

	RW Aqr		140d	Me	Z Aql	129d	Me
JD	2256				2256		
U-B	1.40	1			1.85	2	
B-V	1.38	1			1.53	1	
V	10.61	1			11.00	1	
V-R	1.14	1			1.30	1	
R-I	0.78	2			0.80	2	
63,65	-0.08	3			0.20	4	
65,103	1.18	4			1.58	4	
81c	0.28	4			0.01	5	
103,105	0.06	5			-0.51	5	

	R Cae	392d	Me	
JD	2055		2325	
U-B	0.43	4	-0.28	1
B-V	2.37	3	1.54	1
V	12.96	1	10.75	1
V-R	4.99	3	4.05	1
R-I	3.67	3	3.46	1
63,65	0.10	5	0.54	2
65,103	4.35	4	4.69	1
81c	0.03	5	0.22	1
103,105	-0.29	4	-0.05	1

	R Car	308d	Me					
JD	1812		1847		1847		1849	
U-B	0.00	1	0.11	1	0.09	1	0.11	1
B-V	1.30	1	1.33	1	1.33	1	1.33	1
V	7.81	1	9.24	1	9.25	1	9.27	1
V-R	3.90	1	4.11	1	4.13	1	4.13	1
R-I	3.41	1	3.54	1	3.55	1	3.53	1
63,65	0.42	3	0.46	2	0.45	2	0.47	3
65,103	4.70	2	4.89	2	4.90	2	4.90	2
81c								
103,105								

JD	2197		2226	
U-B	0.27	1	0.43	1
B-V	1.59	1	1.61	1
V	8.74	1	7.48	1
V-R	3.79	1	3 .32	1
R-I	3.14	1	2.78	1
63,65	0.42	1	0.34	1
65,103	4.65	1	4.26	1
81c	0.26	1	0.47	1
103,105	-0.22	1	-0.25	1

	S Car	150d	Me					
JD	1805		1812		1847		1849	
U-B	0.82	1	0.95	1	1.45	1	1.46	1
B-V	1.43	1	1.53	1	1.83	1	1.83	1
V	5.71	1	5.64	1	6.48	1	6.58	1
V-R	1.34	1	1.33	1	1.71	1	1.76	1
R-I	1.06	1	1.10	1	1.58	1	1.63	1
63,65	0.07	3	0.08	2	0.17	2	0.18	2
65,103	1.59	3	1.66	2	2.34	2	2.41	2
81c								
103,105								

JD	2197		2226	
U-B	1.67	1	1.38	1
B-V	1.79	1	1.65	1
V	7.78	1	5.66	1
V-R	2.24	1	1.36	1
R-I	1.97	1	0.97	1
63,65	0.23	1	0.10	1
65,103	2.93	1	1.44	1
81c	0.67	1	0.15	1
103,105	0.13	1	0.02	1

	R Cen	542	Me					
JD	1805		1812		1847		1849	
U-B	0.92	1	0.83	1	0.59	1	0.57	1
B-V	1.94	1	1.95	1	1.88	1	1.89	1
V	7.52	1	7.74	1	8.63	1	8.67	1
V-R	3.20	1	3.28	1	3.96	1	3.70	1
R-I	2.75	1	2.83	1	3.13	1	3.13	1
63,65	0.30	3	0.26	3	0.35	2	0.35	2
65,103	4.15	3	4.23	2	4.55	2	4.56	2
81c								
103,105								

JD	2226		2255	
U-B	1.44	1	1.60	1
B-V	1.99	1	2.05	1
V	6.47	1	5.70	1
V-R	2.62	1	2.28	1
R-I	2.24	1	1.94	1
63,65	0.25	2	0.19	1
65,103	3.45	1	3.05	1
81c	0.53	1	0.44	1
103,105	0.17	1	0.18	1

	T Cen	91d	Me					
JD	1805		1812		1847		1849	
U-B	1.64	1	1.80	1	1.69	1	1.69	1
B-V	1.69	1	1.72	1	1.57	1	1.55	1
V	6.08	1	6.40	1	7.11	1	6.97	1
V-R	1.19	1	1.39	1	1.50	1	1.46	1
R-I	0.99	1	1.22	1	1.45	1	1.38	1
63,65	0.03	3	0.09	2	0.11	2	0.13	2
65,103	1.55	3	1.81	3	2.12	2	2.01	2
81c								
103,10 5								

JD	1912		2226		2255	
U-B	1.96	1	1.50	1	1.83	1
B-V	1.75	1	1.62	1	1.71	1
V	6.99	1	5.87	1	6.42	1
V-R	1.61	1	1.10	1	1.36	1
R-I	1.46	1	0.69	1	1.12	1
63,65	0.17	2	0.02	1	0.07	1
65,103	2,13	2	1,21	2	1.78	1
81c	0.35	3	0.01	2	0.19	2
103,105	0.14	3	0.07	2	0.13	2

	W Cen	201d	Me
JD	2227		
U-B	0.29	1	
B-V	1.44	1	
V	9.41	1	
V-R	2.94	1	
R-I	2.62	1	
63,65	0.32	2	
65,103	3.94	2	
81c	0.69	2	
103,105	0.19	1	

	RT Cen	253d	Me					
JD	1805		1812		1847		1849	
U-B	0.91	1	0.90	1	1.17	1	1.13	1
B-V	1.54	1	1.57	1	1.70	1	1.71	1
V	9,37	1	9.22	1	9.21	1	9.21	1
V-R	2.34	2	2.30	1	2.29	1	2.31	1
R-I	2.25	2	2.16	2	2.15	1	2.15	1
63,65	0.17	5	0.34	5	0.2 1	4	0.18	4
65,103	3.10	5	3.05	5	3.16	4	3.11	4
81c								
103,105								

JD	2226		2255	
U-B	0.65	1	0.59	3
B-V	1.54	1	1.57	1
V	11.03	1	11.53	1
V-R	3.31	1	3.42	1
R-I	2.82	1	2.93	1
63,65	0.33	3	0.31	3
65,103	4.19	3	4.37	3
81c	0.72	3	0.66	3
103,105	0.15	2	0.14	2

	RV Cen 446d		Ce					
JD	1805		1812		1847		1849	
U-B	3.01	1	3.00	2	2.99	3	2.95	3
B-V	3.77	1	3.64	1	3.32	1	3.30	1
V	7.52	1	7.45	1	7.28	1	7.29	1
V-R	1.89	1	1.84	1	1.83	1	1.84	1
R-I	1.32	1	1.33	1	1.37	1	1.36	1
63,65	0.11	4	0.15	3	0.08	2	0.07	2
65,103	2.40	4	2.33	3	2.51	2	2.49	2
81c								
103,105								

JD	2226		2255	
U-B	2.27	2	2.55	2
B-V	4.03	1	3.74	1
V	8.04	1	7.75	1
V-R	2.19	1	2.02	1
R-I	1.42	1	1.37	1
63,65	0.10	1	0.09	1
65,103	2.54	1	2.51	1
81c	-0.40	2	-0.47	1
103,105	0.24	2	0.25	1

	Mira Cet 331d		Me					
JD	1908		1943		1967		1999	
U-B	0.11	1	-0.10	1	-0.12	1	-0.33	1
B-V	1.54	1	1.55	1	1.54	1	1.57	1
V	5.35	1	6.59	1	7.23	1	8.04	1
V-R	3.31	1	3.86	1	4.08	1	4.34	1
R-I	2.79	1	3.13	1	3.26	1	3.46	1
63,65	0.28	1	0.35	1	0.36	1	0.42	1
65,103	4.24	1	4.69	1	4.80	1	4.95	1
81c	0.70	1	0.53	1	0.43	1	0.26	1
103,105	0.15	1	0.07	1	0.01	1	-0.07	1

JD	2049		2255		2323	
U-B	-0.33	1	0.08	1	-0.38	
B-V	1.66	1	1.67	1	1.51	1
V	8.30	1	5.98	1	8.24	1
V-R	4.42	1	3.62	1	4.37	1
R-I	3.47	1	2.92	1	3.56	1
63,65	0.47	1	0.38	1	0.53	1
65,103	4.86	1	4.36	1	4.90	1
81c	0.26	1	0.61	1	0.20	1
103,105	-0.12	1	0.17	1	-0.12	1

	R Cet 166d		Me					
JD	1912		1943		2000		2049	
U-B	1.23	1	1.75	1	0.34	2	0.26	3
B-V	1.68	1	1.73	1	1.63	1	1.73	2
V	9.69	1	8.90	1	12.05	1	13.38	1
V-R	2.37	1	1.89	1	3.93	2	4.48	2
R-I	2.36	1	1.92	1	3.28	2	3.49	1
63,65	0.30	4	0.10	3	0.28	5	0.44	4
65,103	3.49	3	2.97	3	4.76	4	4.81	3
81c	0.48	4	0.49	3	0.53	4	0.34	3
103,105	-0.12	3	0.05	3	-0.07	3	-0.26	2

JD	2255		2323	
U-B	1.20	1	0.29	1
B-V	1.40	1	1.36	1
V	9.25	1	11.15	1
V-R	2.45	1	3.63	1
R-I	2.36	1	3.07	1
63,65	0.25	2	0.41	2
65,103	3.48	2	4.37	1
81c	0.67	2	0.71	2
103,105	-0.05	2	0.06	1

U Cet 236 Me

JD	1912		1943		1999		2255	
U-B	0.79	1	0.60	1	0.48	2	0.37	2
B-V	1.52	1	1.54	1	1.48	1	1.65	1
V	7.31	1	8.6 7	1	11.58	1	12.29	1
V-R	1.57	1	2.25	2	3.57	2	3.73	1
R-I	1.52	1	2.18	2	3.06	2	3.10	1
63,65	0.20	3	0.25	3	0.42	5	0.44	4
65,103	2.17	2	3.23	3	4.29	4	4.52	3
81c	0.44	3	0.67	3	0.61	4	0.47	4
103,105	0.15	3	0.15	3	0.14	4	0.00	2

JD	2325	
U-B	0.74	1
B-V	1.32	1
V	9.53	1
V-R	2.47	1
R-I	2.27	1
63,65	0.22	2
65,103	3.34	1
81c	0.82	1
103,105	0.02	1

	X Cet 177d		Me					
JD	1912		2000		2256		2325	
U-B	1.17	1	1.66	1	1.22	1	1.64	1
B-V	1.50	1	1.79	1	1.52	1	1.76	1
V	9.55	1	10.03	1	10.29	1	9.00	1
V-R	1.82	1	2.12	1	2.17	1	1.65	1
R-I	1.72	1	1.19	2	2.02	1	1.48	1
63,65	0.22	4	-0.05	5	0.21	3	0.13	2
65,103	2.42	4	2.98	4	2.99	3	2.19	2
81c	0.60	4	0.58	5	0.63	3	0.37	1
103,105	0.17	5	0.18	5	0.10	3	0.14	2

	Z Cet 185d		Me
JD	2227		
U-B	0.73	1	
B-V	1.37	1	
V	9.94	1	
V-R	2.41	1	
R-I	2.32	1	
63,65	0.20	2	
65,103	3.45	2	
81c	0.65	2	
103,105	-0.03	2	

	T Col 226d		Me			
JD	1999		2049		2123	
U-B	1.03	1	0.53	1	0.45	1
B-V	1.60	1	1.49	1	1.27	1
V	7.78	1	10.02	1	10.11	1
V-R	2.20	1	3.25	1	3.36	1
R-I	2.10	1	2.83	1	2.78	1
63,65	0.19	2	0.3 2	2	0.27	2
65,103	3.05	2	4.21	2	4.19	2
81c	0.64	2	0.65	2	0.86	2
103,105	0.17	2	0.16	1	0.12	1

	T Eri	252d	Me					
JD	1967		1999		2049		2123	
U-B	0.11	2	0.60	1	0.82	1	0.75	1
B-V	1.62	1	1.44	1	1.41	1	1.61	1
V	12.12	1	10.87	1	8.52	1	9.09	1
V-R	3.90	2	3.39	1	2.18	1	2.47	1
R-I	3.23	2	2.90	1	2.02	1	2.26	1
63,65	0.08	5	0.23	5	0.20	2	0.20	2
65,103	4.71	4	4.24	4	3.00	2	3.47	2
81c	0.39	5	0.82	4	0.71	2	0.69	2
103,105	0.05	3	0.15	3	0.20	2	0.16	1

JD	2325	
U-B	0.70	1
B-V	1.32	1
V	8.45	1
V-R	1.99	1
R-I	2.01	1
63,65	0.17	1
65,103	2.97	1
81c	0.67	1
103,105	0.12	1

	R For	388d	Ce					
JD	1908		1943		1967		1999	
U-B	-0.27	4	0.83	4	0.63	4	1.39	5
B-V	5.35	3	5.49	2	5.63	2	5.55	1
V	10.32	1	9.36	1	9.23	1	9.23	1
V-R	3.13	1	2.84	1	2.74	1	2.76	1
R-I	1.70	1	1.57	1	1.59	1	1.67	1
63,65	0.07	4	0.08	4	0.05	3	0.14	3
65,103	2.70	4	2.55	3	2.56	3	2.65	3
81c	-0.49	4	-0.03	4	-0.17	4	-0.20	4
103,105	0.19	4	0.23	4	0.35	4	0.31	4

JD	2049		2256		2323	
U-B	0.31	3	-0.30	4	0.25	4
B-V	5.29	1	5.86	3	5.60	3
V	9.94	1	11.14	1	9.52	1
V-R	3.13	1	3.70	1	3.01	1
R-I	1.80	1	1.76	1	1.48	1
63,65	0.11	2	0.10	2	0.10	1
65,103	2.95	2	2.90	2	2.40	1
81o	-0.09	2	0.13	3	-0.01	2
103,105	0.26	2	0.22	2	0.20	1

	T Gru	136d	Me					
JD	1847		1908		1943		1967	
U-B	1.53	2	0.97	1	1.24	1	1.79	1
B-V	1.82	1	1.38	1	1.64	1	1.85	1
V	10.50	1	9.37	1	8.79	1	9.74	1
V-R	1.80	3	1.23	1	1.31	1	1.69	1
R-I	1.73	3	1.12	2	1.01	2	1.45	2
63,65	0,41	5	0.32	4	0.00	4	0.10	5
65,103	2.45	5	1.67	5	1.55	5	2.12	5
81o			0.02	5	0.17	5	0.43	5
103,105			-0.11	5	0.02	5	0.45	5

JD	1999		2226		2255		2323	
U-B	1.66	2	0.94	1	1.47	1	1.00	1
B-V	1.73	1	1.67	1	1.75	1	1.48	1
V	11.69	1	9.31	1	10.05	1	8.73	1
V-R	2.38	3	1.45	1	1.71	1	1.18	1
R-I	2.17	3	1.22	1	1.56	1	0.76	1
63,65	-1.87	5	0.06	2	0.14	3	0.05	2
65,103	5.59	5	1.87	3	2.25	3	1.17	2
81o	1.01	5	0.21	3	0.50	3	0.10	2
103,105	-0.03	5	0.09	4	0.13	4	0.25	2

	R Hya	407d	Me					
JD	1805		1812		1847		1849	
U-B	0.29	1	0.27	1	0.22	1	0.21	1
B-V	1.79	1	1.81	1	1.81	1	1.82	1
V	7.51	1	7.68	1	8.43	1	8.46	1
V-R	3.42	1	4.05	1	4.39	1	4.40	1
R-I	3.35	1	3.41	1	3.61	1	3.60	1
63,65	0.38	2	0.43	2	0.48	2	0.47	2
65,103	4.65	2	4.73	1	4.92	1	4.91	1
81o								
10 3,105								

JD	2197		2255	
U-B	0.39	1	0.26	1
B-V	1.73	1	1.88	1
V	7.53	1	8.50	1
V-R	3.86	1	4.57	1
R-I	3.33	1	3.56	1
63,65	0.45	1	0.50	1
65,103	4.68	1	4.86	1
81o	0.39	1	0.20	1
103,105	0.03	1	-0.08	1

	T Hya	287d	Me			
JD	1812		2055		2123	
U-B	0.18	2	0.23	1	0.20	3
B-V	1.59	1	1.57	1	1.78	1
V	11.94	1	9.80	1	12.55	1
V-R	3.85	3	2.98	1	4.09	1
R-I	3.25	3	2.61	1	3.34	1
63,65	-0.28	5	0.33	5	0.47	4
65,103	4.54	5	4.06	4	4.71	3
81o			0.75	4	0.32	3
103,105			0.17	4	-0.05	2

	R Lep	432d	Ce			
JD	1999		2055		2123	
U-B	1.19	2	2.35	1	2.54	1
B-V	4.68	1	4.64	1	4.22	1
V	7.48	1	6.79	1	6.48	1
V-R	2.62	1	2.39	1	2.23	1
R-I	1.53	1	1.42	1	1.55	1
63,65	0.10	2	0.14	2	0.09	1
65,103	2.49	2	2.44	2	2.64	1
81c	-0.25	2	-0.29	3	-0.37	1
103,105	0.31	2	0.32	2	0.24	1

	X Lib	165d	Me
JD	2227		
U-B	1.30	3	
B-V	1.63	1	
V	11.26	1	
V-R	1.49	2	
R-I	1.30	2	
63,65	0.09	4	
65,103	1.99	4	
81c	0.25	5	
103,105	0.10	5	

	S Lup	343d	Se					
JD	1805		1812		1847		1849	
U-B	1.10	1	1.01	1	0.98	4	1.24	5
B-V	2.03	1	2.02	1	2.29	2	2.28	3
V	9.84	1	10.15	1	11.51	1	11.60	1
V-R	2.65	3	2.83	2	3.55	2	3.61	3
R-I	2.10	3	2.18	2	2.67	2	2.70	3
63,65	-0.09	5	-0.72	5	0.38	5	0.12	5
65,103	3.83	5	4.21	5	4.15	5	4.35	5
81c								
103,105								

JD	1849		1908		2226		2255	
U-B	1.30	4	-	-	0.71	4	2.06	5
B-V	2.36	2	4.50	5	2.47	3	1.70	1
V	11.59	1	13.93	1	12.66	1	12.18	1
V-R	3.59	2	4.34	4	3.98	2	1.34	2
R-I	2.69	2	3.49	3	3.08	1	0.97	3
63,65	0.27	5	0.90	5	0.35	4	-0.11	5
65,103	4.08	5	4.40	5	4.57	3	1.81	5
81c			-0.22	5	0.52	3	0.29	5
103,105			0.03	5	0.06	2	1.98	5

	R Mic	138d	Me
JD	2227		
U-B	0.95	1	
B-V	1.59	1	
V	9.96	1	
V-R	2.41	1	
R-I	2.19	1	
63,65	0.26	3	
65,103	3.25	2	
81c	0.62	2	
103,105	0.17	2	

	V Mon	334d	Me			
JD	2000		2049		2055	
U-B	-0.25	1	0.03	1	-0.16	3
B-V	1.40	1	1.60	1	1.84	1
V	10.18	1	11.91	1	11.98	1
V-R	3.91	1	4.57	1	4.54	2
R-I	3.18	1	3.46	1	3.56	2
63,65	0.37	4	0.46	3	0.90	5
65,103	4.60	3	3.76	2	4.72	4
81c	0.64	3	0.55	2	0.08	4
103,105	0.14	2	0.34	2	-0.01	3

	R Nor	496d	Me	
JD	1805		2227	
U-B	1.21	1	1.34	1
B-V	1.75	1	1.88	1
V	8.16	1	8.38	1
V-R	2.39	1	2.45	1
R-I	2.26	1	2.23	1
63,65	0.32	4	0.20	2
65,103	3.42	4	3.43	1
81c			0.53	2
103,105			0.16	1

	T Nor	244d	Me					
JD	1805		1812		1847		1849	
U-B	0.48	1	0.48	1	0.34	4	0.61	4
B-V	1.74	1	1.76	1	1.86	2	1.77	3
V	10.80	1	11.13	1	12.21	1	12.20	1
V-R	3.63	3	3.67	3	4.09	2	4.04	3
R-I	2.94	3	3.04	3	3.27	2	3.27	3
63,65	0.57	5	0.27	5	0.25	5	0.38	5
65,103	4.32	5	4.30	5	4.87	5	4.67	5
81c								
103,105								

JD	1849		1908		2197		2227	
U-B	0.50	4	0.82	1	0.87	1	0.80	1
B-V	1.83	1	1.50	1	1.53	1	1.57	1
V	12.23	1	10.12	1	8.40	1	8.30	1
V-R	4.06	2	3.09	1	2.18	1	2.30	1
R-I	3.26	2	2.62	1	2.13	1	2.15	1
63,65	0.38	5	0.38	4	0.20	2	0.20	2
65,103	4.67	4	3.85	3	3.24	1	3.30	2
81c			0.72	3	0.50	2	0.56	2
103,105			0.01	3	0.00	1	0.12	1

JD	2255	
U-B	0.45	1
B-V	1.53	1
V	9.37	1
V-R	2.92	1
R-I	2.55	1
63,65	0.27	2
65,103	3.89	1
81c	0.72	2
103,105	0.12	1

	R Oct	405d	Me	
JD	2000		2055	
U-B	0.50	1	0.00	1
B-V	1.53	1	1.56	1
V	7.45	1	9.25	1
V-R	2.49	1	3.36	1
R-I	2.35	1	2.93	1
63,65	0.18	2	0.39	4
65,103	3.55	2	4.41	3
81c	0.71	2	0.54	3
103,105	0.17	1	0.22	2

	X Oct	205d	Me
JD	2227		
U-B	0.97	1	
B-V	1.45	1	
V	8.12	1	
V-R	2.30	1	
R-I	2.14	1	
63,65	0.23	2	
65,103	3.22	2	
81c	0.77	2	
103,105	0.15	1	

	V Oph	298d	Ce					
JD	1805		1849		1912		2226	
U-B	4.21	3	-	-	3.22	3	1.59	3
B-V	3.24	1	3.42	1	3.53	1	4.25	1
V	7.50	1	7.81	1	8.78	1	9.34	1
V-R	1.76	1	2.07	1	2.40	1	2.65	1
R-I	1.38	1	1.47	1	1.54	1	1.50	1
63,65	0.12	4	0.05	3	0.06	3	0.07	2
65,103	2.37	3	2.53	2	2.57	2	2.52	2
81c					-0.23	4	-0.14	2
103,105					0.22	3	0.19	2

JD	2255	
U-B	1.40	4
B-V	4.40	1
V	9.33	1
V-R	2.66	1
R-I	1.51	1
63,65	0.07	2
65,103	2.52	2
81c	-0.15	2
103,105	0.21	2

	S Pav	385d	Me	S Phe	141d	Me	
JD	2227			2227		2256	
U-B	0.41	1		1.11	1	1.09	1
B-V	1.64	1		1.45	1	1.56	1
V	8.02	1		6.98	1	7.47	1
V-R	3.65	1		2.01	1	2.22	1
R-I	3.06	1		1.92	1	2.10	1
63,65	0.40	1		0.21	1	0.22	2
65,103	4.45	1		2.82	1	3.12	1
81c	0.44	1		0.60	1	0.69	1
103,105	0.08	1		0.15	1	0.19	1

	W Pup	120d	Me			
JD	2055		2123		2227	
U-B	1.25	1	0.84	1	0.73	1
B-V	1.44	1	1.58	1	1.37	1
V	9.30	1	10.65	1	9.94	1
V-R	1.90	1	2.70	1	2.41	1
R-I	1.83	2	2.48	1	2.32	1
63,65	-0.08	5	0.28	3	0.20	2
65,103	2.59	5	3.73	2	3.45	2
81o	0.49	5	0.69	2	0.65	2
103,105	0.30	5	0.12	2	-0.03	2

	R Sgr	268d	Me					
JD	1812		1847		1849		1851	
U-B	0.60	1	0.34	2	0.31	2	0.32	2
B-V	1.64	1	1.60	1	1.60	1	1.57	1
V	8.85	1	10.73	1	10.85	1	10.92	1
V-R	2.66	1	3.44	1	3.48	1	3.47	2
R-I	2.42	1	3.04	1	3.06	1	3.06	2
63,65	0.30	5	0.41	5	0.37	5	0.47	5
65,103	3.62	4	4.41	4	4.54	4	4.36	4
81o								
103,105								

JD	1908		2226		2255		2323	
U-B	0.28	3	0.89	1	0.94	1	0.91	1
B-V	1.71	2	1.39	1	1.46	1	1.68	1
V	12.57	1	9.22	1	7.78	1	7.98	1
V-R	4.27	2	2.70	1	1.97	1	2.22	1
R-I	3.42	2	2.44	1	1.88	1	2.06	1
63,65	0.22	5	0.25	2	0.19	2	0.22	1
65,103	4.66	4	3.66	2	2.73	1	3.06	1
81o	0.20	4	0.87	2	0.62	1	0.60	1
103,105	-0.06	3	0.10	2	0.11	1	0.15	1

	T Sgr 392d		Se					
JD	1812		1847		1851		1908	
U-B	0.62	1	1.61	1	1.67	2	0.17	2
B-V	1.94	1	1.65	1	1.66	1	1.07	1
V	9.68	1	9.70	1	9.72	1	11.81	1
V-R	3.25	1	1.87	1	1.90	2	3.38	2
R-I	2.77	1	1.89	2	1.79	2	3.57	2
63,65	0.22	5	0.25	5	0.05	5	0.43	5
65,103	4.39	4	2.79	4	2.86	5	4.67	4
81o							-0.26	4
103,105							0.18	3

JD	1943		2226		2255		2323	
U-B	0.10	1	0.37	1	0.19	1	1.82	1
B-V	0.74	1	1.92	1	1.54	1	1.68	1
V	12.18	1	10.13	1	11.03	1	9,83	1
V-R	2.97	4	3.36	1	3.42	1	1.95	1
R-I	3.68	4	2.97	1	3.34	1	1.88	1
63,65	0.30	5	0.31	2	0.38	2	0.19	2
65,103	4.87	5	4.33	2	4.55	2	2.79	2
81o	-0.29	5	0.21	2	-0.12	2	0.51	2
103,105	0.11	4	0.12	1	0.12	1	0.16	2

	RR Sgr 332d		Me					
JD	1812		1847		1908		1943	
U-B	0.63	1	0.20	1	-0.06	1	0.07	1
B-V	1.52	1	1.56	1	1.56	1	1.71	1
V	7.10	1	8.21	1	9.84	1	10.87	1
V-R	2.41	1	3.08	1	3.85	1	4.16	1
R-I	2.24	1	2.65	1	3.16	1	3.42	1
63,65	0.24	3	0.28	2	0.37	3	0.30	4
65,103	3.45	2	4.00	2	4.58	2	4.78	4
81o					0.57	2	0.36	4
103,105					0.10	1	0.00	2

JD	2000		2226		2255		2323	
U-B	0.22	1	0.03	1	0.04	1	0.34	4
B-V	1.92	1	1.81	1	1.82	1	2.04	2
V	11.65	1	9.88	1	11.13	1	12.75	1
V-R	4.35	1	3.75	1	4.21	1	5.07	1
R-I	3.53	1	3.10	1	3.44	1	3.89	1
63,65	0.41	4	0.39	2	0.53	2	0.62	2
65,103	4.89	4	4.51	1	4.79	2	5.03	1
81o	0.20	4	0.42	2	0.15	2	-0.01	1
103,105	-0.10	2	0.10	1	-0.10	1	-0.39	1

	RW Sgr 190d		Me		S Sce 178d		Me	
JD	2227				1805		1805	
U-B	1.15	1			1.08	1	1.07	1
B-V	1.68	1			1.51	1	1.50	1
V	10.55	1			10.68	1	10.67	1
V -R	2.60	1			1.90	4	1.94	4
R-I	2.46	1			1.75	4	1.84	4
63,65	0.27	3			-0.62	5	-0.30	5
65,103	3.72	3			2.64	5	2.80	5
81o	0.61	3						
103,105	0.13	2						

	RR Sco 279d		Me					
JD	1805		1847		1849		1908	
U-B	0.43	1	0.24	1	0.22	1	0.32	1
B-V	1.57	1	1.60	1	1.61	1	1.77	1
V	7.25	1	8.94	1	8.99	1	10.35	1
V-R	2.97	1	3.72	1	3.75	1	4.33	1
R-I	2.62	1	3.19	1	3.20	1	3.50	1
63,65	0.28	3	0.38	2	0.35	3	0.41	3
65,103	3.96	2	4.60	2	4.60	2	4.83	2
81o							0.12	2
103,105							-0.09	1

JD	1943		2197		2226		2256	
U-B	0.28	1	0.28	1	0.38	1	0.59	1
B-V	1.65	1	1.76	1	1.63	1	1.39	1
V	9.91	1	10.56	1	9.79	1	8.03	1
V-R	4.14	1	3.52	1	4.10	1	3.38	1
R-I	3.39	1	4.32	1	3.31	1	2.81	1
63,65	0.34	4	0.47	2	0.39	2	0.28	2
65,103	4.83	3	4.80	1	4.70	1	4.16	1
81c	0.40	3	0.14	1	0.43	1	0.80	1
103,105	-0.04	2	-0.13	1	0.00	1	0.09	1

	RZ Sco 161d		Me					
J D	1812		1848		1849		1912	
U-B	1.18	1	1.34	1	1.34	1	1.46	1
B-V	1.39	1	1.51	1	1.49	1	1.68	1
V	10.92	1	8.81	1	8.77	1	9.52	1
V-R	2.64	3	1.58	1	1.59	1	2.02	1
R-I	2.25	3	1.50	2	1.47	1	1.91	1
63,65	-0.10	5	0.09	4	0.22	4	0.23	4
65,103	3.14	5	2.10	4	2.02	4	2.80	4
81c							0.68	4
103,105							0.17	4

JD	2227	
U-B	1.31	1
B-V	1.72	1
V	9.71	1
V-R	2.04	1
R-I	1.84	1
63,65	0.19	3
65,103	2.78	2
81c	0.53	3
103,105	0.16	3

	KS Sco 429d		Me
JD	2227		
U-B	1.13	1	
B-V	1.61	1	
V	10.56	1	
V-R	2.19	1	
R-I	2.11	1	
63,65	0.20	3	
65,103	3.25	3	
81c	0.45	3	
103,105	0.03	3	

	S Sol	366d	Me					
JD	1908		1943		1967		1999	
U-B	0.06	1	0.51	1	0.58	1	0.34	1
B-V	1.57	1	1.28	1	1.33	1	1.41	1
V	10.38	1	7.73	1	6.85	1	7.45	1
V-R	4.30	1	2.82	1	2.38	1	2.78	1
R-I	3.29	1	2.58	1	2.24	1	2.51	1
63,65	0.35	3	0.21	2	0.18	2	0.25	2
65,103	4.77	2	3.92	2	3.45	1	3.79	2
81c	0.53	2	0.73	2	0.66	1	0.77	2
103,105	-0.19	2	0.00	2	0.09	1	0.14	1

JD	2227		2255		2323	
U-B	0.41	1	0.43	1	0.87	1
B-V	1.59	1	1.44	1	1.45	1
V	10.27	1	9,17	1	6.01	1
V-R	4.23	1	3.80	1	2.13	1
R-I	3.31	1	3.00	1	1.95	1
63,65	0.42	2	0.34	2	0.19	1
65,103	4.67	1	4.41	1	2.92	1
81c	0.55	1	0.81	1	0.70	1
103,105	-0.03	1	0.08	1	0.21	1

	SS Vir 355d		Ce					
JD	1812		1847		1849		2227	
U-B	2.51	1	2.22	4	2.65	5	1.08	3
B-V	3.71	1	3.98	1	4.05	1	4.99	1
V	7.66	1	8.30	1	8.33	1	8.50	1
V-R	2.34	1	2.63	1	2.62	1	2.77	1
R-I	1.49	1	1.58	1	1.59	1	1.50	1
63,65	0.06	4	0.06	2	0.06	3	0.10	2
65,103	2.50	3	2.55	2	2.53	3	2.48	2
81c							-0.12	2
103,105							0.20	2

	V1	47 Tuc	212d	Me
JD	2256		2325	
U-B	1.00	1	0.57	3
B-V	1.55	1	1.59	2
V	10.21	1	12.69	1
V-R	1.33	1	2.48	2
R-I	1.04	1	2.25	2
63,65	0.15	3	0.39	4
65,103	1.36	4	3.40	4
81c	0.13	4	0.61	4
103,105	0.04	4	0.21	4

	V2	47 Tuc	203d	Me
JD	2256		2325	
U-B	0.03	3	0.85	2
B-V	0.76	2	1.23	1
V	14.37	1	12.06	1
V-R	2.96	3	1.95	2
R-I	2.62	3	1.91	2
63,65	0.22	4	0.22	4
65,103	2.65	4	2.78	4
81c	0.54	4	0.77	4
103,105	0.16	4	0.07	4

	V3	47 Tuc	192d	Me		
JD	2226		2256		2325	
U-B	0.84	2	0.56	3	1.08	3
B-V	1.37	1	1.36	2	1.30	1
V	11.97	1	14.12	1	12.61	1
V-R	1.97	2	3.27	3	2.36	2
R-I	1.98	2	2.69	3	2.17	2
63,65			-0.12	5	0.24	4
65,103			5.16	5	3.15	4
81c			0.99	5	0.86	4
103,105			0.57	5	0.18	4

	V4	M69	196d	Me				
JD	2197		2197		2226		2256	
U-B	1,19	5	1.01	5	1.59	3	1.48	4
B-V	2.11	4	1.75	3	1.79	1	1.87	1
V	15.44	2	15.14	1	12.92	1	12.57	1
V-R	3.14	4	2.89	4	1.51	3	1.69	3
R-I	2.30	4	2.28	4	1.47	3	1.29	3
63,65					0.38	5	-	-
65,103					2.19	5	2.32	5
81c					0.35	5	0.16	5
103,105					-0.19	5	-0.40	5

JD	2327	
U-B	1.36	5
B-V	1.98	4
V	15.10	2
V-R	2.94	3
R-I	2.36	3
63,65		
65,103		
81c		
103,105		

Table 3. VRI (S-20) Measurements of Miras

These are measurements made of especially interesting variables on Julian Day 2442171, but using a different photometer than that used for table 2.

Star	Period	V	V-R	R-I
W Cen	202	9.42	3.22	2.30
R Nor	490	7.66	2.42	1.84
S Pav	385	8.17	4.30	3.05
RW Sgr	190	9.83	2.64	2.01
BM Sgr	403	12.97	3.49	2.58
KS Sco	429	12.76	3.87	2.88
V347 Tuc	192	11.42	1.71	1.58

Table 4. The Values of K for the Me Miras

Star	Period	-K	$\overline{V}max + K$
RW Aqr	140	13.5	-4.1
Z Aql	129	13.9	-4.9
R Cae	392	7.7	0.3
R Car	308	5.4	-0.8
S Car	150	8.2	-2.5
R Cen	542	6.4	-0.5
T Cen	91	8.8	-2.7
W Cen	201	9.1	-0.6
RT Cen	253	9.6	-0.3
Mira Cet	331	4.2	-0.5
R Cet	166	9.3	-1.1
U Cet	236	9.4	-1.9
X Cet	177	10.9	-1.9
Z Cet	185	9.9	-1.0
T Col	226	8.6	-1.0
T Eri	252	9.2	-1.1
T Gru	136	11.7	-3.1
R Hya	407	4.2	0.4
T Hya	287	9.1	-1.4
X Lib	165	13.4	-2.4
R Mic	138	10.3	-1.1
V Mon	334	7.8	-0.7
R Nor	496	8.6	-1.4

Star	Period	-K	$\overline{V}max + K$
T Nor	244	9.0	-1.6
R Oct	405	7.4	0.5
X Oct	205	8.6	-1.4
S Pav	385	5.9	-1.3
S Phe	141	8.0	-0.8
W Pup	120	10.3	-1.9
R Sgr	268	8.7	-1.5
RR Sgr	332	7.3	-0.7
RW Sgr	190	10.4	-1.0
BM Sgr	403	12.3	-3.3
S Sco	178	11.9	-1.0
RR Sco	279	6.4	-0.4
RZ Sco	161	10.7	-1.8
KS Sco	429	11.1	-1.1
S Sol	366	7.1	-0.3
V1 47Tuc	212	12.8	-
V2 47Tuc	203	13.3	-
V3 47Tuc	192	13.0	-2.7
V4 M69	196	15.0	-

APPENDIX

OPERATING MANUAL FOR ST. ANDREWS PHOTOMETER

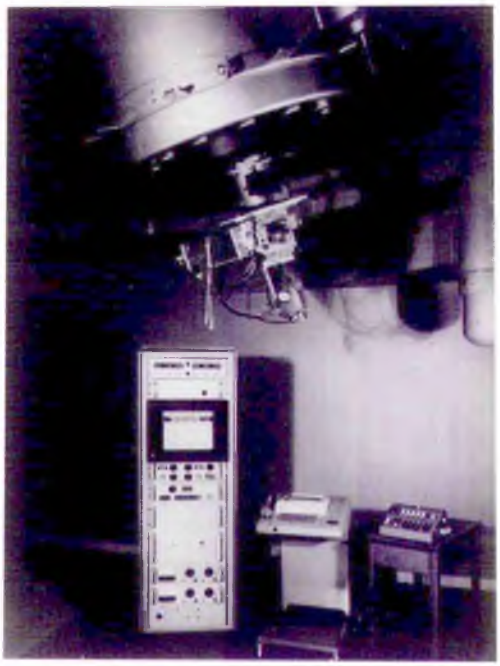

(1)

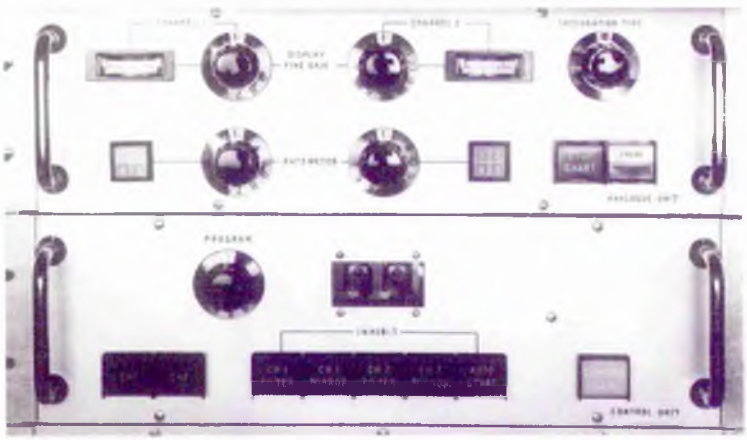

(2)

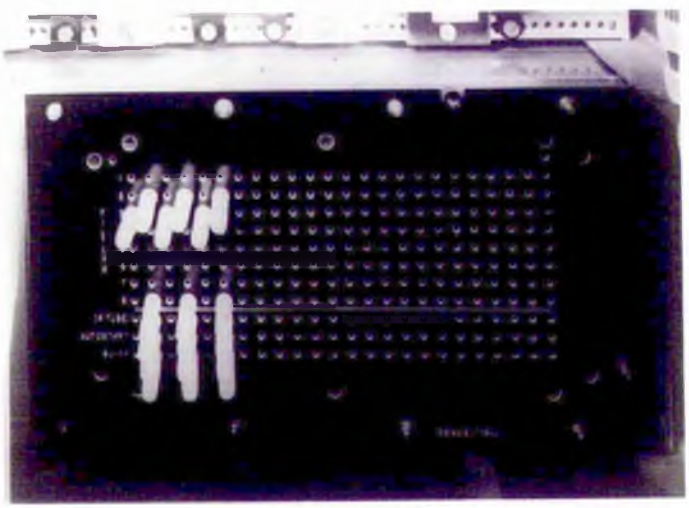

(3)

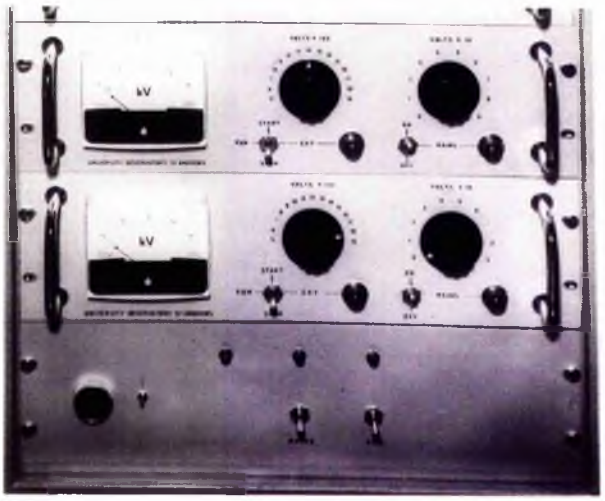

(4)

(5)

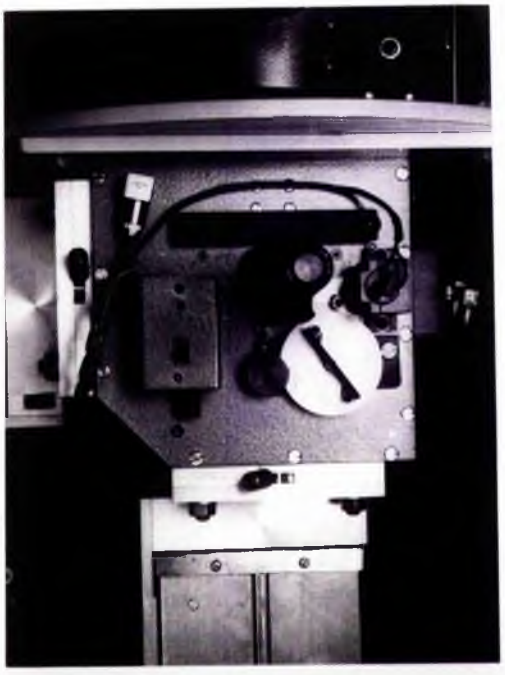

(6)

ST. ANDREWS' PHOTOMETER OPERATORS' MANUAL

SETTING UP

1) Attaching to Telescope

The acquisition head is normally stored with protective wooden covers over the mating surfaces. These must be removed, revealing two sets of four bolt holes in each interface plate. The outer sets (easily identifiable, as the holes are through inserts in the main plates) are the ones of interest. Inspection reveals that one set of holes is tapped, the other being clearance holes. The latter are in the plate which contacts the telescope. Four 9mm. bolts are stored in accessories box 1 in a plastic bag also containing the lable "For Telescope". Any four suitable holes on the telescope interface plate may be used, except those with blue circles around them. Washers are supplied with the bolts. The normal orientation is with the eyepiece pointing south.

The photometer is attached to the acquisition head in such a way that the respective eyepieces point in the same direction. The 10mm. fixing bolts are stored, suitably labelled, in accessories box 1. A small washer from the wooden coverings mentioned above is placed on each bolt, and then the bolts are screwed downwards through the tapped holes in the lower acquisition head plate. The photometer is then slipped onto these four bolts and the large washers

and nuts used to hold it in place.

The cold boxes are fitted such that the blue tube is in the straight-through beam, and that the dark slide handles are on the same side as the photometer eyepieces. The nuts and washers for holding the cold boxes are normally stored on the photometer head. The presence of O-rings on the mating surfaces of the dark slide should be checked.

2) Wiring Connections

a) There is a lead which supplies power to the graticule illumination on the acquisition head. This must be plugged into a socket on the electronics box of the photometer head. Inspection will reveal that the plug is of the 4-way locking type, and there is only one equivalent socket. This connection must be made, even if there is no intention of using the graticule illumination, since this line is also used to inhibit measurement if the acquisition head mirror is left in the light beam.

b) There is a lead from each coldbox with a 2-way plug on the end. These must be connected to the electronics box. There are three suitable sockets adjacent to that of the graticule illumination, any two of which will do. There are also two co-ax leads with screw connectors coming from the electronics box. These are the signal leads and must be connected to the anode socket on each cold box.

c) The inter-connections on the electronics box should be intact, but these should be checked.

d) The main cableform is stored in a large cardboard box next to the electronics rack. The required length of this should be fed through the small hole at the base of the data room wall. All the cables going to the head are strapped together and labelled "HEAD". The cableform is subdivided into three sections, one going to each of the coldboxes for the purpose of powering the coolers and supplying E.H.T. The remaining section goes to the electronics box, and consist of one large connector, one two-pin locking connector and two BNC plugs. The locking connector fits such that the locking button is next to the red dot on the socket. The two BNC's are on the signal leads, and one plugs in on the same surface as the large connector, the other fitting next to the group of short co-ax leads.

The other end of the main cableform splits into two main groups. The first consists of one large conn ector, one two pin locking connector and two BNC's. These all go to the back of the rack. Normally these will be found already connected, excepting one of the BNC's which goes into a socket inside the back of the rack, on the left as viewed, and about one third of the height of the rack from the floor. There are two sockets here, the top one being relevant, the lower normally being out of use. The remaining group goes to the two power supplies for the coolers.

e) The cableform box also contains plastic tubing which is used to supply water to the coldboxes. There are two long tubes, taped together, which are fed to the coldboxes. A short length of tubing connects the two coldboxes together. The remaining short tube should be connected to the "IN" side of the water pump, a long tube being on the "OUT" side. The connections at the water pump are close fitting, but those on the coldboxes are not, and so it is necessary to use wire tourniquets on the coldbox connections to prevent leaks. The water bath should be about two-thirds full of cold water, with one long tube and one short tube dipping into it. These tubes must be taped down or else vibration could cause them to escape.

f) The control box is stored sitting on top of the cableform box, and usually will be found already connected. This should be placed wherever convenient.

g) The electronics rack is best placed just outside the door of the data room, with the teletype and control box next to it.

h) The teletype must be connected using one of the two grey leads coming out of the back of the rack. The second grey lead is for the IBM typewriter; which should only be connected if the teletype fails.

i) The rack, teletype, water pump and coldbox supplies

must all be plugged into the mains. The rack must not be plugged in until it is properly connected to the photometer head.

3) Switch on Procedures

a) It is sensible to start the cooling system as early as possible. The red (FW-118) tube should be turned right down. The blue tube is normally operated at -15°C or warmer. There are thermometers on the coldboxes which indicate the temperatures actually achieved.

b) When the electronics rack is plugged in, a green light shines on the front of the rack near ankle level. This indicates that the power supplies to the clocks and window heaters are operational. The system should be left in this state for five minutes or so to enable the sidereal clock to start. The switch labelled "MAINS" should then be switched up, whereupon the red light next to it comes on. The sidereal time display must be immediately inspected to check that it is counting. If it is not, turn the "MAINS" switch off again and wait a few moments before repeating the procedure.

c) The teletype is activated by a green on-off button which is next to the red mains indicator. There is no line-local switch. The paper tape punch has the usual separate switch.

d) The U.T. and L.S.T. clocks require setting. It is normal at first switch-on for some of the digits in the clock

display to be multiple. Once set, the mains switch may be turned off without affecting the clocks, which are operational as long as the green indicator ((b) above) is lit.

e) The MAINS switches on the EHT's are normally left in the ON position. The FW-118 (red) and EMI 6256A (blue) tubes are normally operated at 1850 and 1000 volts respectively.

The photometer should now be fully operational.

PHOTOMETER OPERATION

Description

Plate (1) gives an overall view on the photometer attached to the St. Andrews 37-inch telescope. This picture shows all the principal components of the photometer, with the exception of the coldbox power supplies and the water supply.

To understand fully the operation of the photometer, it is first necessary to realise that the electronics section is capable of driving two separate photometer heads, each bearing two photomultipliers. Hence, where applicable all the controls appear in pairs, one for channel 1 and one for channel 2. Only one head is supplied, and so only channel 1 is of interest under normal operating circumstances. It must be emphasized that tube 1 (blue) and tube 2 (red) are both associated with channel 1, i.e. Tubes do not correspond to channels.

A) MAIN ELECTRONICS RACK

It will be seen from plate (1) that the rack is divided into modules. These are described in order from the top of the rack downwards.

1) Display Unit

This consists of two six-digit nixie displays which are labelled UT/CHI COUNT and LST/CH2 COUNT respectively. Between them are a pair of switches which enable the operator to select which of the two possibilities is displayed in each case. Normally one would choose CHI COUNT and LST respectively. Below each digit is a small button concerned with setting the clocks. Holding such a button down causes that digit to increase by one every second, unless the digit is the seconds display, in which case the increment is two per second. Holding down the left-hand button of a pair (e.g. the tens of minutes digit) inhibits the carry to the next pair. For example, the display might produce a sequence:-

10 43 26

10 53 27

10 03 28

Once the clocks are set, they remain correct so long as the rack is plugged into the mains (power failures permitting). The remaining switch on this unit enables all the nixies to be turned off when low dome lighting conditions are required.

2) Serializer Unit

This has one switch upon it, labelled UT, with two positions, IN and OUT. IN results in the UT of each observation being outputted on the teletype. LST is always outputted. It is recommended that unless UT is specifically required, UT OUT be normally selected. (This is to reduce wear on the teletype).

3) Chart Recorder

This is a normal Brown recorder, but its operation is controlled by the rack. The ON/OFF switch inside its door should be in the OFF position. The rack then causes the chart drive to operate only during a measurement. The rear of the recorder, accessed by opening the back door of the rack, bears an illuminated switch enabling the choice of CHI or CH2 output. This should be in the CHI position. The chart recorder pen has a remote reservoir which is reached by unlatching the chassis on the right and swinging it out. The reservoir is a plastic bottle with an open cap. Ink is forced to the pen by placing a finger over the cap and squeezing the bottle. Further details are in the Honeywell manual housed in the electronics section of the technical building.

4) Analog Unit

This section is shown in close-up in plate (2).

This unit has two illuminated switches, both concerned with the chart recorder. The STOP CHART switch, when

illuminated, renders the chart recorder inoperable. LINEAR/LOG enables the operator to choose between a linear or logarithmic scale of chart recorder output. The LOG is for display purposes only, but the LINEAR can be used as a normal chart recorder output - i.e. it provides a standby in case the digital output fails.

The remaining facilities on this unit are paired for CH1 and CH2. The DISPLAY FINE GAIN is a normal fine gain used for moving the trace to a suitable place on the chart recorder. By it is a meter showing the deflection. The coarse gain steps are selected elsewhere. (see CONTROL BOX). The RATEMETER enables chart recorder output to be used when the system is pulse counting. The switches allow choice of one of three coarse gains, the gain ratios being ten. The small square displays indicate which of the gains, 1, 2 or 3, are actually being used. (Position 4 is redundant). This is necessary because there is an auto-ranging facility, in that if too high a gain is selected, the system will change down automatically. There is no change-up, therefore star and sky can be measured on the same gains if the star gain is selected manually prior to the sky measurement. The fine gain operates normally.

The INTEGRATION TIME switch allows choice of a 10 sec, 30 sec or 60 sec measurement time.

5) CONTROL UNIT

Not to be confused with control box.

The COMMON GAIN switch should be in the off state,

i.e. not illuminated. This switch is only relevant for two channel operation.

The CHI and CH2 switches enable the selection of which channel is in operation. Normally CHI should be illuminated and CH2 not.

The INHIBIT switches enable the operator to cause the system to ignore certain factors. When the associated switch is illuminated that factor is ignored. Normally all these lights should be off.

CHI FILTER: This causes the system to ignore which filter has been selected.

CHI MIRROR: The mirror referred to is the one which selects which photomultiplier is receiving light. This switch stops the automatic selection of the photomultiplier.

AUTOSTART: This causes every measurement to have to be started by the operator pressing a start button.

The INHIBIT: Facilities are basically of use when testing the system, and are not at present of interest to the observer.

The PROGRAM switch enables the choice of seven different measurement sequences. Number 1 is the plug-in SEALECTRO diode matrix which is found by opening the back door of the rack, and is shown in plate (3). (Spare plug-in diodes are to be found in accessories box 2). Each vertical column

of holes corresponds to a single instruction. The system works from left to right. The section labelled FILTERS consists of eight numbered rows, each of which corresponds to a filter position. The filter position number is defined as the number of the filter which is in front of the blue tube. There are ten filters altogether, positions 9 and 10 (equivalent to 0) being obtained by using two diodes in the same column, namely 8+1 and 8+2. A blank filter column is interpreted as the end of the sequence, and the system returns to the beginning.

When there is a diode in the IR row, then the measurement associated with that column is performed on the red tube. Otherwise the blue tube is selected.

N.B. The red tube is perpendicular to the blue tube, and hence is presented with the filter which is five away from the filter in front of the blue tube. Hence the distinction between filter position and filter number. For example, if one wished to measure through filter number 5 using the red tube, one would have diodes in 8+2 (=10) and IR.

If a column has a diode in the AUTOSTART position, then that measurement starts as soon as the previous measurement has ended, without operator interference. (Provided AUTOSTART is not inhibited, see above).

Suppose one wishes to use (B,V) sky, (V,B,U) star, (U,B) sky. The matrix should be programmed as shown.

FILTERS	1	0	0	0	0	X	X	0	0
	2	X	0	0	X	0	0	X	0
	3	0	X	X	0	0	0	0	0
	4	0	0	0	0	0	0	0	0
	5	0	0	0	0	0	0	0	0
	6	0	0	0	0	0	0	0	0
	7	0	0	0	0	0	0	0	0
	8	0	0	0	0	0	0	0	0
IN TUBE		0	0	0	0	0	0	0	0
AUTOSTART		0	X	0	X	X	0	X	0
BLEEP		0	X	0	0	X	0	X	0

This assumes that U, B, V, correspond to positions 1, 2, 3. A cross represents a plugged-in diode.

When the observer presses a START button, the system selects filter position 2, sees that the red tube is not required and commences the first integration. When this is completed, column 2 is inspected. This causes filter 3 to be selected and the measurement proceeds immediately since AUTOSTART is specified. At the end of the integration the system BLEEPS, to warn the observer. Column 3 is inspected, but it contains no AUTOSTART, so that the system waits until the observer presses a START button, thereby allowing him to move the telescope. The sequence proceeds until column 8 is reached, whereupon the system returns to column 1 as column 8 requests no filter. At column 1 there is no AUTO-START so the system waits until the observer is ready to

start the sequence again.

The plug-in matrix thus allows the observer to specify his own preferred observing sequence. Up to 24 operations can be accommodated.

The sequence given as an example above is available as a standard facility, and is obtained by setting the PROGRAM switch to position 2. A list of pre-programmed sequences will be found posted on the inside of the back door of the cabinet, along with data on the filters.

The front of the CONTROL unit also bears a two digit display. This shows the number of the instruction that the system has reached, counting the first instruction as zero, i.e. V star above would be indicated by 02.

6) Battery Charger

There is a standby system allowing the use of batteries to keep the clocks running in the event of a power failure. At present batteries are not supplied, but they can be easily connected if there should be a demand.

7) EH T's

The EHT's should be left with their MAINS switches in the ON position. The voltages for the FW-118 (red) and EMI 6256A (blue) tubes are 1850v and 1000 v respectively. These voltages apply to both integrating and pulse counting measurements.

If other tubes are used, they should be inspected closely

for informative labels.

8) Power Unit plate (4)

This has three indicator lamps. The green one lights up as soon as the rack is plugged into the mains. This indicates that the clocks and the window heaters in the coldboxes are in operation. When the MAINS switch and its associated red light are on, the whole system is powered. The MAINS switch should only be left on if the sidereal clock is running.

The FAN switch and its indicator are associated with a device to blow air through the rack to prevent overheating. Use of this should be unnecessary.

On the left of the power unit is the BLEEPER. It has an ON/OFF switch which enables the observer to eliminate the bleeps if they annoy him.

B) CONTROL BOX plate (5)

The control box is connected to the rack by a cableform. The switches on this unit are illuminated and so perform a dual function as selection switches and indicators. The MANUAL FILTER SELECT enables the programming to be overriden and the observer can then select filters and tubes either manually at the photometer head or by pressing the relevant switch on the control box. Note that MANUAL FILTER SELECT causes the system to make one measurement after another without stopping, unless AUTOSTART is inhibited.

START starts a measurement, and its illumination is off when a measurement is in progress. CLEAR stops a measurement, and the system waits for a start switch to be pressed irrespective of the state of AUTOSTART. The illumination for CLEAR is always on.

RESET PROGRAM shifts the system back to the first instruction of the program. SHIFT advances the program by one place. The position of the program is indicated by the nixies on the CONTROL UNIT. The illuminations for RESET and SHIFT are always on.

The Tube 1 (blue) and Tube 2 (red) switches enable selection of the photomultiplier when MANUAL FILTER SELECT is operational. Otherwise these indicate which tube is in use.

The block of switches labelled 0 to 9 are the filter selection switches and indicators. The tube and filter switches are all double because of the two channel facility.

PULSE COUNT TUBE 1 and its equivalent for tube 2 enable one to require the system to pulse count with the blue tube or the red tube or both or neither. A tube which is not pulse counting is connected to the integrator.

The six double switches labelled 1, 2, 3 are the integrator gain selectors. The top row of double switches applies to CHI. The top halves of the switches indicate the gain actually used for the measurement, whereas the bottom halves show the gain selected by the operator. This is necessary because there is an autorange facility on the integrator which

reduces the gain if the gain selected is too high. (The bleeper gives a warning if the system overranges). The autorange cannot increase the gain, thus it is possible to measure star and sky on the same gain. Normal procedure is to select gain 3 at the beginning of the night and thereafter leave the system to its own devices. The gain ratios are approximately 20.

On the side of the box is the dimmer, which can be used to adjust the brightness of the illumination of all the switches on the control box and also the rack. The nixies can be switched off as mentioned above. The MAINS indicator lights cannot.

The circular button on top of the control box enables measurement of the integrator zero. The button should be held down continuously and the system started, giving rise to a series of 3 second integrations showing the zero offset of the integrator. It is probably good practice to check this at the end of every night.

C) TELETYPE

A green indicator lights on the teletype when it is plugged in. Near the green light is a red button which activates the teletype. There is no line/local switch. When activated the teletype will respond either to signals from the rack or to typing by the operator. The tape punch has its own ON/OFF switches as usual.

D) TYPEWRITER

The typewriter is a standby for the teletype and is not normally connected to the system. It is mounted on a trolley along with its drive unit. The typewriter mains lead is plugged into the drive unit, and the drive unit plugged into the mains.

E) MECHANICAL SECTION

1) Acquisition Head

The aequisition head has a hinged mirror which is operated by the handle on the observer's right. The eyepiece has a two inch diameter field of view, which corresponds to eleven minutes of arc on the 40-inch. The eyepiece has a screw-type focussing mount which enables it to be focussed on the perspex graticule. The graticule has X and Y motions. The entire eyepiece-graticule assembly is mounted on a tube which slides into the side of the acquisition head, enabling focussing on stars and rotation of the direction of the graticule lines. The graticule has an illumination with a dimmer and on/off switch. There is also a switch on the viewing mirror such that the graticule illumination is off unless the mirror is in the light beam. The same switch prevents measurements being started from the start switch on the head of the mirror is in the light beam.

2) Photometer Head plate (6).

Slight modifications have been made since plate (6) was produced.

Down from the interface plate there is a slide which covers the rim of the aperture disc. At the right hand end of this is a catch which, when lifted, enables the slide to be moved out to the right. Apertures are then changed by pushing the knurled edges of the disc.

The aperture viewer operates by pushing a prism down into the light beam. The two nuts on this system should be kept slack in operation to facilitate proper extraction of the prism. This is necessary as there is a switch which prevents measurements being started from the head if the prism is not fully retracted.

To the left of the eyepiece is the head indicator. This consists of a red lamp which is lit when the red tube is selected, and a numeric indicator which displays the current filter position. The latter goes out when the prism is in the light beam. There are brightness controls on this display.

To the right of the eyepiece is the motor which drives the tube selection mirror. If the red tube is the operational one when the prism is pushed into the light beam, the motor moves the selector mirror out of the way until the prism is retracted.

The large gear with a handle mounted on it is a manual override for the mirror motor. This is on a hinged mounting and is normally left disengaged from the drive shaft. It is a standby in case the motor fails. About $3\frac{1}{2}$ turns are required to change tubes.

Sticking out diagonally from the bottom left hand side of the head is the stepping motor. This drives the filter wheel. On its extremity is a knob with a detent. The latter must be left disengaged at all times. This is another standby system enabling manual selection of filters should the stepping motor fail. Engaging the detent in normal circumstances, even when the motor is not driving, could cause trouble with the delicate optical encoder used to determine the position of the filter wheel. Filter positions are engraved on the knob, and the detent is the fiducial mark.

The surface of the photometer opposite to that shown in plate (6) carries the electronics box. From this hang two switches which are visible draped over the tube 2 coldbox in plate (1). The switch in the cylindrical housing is the head START switch, the other being CLEAR. START is wired in series with switches on the acquisition head mirror and the aperture viewer prism. These prevent measurements being started from the head while either of these is blocking the light beam. The START switch on the control box is not subject to this limitation. Therefore an observer should normally start using the switch on the photometer head.

3) Coldboxes

The coldboxes are fitted with dark slides. Opening the dark slides requires a pulling and turning motion followed by a pushing motion to move them from the position marked SHUT to that marked OPEN, or vice-versa. This is because the actual slides rotate about an axis parallel to the optic axis. Excessive force is not required.

REFERENCES

Barbaro, G., Dallaporta, N., and Nobili, L. 1966. Colloquium on Late Type Stars. Ed. M. Hack. p.386.

Barnes, T. G. 1973. Ap.J. Supp. 25, 369.

Beals, C. S. 1951. Victoria Publ. 9, 1.

Bonneau, D. and Labeyrie, A. 1973. Ap.J. 181, L 1.

van Breda, I. G. and Hill, P. W. 1972. Proceedings of ESO/CERN Conference on Auxiliary Instruments for Large Telescopes. p. 493.

Cousins, A. W. J. 1973 Mem. R.A.S. 77, 223.

Campbell, L. 1955. Studies of Long Period Variables.

Clayton, M. L. and Feast, M. W. 1969. M.N. 146, 411.

Cox, J. P. and Giuli, R. T. 1968. Principles of Stellar Structure.

Eggen, O. J. 1967. Ap.J.Supp. 14, 307.

Eggen, O. J. 1971. Ap.J. 163, 313.

Eggen, O. J. 1975. Ap.J. 195, 661.

Feast, M. W. 1963. M.N. 125, 367.

G.C.V.S. General Catalogue of Variable Stars. Moscow 1969.

Hartwick, F. D. A. and Hesser, J. E. 1974. Ap.J. 194, L 129.

Hartwick, F. D. A. and Sandage, A. 1968. Ap.J. 153, 715.

Hawarden, T. G. 1976. In preparation.

Johnson, H. L. 1966. Ann. Rev. 4, 193.

Johnson, H. L., Mitchell, R. I., Iriarte, B. and Wisniewski, W. Z. 1966. Commun. L.P.L. 4, 99.

Joy, A. H. 1926. Ap.J. 63, 281. 1954. Ap.J.Supp. 1, 39.

Keeley, D. A. 1970a. Ap.J. 161, 657.

Keeley, D. A. 1970b. Ap.J. 161, 657.

Kelly, B. D. 1974. M.N.A.S.S.A. 33, 79.

Kelly, B. D. and Kilkenny, D. 1973. Observatory 93, 145.

Langer, G. E. 1971. M.N. 155, 199.

Lloyd Evans, T. and Menzies, J. W. 1971. Observatory 91, 35.

Lockwood, G. W. 1973. Ap.J. 180, 843.

Lockwood, G. W. and Wing, R.F. 1971. Ap.J. 169, 63.

Mendoza V, E. E. 1967. Bol. Tonanzintla, 4, 114.

Merrill, P. W. 1940. Spectra of Long-Period Variable Stars.

Merrill, P. W. 1960. Stars and Stellar Systems: Stellar Atmospheres.

Merrill, P. W. and Deutsch, A. J. 1959. Ap.J. 130, 570.

Nather, R. E. and Wild, P. A. T. 1973. A.J. 78, 628.

Oke, J. B. and Schild, R. E. 1968. Applied Optics 7, 617.

Osvalds, V. and Risley, R. M. 1961. Publ. Leand. McC. 11, pt XXI.

Pease, F.G. 1931. Quoted in Bonneau and Labeyrie, 1973.

Pettit, E. and Nicholson, S. B. 1933. Ap.J. 78, 320.

Photoelectric Catalogue. U.S. Naval Observatory Publications.

Scott, R. M. 1942. Ap.J. 95, 58.

Smak, J. 1966. Ann. Rev. 4, 19.

Willson, L. A. 1976. Ap.J. 205, 172.

Wilson, R. E. and Merrill, P. W. 1942. Ap.J. 95, 248.

Wing, R. F. 1966. Colloquium on Late Type Stars. Ed. M. Hack. p. 205.

Wing, R. F., Spinrad, H. and Kuhi, L. V. 1967. Ap.J. 147, 117.